

Modeling and Simulation of Hybrid Electric Vehicles

By

Yuliang Leon Zhou

B. Eng., University of Science & Tech. Beijing, 2005

A Thesis Submitted in Partial fulfillment of the Requirements for the Degree of
MASTER OF APPLIED SCIENCE
in the Department of Mechanical Engineering

© Yuliang Leon Zhou, 2007

University of Victoria

All rights reserved. This thesis may not be reproduced in Whole or in part, by
photocopy or other means, without the permission of the author.

SUPERVISORY INFORMATION

Modeling and Simulation of Hybrid Electric Vehicles

By

Yuliang Leon Zhou

B.Eng., University of Science and Technology Beijing, 2005

Supervisory Committee

Supervisor

Dr. Zuomin Dong (Department of Mechanical Engineering)

Department Member

Dr. Afzal Suleman (Department of Mechanical Engineering)

Department Member

Dr. Andrew Rowe (Department of Mechanical Engineering)

External Examiner

Dr. Subhasis Nandi (Department of Electrical Engineering)

Supervisory Committee

| | | |
|---------------------------|---------------------|------------------------|
| <u>Supervisor:</u> | Dr. Zuomin Dong, | Mechanical Engineering |
| <u>Department Member:</u> | Dr. Afzal Suleman, | Mechanical Engineering |
| <u>Department Member:</u> | Dr. Andrew Rowe, | Mechanical Engineering |
| <u>External Examiner:</u> | Dr. Subhasis Nandi, | Electrical Engineering |

Abstract

With increasing oil price and mounting environment concerns, cleaner and sustainable energy solutions have been demanded. At present transportation constitutes a large portion of the energy consumed and pollution created. In this work, two hybrid vehicle powertrain technologies were studied, a fuel cell - battery hybrid and two internal combustion engine - battery/ultracapacitor hybrids. Powertrain performance models were built to simulate the performance of these new designs, and to assess the feasibility of a fuel cell hybrid power backup system for a special type of vehicles, elevators in high-rise buildings, using the ADvanced VehIcle SimulatOR (ADVISOR) first. The model was then applied to evaluate the two-mode hybrid powertrain for more common vehicles - commercial trucks, showing potential fuel consumption reduction. To improve modeling accuracy, a new and more flexible tool for modeling multi-physics systems, Modelica/Dymola, was used to carry out the modeling and analysis of next generation hybrid electric vehicles, exploring the potentials of new hybrid powertrain architectures and energy storage system designs. The study forms the foundation for further research and developments.

Table of Contents

| | |
|--|-------------|
| Modeling and Simulation of Hybrid Electric Vehicles | i |
| Supervisory Committee | ii |
| Abstract | iii |
| Table of Contents | iv |
| List of Figures | viii |
| List of Tables | xiii |
| List of Abbreviations..... | xv |
| Acknowledgements | xvi |
| CHAPTER 1 Introduction..... | 1 |
| 1.1. The Need of Hybrid Electric Vehicles | 1 |
| 1.1.1. Environmental Concerns | 1 |
| 1.1.2. Energy Consumption..... | 2 |
| 1.1.3. Current Global HEV Market..... | 3 |
| 1.2. HEV Classifications by Power Source..... | 3 |
| 1.2.1. Internal Combustion Engine Based HEV..... | 4 |
| 1.2.2. Fuel cell Based HEV | 4 |
| 1.3. HEV Classifications by Drivetrain Architectures | 5 |
| 1.3.1. Series Hybrid..... | 5 |
| 1.3.2. Parallel Hybrid | 6 |
| 1.3.3. Series-Parallel Configurations..... | 9 |
| 1.4. Thesis Outline | 10 |
| CHAPTER 2 Review on Hybrid Electric Vehicles Energy Storage System..... | 12 |
| 2.1. Research Issues in Hybrid Electric Vehicles Design | 12 |
| 2.2. Energy Storage System | 12 |
| 2.2.1. Sizing Considerations of Energy Storage System..... | 12 |
| 2.2.2. ESS Power and Capacity Rating | 13 |
| 2.2.3. ESS for a Electric Vehicle | 15 |

| | | |
|--|--|-----------|
| 2.2.4. | ESS for a Hybrid Electric Vehicle | 17 |
| 2.2.5. | ESS for a Plug-in Hybrid Electric Vehicle | 18 |
| 2.3. | Advance of Energy Storage Technologies and Hydrogen Fuel Cells | 19 |
| 2.3.1. | Sealed Lead Acid Battery (SLA)..... | 20 |
| 2.3.2. | Nickel Metal Hydride Battery (Ni-MH)..... | 20 |
| 2.3.3. | Lithium Ion Battery (Li-ion) | 21 |
| 2.3.4. | Ultracapacitors | 22 |
| 2.3.5. | Hydrogen Fuel Cells..... | 22 |
| CHAPTER 3 Review on Vehicle Simulation Tools | | 24 |
| 3.1. | Vehicle Simulation Tools | 24 |
| 3.2. | ADvanced VehIcle SimulatOR (ADVISOR)..... | 24 |
| 3.2.1. | ADVISOR Background..... | 24 |
| 3.2.2. | ADVISOR Modeling Approaches..... | 25 |
| 3.2.3. | ADVISOR Interface | 26 |
| 3.2.4. | Models in ADVISOR | 30 |
| 3.3. | Modelica and Dymola | 31 |
| 3.3.1. | Modelica..... | 31 |
| 3.3.2. | Dymola | 31 |
| 3.3.3. | Vehicle Modeling and Simulation Libraries..... | 32 |
| CHAPTER 4 Modeling of a Fuel Cells Hybrid Power System for Elevator Power Backup Using ADVISOR..... | | 34 |
| 4.1. | Modeling High Speed Elevators as Electric Vehicles | 34 |
| 4.2. | Power Failures of Elevators in High-rise Buildings | 35 |
| 4.3. | Backup Power Solutions | 36 |
| 4.3.1. | Batteries for Power Backup..... | 37 |
| 4.3.2. | Ultracapacitors for Power Backup | 37 |
| 4.3.3. | ICE Generator for Power Backup | 38 |
| 4.4. | A Fuel Cells Hybrid Power Backup Solution | 38 |
| 4.4.1. | A Hybrid Energy Storage System | 38 |
| 4.4.2. | Operation of Battery Ultracapacitor Hybrid..... | 40 |
| 4.5. | Modeling of High-rise Building Elevator | 40 |

| | | |
|--|--|-----------|
| 4.5.1. | Elevator Model | 41 |
| 4.5.2. | Powertrain Model | 41 |
| 4.5.3. | Modeling of PEM Fuel Cell system | 43 |
| 4.5.4. | Modeling of Motors | 46 |
| 4.5.5. | Modeling of Energy Storage System | 47 |
| 4.6. | Elevator Power Management | 49 |
| 4.7. | Computer Simulation | 51 |
| 4.7.1. | Elevator Traffic Patterns (Drive Cycles) | 51 |
| 4.7.2. | Low Power Mode Simulation | 52 |
| 4.7.3. | High Power Mode Simulation | 55 |
| 4.8. | Optimal Battery and Ultracapacitor Units | 57 |
| 4.9. | Cost Analysis | 59 |
| 4.9.1. | Cost of PEM Fuel Cell System | 59 |
| 4.9.2. | Costs of Batteries and Ultracapacitors | 60 |
| 4.9.3. | Power Converter and Controller | 60 |
| 4.10. | Discussion and Conclusions | 61 |
| CHAPTER 5 Modeling of a ICE Hybrid Powertrain for Two-mode Hybrid Trucks Using ADVISOR..... | | 63 |
| 5.1. | Planetary Gear Based Power Transmission | 63 |
| 5.1.1. | Speed, Torque and Power of the Planetary Gears | 63 |
| 5.1.2. | Toyota Hybrid System | 67 |
| 5.1.3. | The First Mode of a Two-mode Transmission | 73 |
| 5.1.4. | The Second Mode of a Two-mode Transmission | 78 |
| 5.2. | Vehicle Modeling in ADVISOR | 84 |
| 5.2.1. | Modeling of Drivetrain | 85 |
| 5.2.2. | Modeling of Engine | 86 |
| 5.2.3. | Modeling of a Two-mode Transmission | 88 |
| 5.3. | Control Strategy of a Two-mode Hybrid Vehicle | 92 |
| 5.3.1. | Review on HEV Control Development | 92 |
| 5.3.2. | Mode Selection | 93 |
| 5.3.3. | Power Management of First Mode | 94 |

| | | |
|--|--|------------|
| 5.3.4. | Power Management of Second Mode | 96 |
| 5.4. | Computer Simulation | 97 |
| 5.4.1. | Drive Cycles | 97 |
| 5.4.2. | Road Performance | 99 |
| 5.4.3. | System Operation | 102 |
| 5.4.4. | System Efficiency..... | 104 |
| 5.4.5. | All Electric Range | 108 |
| 5.5. | Conclusions..... | 109 |
| CHAPTER 6 Modeling of ICE Hybrid Powertrain for a Parallel Hybrid Truck Using Modelica/Dymola and Validation..... | | 111 |
| 6.1. | Parallel Hybrid Electric Vehicle..... | 111 |
| 6.2. | Vehicle Modeling in Dymola | 112 |
| 6.2.1. | Engine Modeling | 113 |
| 6.2.2. | Transmission Modeling..... | 115 |
| 6.2.3. | Chassis and Resistance Modeling | 116 |
| 6.2.4. | Driver Modeling..... | 118 |
| 6.3. | Models Simulation and Validations | 118 |
| 6.3.1. | Engine Model Validation..... | 118 |
| 6.3.2. | Torque Converter Model Validation..... | 119 |
| 6.3.3. | Transmission Model Validation..... | 121 |
| 6.3.4. | Chassis and Resistance Model Validation..... | 122 |
| 6.4. | Overview and Conclusions | 123 |
| CHAPTER 7 Summary..... | | 124 |
| 7.1. | Research Problem | 124 |
| 7.2. | Technology Review..... | 124 |
| 7.3. | Vehicle Modeling | 124 |
| 7.4. | Future Work | 125 |
| REFERENCES | | 126 |

List of Figures

| | |
|--|----|
| Figure 1-1 Globe Oil Consumption Perspective [4] | 2 |
| Figure 1-2 Toyota Prius-Most Sold HEV | 3 |
| Figure 1-3 a Series Hybrid Electric Vehicle Configuration | 5 |
| Figure 1-4 a Fuel cell HEV Configuration | 6 |
| Figure 1-5 a Pre-Transmission Parallel HEV Configuration | 7 |
| Figure 1-6 a Post-Transmission Parallel HEV Configuration | 7 |
| Figure 1-7 A All Wheel Drive Parallel HEV Configuration | 8 |
| Figure 1-8 Toyota THS Configuration | 10 |
| Figure 2-1 Power/Energy Ratio of Vehicle Demand and ESS Capability | 15 |
| Figure 3-1 Flow Chart of an Backward Modeling Approach | 26 |
| Figure 3-2 ADVISOR/Simulink Block Diagram of a Two-mode Truck | 26 |
| Figure 3-3 ADVISOR Vehicle Input Interface..... | 28 |
| Figure 3-4 Simulation Setup Interface | 28 |
| Figure 3-5 Simulation Result Window | 29 |
| Figure 4-2 a Fuel cells Super Hybrid Power System..... | 39 |
| Figure 4-3 Physical Model of an Elevator | 41 |
| Figure 4-4 Modeling a Fuel Cell Hybrid Vehicle/Elevator in ADVISOR..... | 42 |
| Figure 4-5 A PEM Fuel Cells Stack..... | 44 |
| Figure 4-6 a Fuel cell system Model in ADVISOR..... | 45 |

| | |
|--|----|
| Figure 4-8 Motor Model Power Flow | 46 |
| Figure 4-9 Motor Model in ADVISOR..... | 46 |
| Figure 4-10 AC30 Motor Power Efficiency..... | 47 |
| Figure 4-11 Energy Storage System Model | 47 |
| Figure 4-12 Energy Storage System Model in ADVISOR | 48 |
| Figure 4-13 Power Management System of a Fuel Cells Hybrid Powertrain..... | 49 |
| Figure 4-14 Fuel cell system Power Management Flow Chart..... | 50 |
| Figure 4-15 Simulation of Low Power Cycle | 52 |
| Figure 4-16 System Power Demand-Low Power Cycle | 53 |
| Figure 4-17 Fuel cells Power Demand-Low Power Cycle | 53 |
| Figure 4-18 Battery SOC-Low Power Cycle | 54 |
| Figure 4-19 Ultracapacitor SOC-Low Power Cycle | 54 |
| Figure 4-20 Performance Simulation of High Power Cycle..... | 55 |
| Figure 4-21 System Power Demand-High Power Cycle | 55 |
| Figure 4-22 Fuel cells Power Demand-High Power Cycle..... | 56 |
| Figure 4-23 Battery SOC-High Power Cycle | 56 |
| Figure 4-24 Ultracapacitor SOC-High Power Cycle | 57 |
| Figure 4-25 Optimal Battery Units | 58 |
| Figure 4-26 Optimal Ultracapacitor Units | 58 |
| Figure 5-1 A General Planetary Gear..... | 64 |
| Figure 5-2 Power Flow Chart of Planetary Gear | 67 |
| Figure 5-3 Toyota THS Configuration..... | 68 |

| | |
|--|----|
| Figure 5-4 Engine, M/G1 and M/G2 Speed of THS | 69 |
| Figure 5-5 THS Power Flow Chart Engine Off | 69 |
| Figure 5-6 THS Power Flow Chart Engine Start | 70 |
| Figure 5-7 THS Power Flow Chart $V_1 < V < V_2$ | 71 |
| Figure 5-9 First Mode Drivetrain Configuration | 73 |
| Figure 5-10 Speed of Engine, M/G 1, M/G2 and Output Shaft..... | 74 |
| Figure 5-11 First-mode Power Flow Chart-Engine Off..... | 75 |
| Figure 5-12 Power Flow Chart of Forward Movement in the First Mode..... | 76 |
| Figure 5-13 Power Flow Chart of Backward Movement in the First Mode..... | 77 |
| Figure 5-14 Second Mode Drivetrain Configuration..... | 78 |
| Figure 5-15 Power Flow of Second Mode at Vehicle Speed of V_{s3} or Lower.... | 80 |
| Figure 5-16 Power Flow of Second Mode during Brake at a Vehicle Speed of V_{s3} or Lower..... | 81 |
| Figure 5-17 Power Flow of Second Mode at a Vehicle Speed Greater than V_{s3} | 82 |
| Figure 5-18 Power Flow of Second Mode Brake at Speed over V_{s3} | 83 |
| Figure 5-19 Free Body Diagram of a Truck..... | 85 |
| Figure 5-20 Engine Model Schematic Diagram | 87 |
| Figure 5-21 Simulink Block Diagram of Engine Thermal and Fuel Model | 88 |
| Figure 5-22 A Schematic Diagram of Two-mode HEV | 88 |
| Figure 5-23 Two-mode Transmission Model and its Controller..... | 91 |
| Figure 5-24 First Mode Block in Transmission Model..... | 92 |
| Figure 5-25 Mode Switch Control | 93 |

| | |
|--|-----|
| Figure 5-26 Speed Profile of All Shafts (Engine Speed predefined)..... | 94 |
| Figure 5-27 Power Management Chart Mode 1 | 95 |
| Figure 5-28 Power Management Chart Mode 2 | 96 |
| Figure 5-29 Vehicle Speed on the UDDSHEV Cycle..... | 99 |
| Figure 5-30 Vehicle Speed on NYCTRUCK Cycle..... | 100 |
| Figure 5-31 Vehicle Speed on CSHVR Cycle | 101 |
| Figure 5-32 Vehicle Speed on HWFET Cycle..... | 101 |
| Figure 5-33 Engine Power on NYCCTRUCK Cycle | 102 |
| Figure 5-34 Electric Motors Power Demand over NYCCTRUCK Cycle..... | 103 |
| Figure 5-35 Speed of Engine and Electric Motors on NYCTRUCK Cycle | 103 |
| Figure 5-36 Battery SOC History on NYCTRUCK | 104 |
| Figure 5-37 Efficiency of Two Mode HEV and Conventional ICE Vehicle on UDDSHEV Cycle | 105 |
| Figure 5-38 Efficiency of Two Mode HEV and Conventional ICE Vehicle on NYCCTRUCK Cycle..... | 106 |
| Figure 5-39 Efficiency of Two Mode HEV and Conventional ICE Vehicle on CSHVR Cycle..... | 106 |
| Figure 5-40 Efficiency of Two Mode HEV and Conventional ICE Vehicle on HWFET Cycle | 107 |
| Figure 5-41 Summery of Fuel Consumptions..... | 107 |
| Figure 5-42 All Electric Mode Operation on NYCCTRUCK | 108 |
| Figure 5-43 Battery SOC on NYCTRUCK at AEM..... | 109 |
| Figure 6-1 a Post-Transmission Parallel HEV Configuration | 112 |

| | |
|---|-----|
| Figure 6-2 Forward Vehicle Modeling Algorithm in Dymola | 113 |
| Figure 6-3 Engine Model in Dymola | 114 |
| Figure 6-4 Base Engine Modeling | 115 |
| Figure 6-5 Engine Speed Governor Modeling..... | 115 |
| Figure 6-6 Transmission Model in Dymola..... | 116 |
| Figure 6-7 Chassis Model in Dymola | 117 |
| Figure 6-8 Vehicle Resistance Model | 117 |
| Figure 6-9 Driver Model..... | 118 |
| Figure 6-10 Engine Model Validation..... | 119 |
| Figure 6-11 Torque Converter Validation - Output Torque..... | 120 |
| Figure 6-12 Torque Converter Validation - Output Speed..... | 121 |
| Figure 6-13 Transmission Model Validation - Output Speed | 122 |
| Figure 6-14 Vehicle Chassis Model Validation - Vehicle Speed..... | 123 |

List of Tables

| | |
|--|----|
| Table 1-1 An Incomplete List of HEV been developed at present..... | 4 |
| Table 2-1 Characteristic of a Benchmark EV | 16 |
| Table 2-2 ESS Sizing for a Benchmark EV | 17 |
| Table 2-3 Specs of Ni-MH on a 2004 Toyota Prius [16] | 17 |
| Table 2-4 ESS Sizing for a HEV..... | 18 |
| Table 2-5 UC-battery Hybrid ESS for Prius | 18 |
| Table 2-6 UC-battery Hybrid ESS for Prius | 19 |
| Table 2-7 Battery Performance Characterizes for HEV and EV | 21 |
| Table 3-1 Vehicle Modeling Packages in Modelica..... | 33 |
| Table 4-1 Parameters of a Prototype Elevator | 43 |
| Table 4-4 Power Source Unit Sizes on Initial Simulation Test..... | 52 |
| Table 4-5 Specification of Optimized Powertrain | 59 |
| Table 4-6 Specification of Battery Based Elevator Backup Power System..... | 59 |
| Table 4-7 Overall System Cost Prediction..... | 61 |
| Table 5-1 Engine and Motor Operating Condition of THS | 72 |
| Table 5-3 Summery of Engine, M/G1 and M/G2 in First Mode | 78 |
| Table 5-4 Power Flow Summery of First Mode | 78 |
| Table 5-5 Summery of Engine, M/G1 and M/G2 in Second Mode..... | 83 |
| Table 5-6 Power Flow Summery of Second Mode..... | 84 |

| | |
|--|-----|
| Table 5-7 Modeling Parameters | 86 |
| Table 5-8 Signal Interface Explanation of a Two-mode Transmission Model..... | 91 |
| Table 5-9 ESS SOC Management..... | 95 |
| Table 5-10 Simulation Vehicles Specification | 97 |
| Table 6-1 Engine Model Input | 119 |
| Table 6-2 Torque Converter Model Input | 120 |
| Table 6-3 Transmission Input..... | 121 |
| Table 6-4 Transmission Input..... | 122 |

List of Abbreviations

| | |
|--------|---|
| AEM | All Electric Mode |
| AER | All Electric Range |
| BOP | Balance of Plant |
| CVT | Continuous Variable Transmission |
| DOE | Department of Energy |
| DOH | Degree of Hybridization |
| EM | Electrical Machine |
| ESS | Energy Storage Systems |
| EV | Electric Vehicle |
| FCHEV | Fuel Cell Hybrid Electric Vehicle |
| GHG | Green house Gasses |
| GUI | Graphic User Interface |
| HEV | Hybrid Electric Vehicle(s) |
| ICE | Internal Combustion Engine(s) |
| IESVic | Institute for Integrated Energy Systems |
| L-A | Lead Acid Battery |
| Li-ion | Lithium-ion |
| M/G | Motor/Generator |
| Ni-MH | Nickel Metal Hydride Battery |
| NYCC | New York City Cycle |
| SLA | Sealed Lead Acid Battery |
| SOC | State of Charge |
| THS | Toyota Hybrid System |
| PEM | Proton Exchange Membrane |
| PF | Power Flow Factor |
| PHEV | Plug-in Hybrid Electric Vehicle |
| PSD | Power Split Devices |
| UVic | University of Victoria |

Acknowledgements

I would like to first acknowledge and express my sincere thanks to my supervisor, Professor Zuomin Dong for the opportunity that he gave me to work on this highly promising and exciting research area. I would like to express my gratitude to Jeff Wishart and Adel Younis, both Ph.D. candidates in the research laboratory, and Dr. Jianxiong Liu for their encouragement and warm assistance on their respective expertise. I would also like to thank Matthew Guenther, a recent graduate from the laboratory, whose Master thesis on related topics has provided solid foundation for the initiation of my research.

Financial supports from the Natural Science and Engineering Research Council of Canada, University of Victoria, Azure Dynamic and MITACS program are gratefully acknowledged.

Finally, a special thank you goes to my parents Zhou Yong and Yu Dongmei for their moral and financial supports during my study in Canada.

CHAPTER 1 Introduction

1.1. The Need of Hybrid Electric Vehicles

In recent years, a significant interest in hybrid electric vehicle (HEV) has arisen globally due to the pressing environmental concerns and skyrocketing price of oil. Representing a revolutionary change in vehicle design philosophy, hybrid vehicles surfaced in many different ways. However, they share the hybrid powertrain that combines multiple power sources of different nature, including conventional internal combustion engines (ICE), batteries, ultracapacitors, or hydrogen fuel cells (FC). These vehicles with onboard energy storage devices and electric drives allows braking power to be recovered and ensures the ICE to operate only in the most efficient mode, thus improving fuel economy and reducing pollutants. As a product of advanced design philosophy and component technology, the maturing and commercialization of HEV technologies demand extensive research and developments. This research intends to address many key issues in the development of HEV.

1.1.1. Environmental Concerns

The United Nations estimated that over 600 million people in urban area worldwide were exposed to traffic-generated air pollution [1]. Therefore, traffic related air pollution is drawing increasing concerns worldwide. Hybrid electric vehicles hold the potential to considerably reduce greenhouse gas (GHG) emission and other gas pollution. A fuel cell HEV, which only produce water and heat as emissions during operation, makes pollution more controllable by centralizing GHG emission and air pollution to the hydrogen production process at large scale manufacturing facilities. ICE based hybrids, on the other hand, can improve the fuel economy and reduce tailpipe emission by more efficient engine operation. The improvements come from regenerative braking, shutting down the ICE while stationary and allowing a smaller, more efficient engine which is not required to follow the power at the wheel as closely as the engine in

a conventional vehicle must [2]. In an emission effect comparison of the Toyota Prius (HEV) and Toyota Corolla, it was reported that the Prius only produced 71% of CO₂, 4% of CO and 0.5% of NO_x compared with the Toyota Corolla. The Corolla is one of most efficient conventional vehicles on the market.

1.1.2. Energy Consumption

Around the world, we are experiencing a strong upward trend in oil demand and tight supply. Maintaining a secure energy supply becomes an on-going concern and a high priority. The US Department of Energy (DOE) states that over 15 million barrels of crude oil are being consumed in the nation of which 69% are for the transportation sector [3]. The transport energy consumption worldwide are also continue to rise rapidly. In 2000 it was 25% higher than in 1990 and it is projected to grow by 90% between 2000 and 2030 as shown in Figure 1-1.

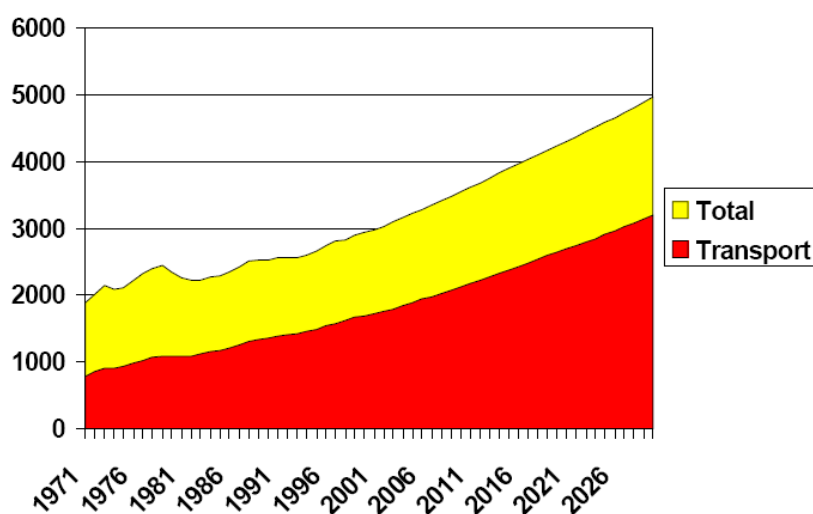


Figure 1-1 Globe Oil Consumption Perspective [4]

Many HEV projects reported fuel economy improvement from 20% to 40% [5]. Therefore, HEV provides a promising solution to relieve the energy shortage.

1.1.3. Current Global HEV Market

In 1970s, many auto makers such as GM, Ford and Toyota started to develop electric vehicles powered by batteries due to the oil shortage. However, these electric vehicles powered solely by battery power did not go far enough. The interest in hydrogen fuel cell cars has arisen as a result to address the range problem associated with battery power cars. However, with more than 15 years of intensive development, there are still not any fuel cell hybrid cars on market mainly due to the high manufacturing cost. In the meantime, other automotive manufacturers have moved in another direction of ICE based HEV. In 1997, Toyota introduced the Prius (Figure 1-2), the first ICE based HEV to the Japanese market. Ever since, an increasing number of HEV have become available.



Figure 1-2 Toyota Prius-Most Sold HEV

The sales of HEV are growing rapidly. An estimated 187,000 hybrids were sold in the first six months of 2007 in US, accounting for 2.3 percent of all new vehicle sales according to J.D. Power. J.D. Power also forecasted a total sale of 345,000 hybrids for 2007, a 35% increase from 2006.

1.2. HEV Classifications by Power Source

There are many ways to classify hybrid electric vehicles. One way is based on principal power sources. Two major principal power sources for HEV are ICE and fuel cell system.

Table 1-1 An Incomplete List of HEV been developed at present

| Manufacturers and Vehicles | | Year | Type |
|-----------------------------------|--|-------------|-------------|
| Toyota | Prius, Camry, Highlander | 1997 | Sedan, SUV |
| Lexus | RX400h, LS600H | 2005 | Sedan, SUV |
| Honda | Insight, Civic, Accord | 2005 | Sedan, SUV |
| GM | Silverado, Saturn, Equinox, Tahoe, Yukon | 2007 | Truck, SUV |
| GM | New Flyer | 2004 | Heavy Bus |
| Chrysler | Durango, Ram | 2005 | Truck |
| Mercedes | Benz S | 2006 | Sedan |
| Ford | Escape, Mariner | 2005 | SUV |
| Hyundai, Renault, IVECO | | 2004 | Various |

1.2.1. Internal Combustion Engine Based HEV

In an ICE based HEV, the engine is coupled with electric machine(s). This modification creates integrated mechanical and electrical drive trains that merge power from both the ICE and the electric motors to drive the vehicle. By using the energy storage system as a power buffer, the ICE can be operated at its most efficient condition and reduced in size while maintaining the overall performance of the vehicle. In this type of vehicles, fossil fuel, however, is still the sole energy source to the vehicle system, (except for plug-in HEV where electricity obtained from electrical grid provides another power source). The charge of the battery is maintained by the ICE and the electric machines. As a consequence of the reduced engine size, more efficient engine operation, and recovered braking power, fuel usage and emissions of the vehicle are considerably lower than comparable conventional vehicles.

At present, all commercialized HEV are ICE based. Many possible mechanical configurations can be implemented for an ICE based HEV. More detailed vehicle configurations will be explained in Section 1.3.

1.2.2. Fuel cell Based HEV

A fuel cell hybrid electric vehicle operates solely on electric power. The fuel cells continuously

produce electrical power while energy storage devices buffer the power flow in the electric power train. A fuel cell system is an electric power-generating plant based on controlled electrochemical reactions of fuel and oxidant [6]. In principle, fuel cells are more efficient in energy conversion and produce zero emission. Due to many attractive features, such as low operation temperature, compact structure, fewer corrosion concerns, and quick start-up, the Proton Exchange Membrane (PEM) fuel cells serves as an ideal power plant for automotive applications.

1.3. HEV Classifications by Drivetrain Architectures

One of the most common ways to classify HEV is based on configuration of the vehicle drivetrain. In this section, three major hybrid vehicle architectures introduced are series, parallel and series-parallel. Until recently, many HEV in production are either series or parallel. In terms of mechanical structure, these two are primitive and relatively simple. A series-parallel powertrain brings in more degrees of freedom to vehicle engine operation with added system complexity.

1.3.1. Series Hybrid

One of the basic types of HEV is series hybrid. In this configuration, as shown in Figure 1-3, the ICE is used to generate electricity in a generator. Electric power produced by the generator goes to either the motor or energy storage systems (ESS). The hybrid power is summed at an electrical node, the motor.

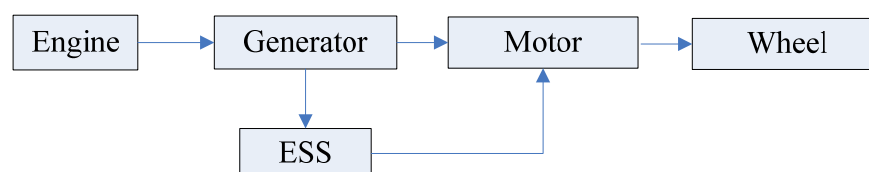


Figure 1-3 a Series Hybrid Electric Vehicle Configuration

Early on in the latest renaissance of the hybrid vehicle, several automotive OEMs explored the possibility of series hybrid vehicle development. Some of the most notables are the Mitsubishi ESR, Volvo ECC, and BMW 3 Series [7]. Despite the early research and prototypes, the possibility for series hybrids to be commonly used in vehicular applications seems to be remote. The series hybrid configuration tends to have a high efficiency at its engine operation. The capacity for the regenerative braking benefits from the full size motor. However, the summed electrical mode has tied up the size of every component. The weight and cost of the vehicle is increased due to the large size of the engine and the two electric machines needed. The size of the power electronic unit is also excessive.

The configuration of fuel cell HEV is also technically in series as shown in Figure 1-4. Since fuel cell generate electric, rather than mechanical power, it functions as a power generator replacing both of the engine and the electric generator. This is the uniqueness of fuel cell powered HEV.

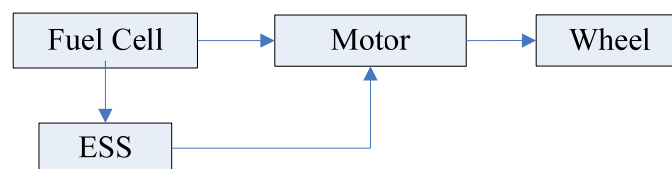


Figure 1-4 a Fuel cell HEV Configuration

1.3.2. Parallel Hybrid

The parallel hybrid is another HEV type that has been closely studied. In parallel configurations, both the engine and the motor provide traction power to the wheels, which means that the hybrid power is summed at a mechanical node to power the vehicle. As a result, both of the engine and the motors can be downsized, making the parallel architecture more viable with lower costs and higher efficiency. Some early developments of parallel hybrid vehicles include the BMW 518, Citroën Xzara Dynactive and Saxo Dynavolt, Daimler-Chrysler ESX 3, Fiat Multipla, and the Ford Multipla and P2000 Prodigy [7].

The parallel hybrid vehicles usually use the same gearboxes of the counterpart conventional vehicles, either in automatic or manual transmissions. Based on where the gearbox is introduced in the powertrain, there are two typical parallel HEV architectures, named pre-transmission parallel and post-transmission parallel, as shown in Figure 1-5 and Figure 1-6, respectively.

In a pre-transmission parallel HEV, the gearbox is located on the main drive shaft after the torque coupler. Hence, gear speed ratios apply on both the engine and the electric motor. The power flow is summed at the gearbox. On the other hand, in a post-transmission parallel hybrid, the gearbox is located on the engine shaft prior to the torque coupler. The gearbox speed ratios only apply on the engine. A continuous variable transmission (CVT) can be used to replace conventional gearbox to further improve the engine efficiency.

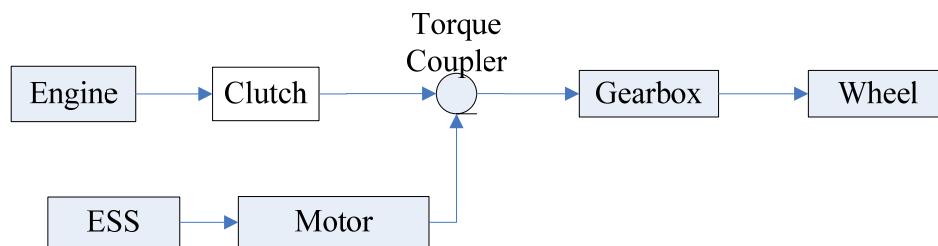


Figure 1-5 a Pre-Transmission Parallel HEV Configuration

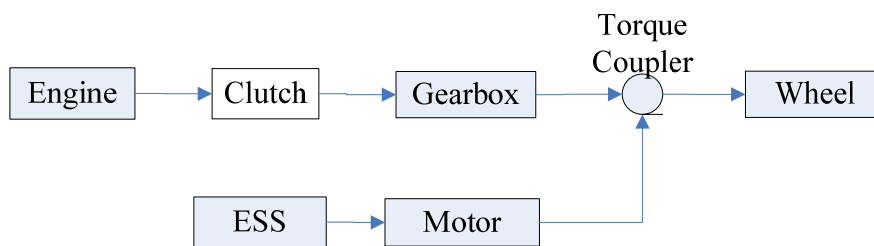


Figure 1-6 a Post-Transmission Parallel HEV Configuration

In a pre-transmission configuration, torque from the motor is added to the torque from the engine at the input shaft of the gearbox. Contemporary mild parallel hybrid vehicles employ this strategy exclusively. In a post-transmission, the torque from the motor is added to the torque from the engine delivered on the output shaft of the gearbox. A disconnect device such as a clutch is used to disengage the gearbox while running the motor independently [8].

Post-transmission electric hybrids can also be used in hybrid vehicles with a higher degree of hybridization. Hydraulic power can be used on launch-assist devices in heavy-duty trucks and commercial vehicles.

There are attempts from different perspectives to improve the operation of a parallel HEV. One possibility is to run the vehicle on electric machine alone in city driving while running engine power alone on highways. Most contemporary parallel vehicles use a complex control system and special algorithms to optimize both vehicle performance and range. The flexibility in powertrain design, in addition to the elimination of the need for a large motor, of parallel hybrids has attracted more interest in HEV development than the series hybrids.

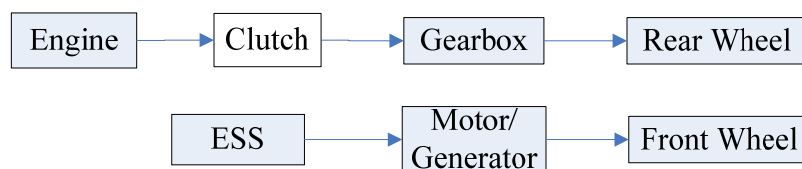


Figure 1-7 A All Wheel Drive Parallel HEV Configuration

One unique implementation of the parallel hybrid technology is on an all wheel drive vehicle as shown in Figure 1-7. The design is most beneficial if the ICE powers the rear wheels while the electric motor powers the front wheels. The more weight borne by the front wheels during braking will result in more power captured during regenerative braking. The design is also effective on slippery surfaces by providing vehicle longitudinal stability control that is not as easy with other types of hybrid designs. The power to each axle is manipulated by a single controller, although this requires a fast data communication. It is unclear whether any automotive OEM has planned to incorporate this design into real vehicles.

The Honda Insight was the first commercialized hybrid vehicle, although the vehicle line was discontinued in September 2006. The Insight was considered as a test vehicle to gauge public opinion on hybrid technology, and the 18,000 USD price tag is estimated to be 10,000 USD less than the actual production cost [7]. Despite the cost distortion, the Insight never became a

commercial success largely because of its two-seater format. Honda has promised a replacement to arrive in 2009 [9].

The Insight is a mild-hybrid, with the electric motor being the key to the Integrated Motor Assist (IMA) technology that boosts the engine power. The engine is an inline 3 cylinders 0.995 litre gasoline engine that delivers 50 kW peak power at 5700 rpm, and 89 N·m peak torque at 4800 N·m with a manual transmission. When the IMA system is activated, these numbers rise to 54.4 kW and 107 N·m for the manual transmission and 53 kW and 121 N·m for the CVT. The electric motor is a permanent magnet machine that supplies 10.4 kW of power at 3,000 rpm with a manual transmission, and 9.7 kW of power at 2,000 rpm in a CVT model. The ESS consists of 120 cells of Nickel Metal Hydride (Ni-MH) batteries of 1.2 V each, for a total voltage of 144 V with a rated capacity of 6.0 Ah. The schematic of the Insight is similar to Figure 1-5 on a pre-transmission parallel HEV.

1.3.3. Series-Parallel Configurations

In the series-parallel configurations, the vehicle can operate as a series hybrid, a parallel hybrid, or a combination of both. This design depends on the presence of two motors/generators and the connections between them, which can be both electrical and mechanical. The mechanical connections between the engine and electric machines are usually accomplished by planetary gears known as power-splitting devices (PSDs), which are discussed in more detail in Section 5.1. One advantage of a series-parallel configuration is that the engine speed can be decoupled from the vehicle speed. This advantage is partially offset by the additional losses in the conversion between mechanical power from engine and electrical energy [10].

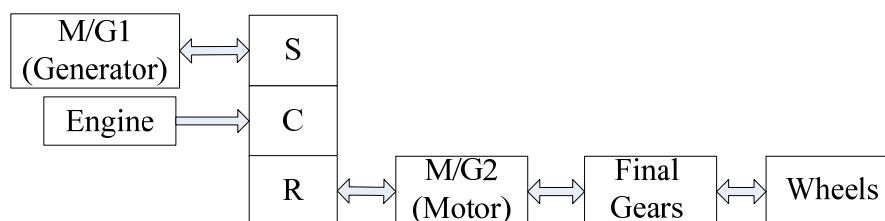


Figure 1-8 Toyota THS Configuration

There are a number of variations of series-parallel configurations. A most well known one is the Toyota THS design that was first used on a Toyota Prius. The THS configuration is shown on Figure 1-8. Today, most hybrid vehicles at the production stage have been either of parallel or series configuration, as the series-parallel design is less mature in its development. However, a review of the literatures from both academic and commercial sources reveals that the current state-of-the-art of hybrid technology employs the series-parallel configuration [11]. In this study, a new series-parallel configuration known as two-mode configuration will be introduced and analyzed.

1.4. Thesis Outline

In this thesis, Chapter 1 has defined the research problem and presented the importance of the HEV technology. Classifications of various HEV configurations were introduced based on different criteria. Chapter 2 explains the power and energy demands from vehicle on board energy storage system. Based on these demands, a review on recent advances of HEV related energy storage system technologies was presented. Chapter 3 discusses the state-of-the-art of HEV design and simulation tools. Two widely used modeling platforms are discussed in details. Chapter 4 explains the modeling of a fuel cell hybrid power system for the application of high rise building elevator power backup. Both system performance and cost analysis are carried out in examining the feasibility of the technology. Chapter 5 presents the new models of a hybrid commercial truck using the two-mode hybrid powertrain, with vehicle performance simulation

results presented at the end. Chapter 6 discusses the modeling of a parallel hybrid vehicle in the new Dymola modeling and simulation environment. Validations of the powertrain model using empirical data from tests are carried out. Finally, Chapter 7 summarizes the work of this thesis, and Chapter 8 points out the future work needed.

CHAPTER 2 Review on Hybrid Electric Vehicles Energy Storage System

2.1. Research Issues in Hybrid Electric Vehicles Design

The focus of HEV design is mostly on powertrain efficiency. This efficiency depends on contributions from the engine, motor, battery, and mechanical transmissions. The peak efficiency of an ICE can be as high as 36% (based on 1998 Prius 1.5L Gasoline Engine), while the overall efficiency of its operation, on the other hand, is usually no more than 20%. Therefore, the objective of HEV design is to improve the overall vehicle efficiency by optimizing the sizes operations of its powertrain components. Although there is a great potential to improve the vehicle fuel economy and driveability in principle, present control strategies based on engineering intuition frequently fail to capture these potentials. Due to the existence of multiple power sources on these vehicles, an overall fuel consumption and emission control strategy needed be developed.

2.2. Energy Storage System

2.2.1. Sizing Considerations of Energy Storage System

For different types of vehicle technology, the electrical energy storage system (ESS) is utilized differently. HEV are classified into three categories following the types of power source: electric vehicles (EV), hybrid electric vehicles (HEV), and plug in hybrid electric vehicles (PHEV). An EV uses ESS as the sole energy source. Technically an EV would not be considered as a HEV; it is discussed here in order to compare with the other two types. The ESS on an EV, usually a battery pack, is only charged from grid electricity except for during

regenerative braking. The vehicle range with one charge is directly related to the energy capacity of the ESS. A HEV on the other hand, has more than one energy sources. The ICE or FC is usually hybridized with an ESS on a HEV. The ESS would be charged by the ICE or FC during the vehicle operation according to power demand, and no external power source is necessary to charge the ESS. A plug-in hybrid electric vehicle is also a HEV with its ESS being charged either by the on board power source, such as ICE and FC, or the stationary grid power.

In HEVs, the size of the ESS is determined to provide sufficient energy storage (*kWh*) capacity and adequate peak power (*kW*) ability. In addition, appropriate cycle life and hardware cost have to be considered. The size requirement of ESS varies significantly depending on the characteristics of different vehicle's powertrains (EV, HEV and PHEV) [12]. This requirement can be obtained once the vehicle is specified and the performance target is established. However, what is less straightforward and more challenging is to find an optimal ESS design that would satisfy the special characteristics of vehicle power requirements. Normally, energy storage units are primarily sized by either the energy or power capability. Charging-discharging efficiency is also considered. In this study, a comparison of the performance characteristics (*Wh/kg*, *Wh/L*, *W/kg* etc.) of various energy storage technologies for different vehicle power requirements is made to guide the ESS design.

2.2.2. ESS Power and Capacity Rating

ESS can consist of various types of batteries, ultracapacitors, and their combinations.

An expression $P_{peak} = V_0^2 / 4R$ is commonly used to rate the peak power of the battery, where V_0 is the nominal voltage of the battery and R is the battery's internal resistance. The efficiency at the peak power of the battery is relatively low (close to 50%). A generic expression of battery power and efficiency is given by the following equation

$$P_{peak} = \eta \times (1 - EF) \times V_0^2 / R \quad (2.1)$$

where η is the efficiency at peak power pulse. It is assumed that the peak power occurs when $V_{peak} = V_0 \times \eta$. For an efficiency of 85%, the peak power will be reduced by 1/2 from the peak power at lower efficiency.

Ultracapacitors are also sized by power and energy. Energy storage capacity (Wh) is usually used to size ultracapacitors due to their low specific energy (5-10 Wh/kg). The useable peak power from an ultracapacitor is given by Eq. (2.2):

$$P_{peak} = 9/16 \times (1 - \eta) \times V_0^2 / R \quad (2.2)$$

The peak power occurs at a voltage of $3/4 V_0$, where $I = P_{peak} / 3/4 V_0$. As internal resistance of an ultracapacitor is considerably lower than that of a battery, the peak power is much higher.

Figure 2-1 shows specific power and energy of the most popularly used energy storage devices, including lead acid batteries, Ni-MH batteries, Li-ion batteries and ultracapacitors. With the differences of battery chemistry, there are tradeoffs between energy density and power density. The specific energy and power of the batteries thus vary over a range, as illustrated by the shaded area shown in Figure 2-1, and data summarized in Table 2-7. The size of ESS on different types of vehicles is determined by the specific energy and power demands. In sections 2.2.3 - 2.2.5, three typical hybrid vehicles were analyzed. The ratio of their specific power and energy needs were calculated. Reference lines were drawn in Figure 2-1 to represent the ESS demand characteristics of these vehicles. For a HEV, the reference line for the ESS power/energy ratio appears between the specific power and specific energy regions of ultracapacitor and batteries. Therefore, for a HEV, the size constraint of a battery based ESS is the specific power while the size constraint of an ultracapacitor based ESS is the specific energy. An ideal match of both energy and power would be a combination of battery and ultracapacitor. For PHEV and EV, the ESS specific power/energy ratio lines appear in the battery regions, and the size constraint of ESS is the specific power of the batteries. Ultracapacitors with much lower specific energy are

normally not considered; however, it may still be beneficial to added ultracapacitors to the batteries to extend the operation life of the battery [13].

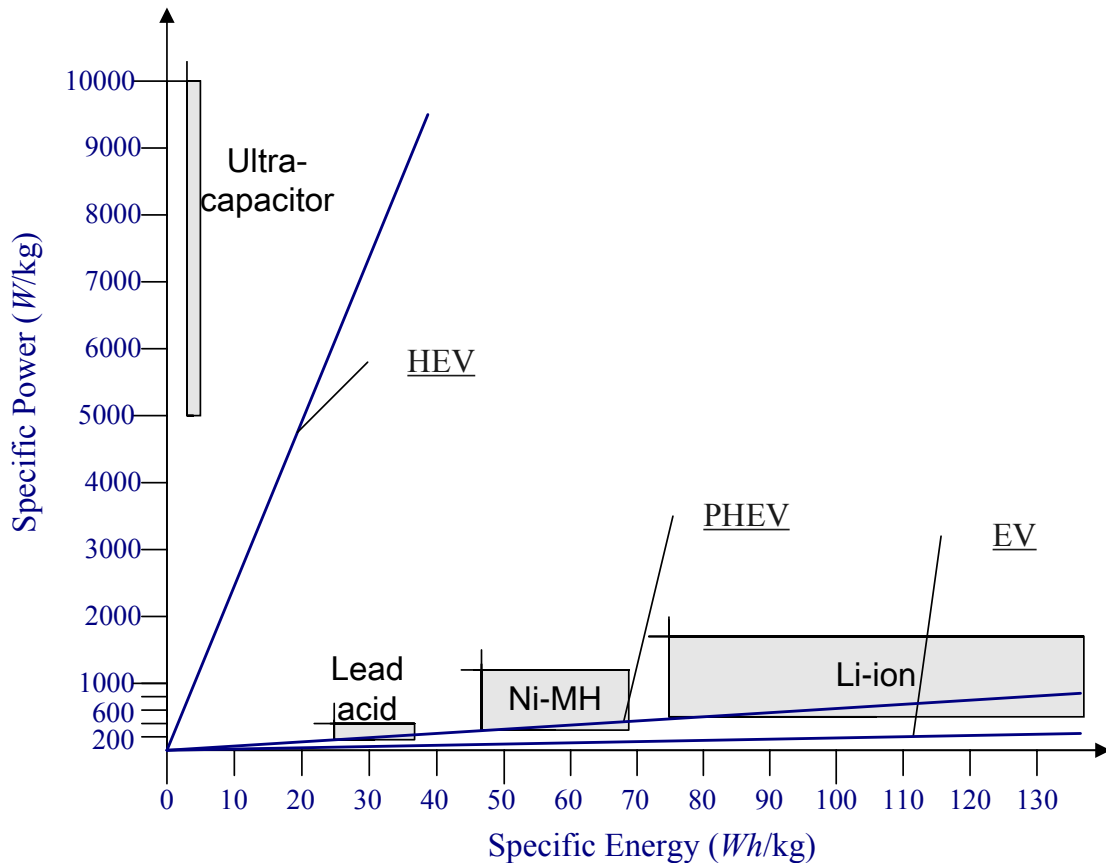


Figure 2-1 Power/Energy Ratio of Vehicle Demand and ESS Capability

2.2.3. ESS for a Electric Vehicle

The focus of an EV design tends to be the acceptable range with a single charge. Therefore, the ESS is sized to meet the designed range of the vehicle. For battery powered vehicles, the size of batteries is determined by its energy requirements (kWh/kg) as power requirements (kW/kg) can be easily satisfied for a reasonable vehicle acceleration performance need. The load cycles of batteries on an EV are usually deep discharging and charging. The shortened life of deeply discharged battery is a major consideration since the minimum battery life has to be satisfied. Battery charging time is another major consideration as this time is significantly longer than

refilling a gasoline tank. An alternative is to replace the discharged battery pack with a fully charged one at a battery station with a reasonable cost of service charge. However, certain challenges arise for battery replacement such as weight and volume, especially for the heavier and bulkier lead-acid batteries. Meanwhile, ultracapacitors are not likely to be employed in EV at present due to their characteristically low energy density.

In order to quantify the power and energy consumption on an EV, a performance characteristics benchmark is used, as given in Table 2-1. The fuel consumption of 100 MPG is accepted as a benchmark for passenger vehicles. The gasoline consumption is translated into battery energy using net calorific value (NCV).

Table 2-1 Characteristic of a Benchmark EV

| | |
|----------------------------------|-------------------------------------|
| Peak Power | 100 <i>kW</i> |
| Range | 300 <i>km</i> |
| Fuel Economy (Equivalent) | 0.024 <i>L/km</i> (100 <i>MPG</i>) |
| Discharge Depth | 70% |

The energy consumption (*kWh*) is calculated from fuel economy equivalent using the following equation.

$$E = \frac{300\text{km} \times 0.024\text{L} / \text{km} \times 0.73\text{kg} / \text{L} \times 42,900\text{kJ} / \text{kg}}{1\text{W} \times 3600\text{s} / \text{hr} \times 0.70} \approx 89\text{kWh} \quad (2.3)$$

As a result, an ideal energy/power ratio of 0.89 (89 *kWh*/100 *kW*) or lower (for longer ranged) is necessary for an EV. A reference line for the EV was drawn in Figure 2-1. It is shown that all types of batteries are able to satisfy this power demand with the requested energy capacity. The main criterion for sizing an EV is energy rather than power capability. For EV applications the objective should be to develop batteries with high energy density and acceptable power density. The weight and capability of batteries for EV are shown in Table 2-2. As battery power is mostly sufficient for vehicle power demand, ultracapacitors are unlikely needed to boost power.

Table 2-2 ESS Sizing for a Benchmark EV

| | Energy | Power | Weight | Volume |
|-----------|---------------|-------------------------|----------------|---------------|
| Lead acid | 89 <i>kWh</i> | 122 <i>kW</i> @ Ef. 95% | 2602 <i>kg</i> | High |
| Ni-MH | 89 <i>kWh</i> | 114 <i>kW</i> @ Ef. 90% | 1308 <i>kg</i> | Medium |
| Li-ion | 89 <i>kWh</i> | 108 <i>kW</i> @ Ef. 90% | 635 <i>kg</i> | Low |

2.2.4. ESS for a Hybrid Electric Vehicle

For a hybrid electric vehicle (HEV) using either an engine or fuel cells as the primary energy source, the ESS is sized differently depending on the degree of hybridization (DOH) and power management strategy of the vehicle. As the operation cycles of ESS on a HEV are significantly longer than on an EV, the life of ESS therefore will be a main concern. One approach to extend battery life is “shallow charging” which confines the battery operation at relatively narrow state-of-charge range (5%-10%). Reference [14] showed shallow cycle life can be greatly enhanced to satisfy consumer expectation on a HEV. Even though not used in commercialized vehicles yet, ultracapacitors have the potential to be used in a HEV due to its much longer life cycle that passes 500,000. Reference [15] reviewed ultracapacitor applications and provided guidelines for sizing ultracapacitors on HEV. Due to the vehicle dependent nature of ESS on HEV, it is difficult to standardize the generic power demand for a HEV. The ESS on a 2004 Toyota Prius[16] was set as reference while other ESS technologies were explored.

Table 2-3 Specs of Ni-MH on a 2004 Toyota Prius [16]

| Type | Module Volt. | Capacity | Cells | Power Specified |
|-------------|---------------------|-----------------|--------------|------------------------|
| Ni-MH | 7.2 <i>V</i> | 6 <i>Ah</i> | 168 | 21 <i>kW</i> @60% |

The energy capacity of Prius is 1209.6 *Wh*. According to the shallow charge operation condition on battery, the useable energy is 60 *Wh*-120*Wh*. The battery efficiency at 21 *kW* is 60%.

There is a distinct difference on cycle life between a battery and an ultracapacitor. Battery size is greatly influenced by the amount of power needed and its normal state of charging, related to battery cycle life. Ultracapacitor sizing, on the other hand, is only related to the usable energy.

Table 2-4 ESS Sizing for a HEV

| | Rated Energy (Wh) | Usable Energy (Wh) | Power | Weight |
|--------------------------------|--------------------------|---------------------------|--------------|---------------|
| Lead acid | 1419 Wh | 71 Wh-141 Wh | 21 kW | 54 kg |
| Ni-MH | 1209 Wh | 60 Wh-120 Wh | 21 kW | 27 kg |
| Li-ion | 1200 Wh | 60 Wh-120 Wh | 24 kW | 15 kg |
| Ultra-capacitor power-match | 13.35 Wh | 13.35 Wh | 24 kW | 3 kg |
| Ultra-capacitor capacity-match | 90 Wh | 90 Wh | 160 kW | 20 kg |

In this case, power demand can be easily satisfied. The result of the Prius example shown in Figure 2-1 used the same energy power ratio as that of the EV. Ideally, a combination of battery and ultracapacitor will reach a point at which both power and energy can be satisfied simultaneously. Table 2-5 shows a combination of batteries and ultracapacitors which reaches the same performance characteristics with much lower weight.

Table 2-5 UC-battery Hybrid ESS for Prius

| | Rated Energy (Wh) | Power | Weight |
|----------------|--------------------------|--------------|---------------|
| Ni-MH | 78.2 Wh | 1.9 kW | 1.7 kg |
| Ultracapacitor | 11 Wh | 19 kW | 2.4 kg |
| Total | 90 Wh | 21 kW | 4.1 kg |

2.2.5. ESS for a Plug-in Hybrid Electric Vehicle

The only difference of a PHEV from the HEV is its larger battery that allows energy to be charged from grid electricity. In addition to the power and energy demand of a HEV, additional ESS capacity requirement depends on its “all electric range” (AER). However, sizing the ESS for a PHEV is more complex for several reasons. First, in the AER, not only the energy but also the power is a concern, since the battery is the only source of power for most operations. Secondly, battery life is affected by the depths of charge and discharge. The depth of discharge on a PHEV is far more than that of a HEV with limited, shallow discharges. It is therefore more difficult to satisfy energy and power requirements with a reasonable life expectancy of the ESS. More detailed power and energy requirement on a parallel PHEV is discussed in [17].

To further explore the ESS characteristics of a PHEV, a hypothetical PHEV based on Prius is used. The AER power is confined at 30 kW which allows limited speed and acceleration.

Table 2-6 UC-battery Hybrid ESS for Prius

| | |
|----------------|---------|
| AER Power | 30 kW |
| Range | 20 km |
| Charging Depth | 70% |
| AER Efficiency | 100 MPG |

The energy demand can be expressed in the following equation where the energy/power ratio is 0.2 (6 kWh/30 kW).

$$E = \frac{20km \times 0.024L / km \times 0.73kg / L \times 42,900kJ / kg}{1W \times 3600s / hr \times 0.70} + 0.09kWh \approx 6kWh \quad (2.4)$$

The energy/power ratio was shown in Figure 2-1. As a result, batteries are more appropriate to be used as the energy storage unit. However, there exists a possibility of using ultracapacitors when vehicle speed and acceleration demand is higher. The AER peak power will be higher than 30 kW and this demands a lower energy/power ratio.

2.3. Advance of Energy Storage Technologies and Hydrogen Fuel Cells

In this section, the technical backgrounds and state of art on the developments of battery and ultracapacitor are briefly reviewed. At present three types of batteries are widely used, including lead acid (L-A), Ni-MH, and lithium-ion (Li-ion) batteries. Following the same order are their improved performance, energy density, and increased cost. For economic reasons, L-A batteries were used in earlier production electric vehicles. Ni-MH is gaining popularities on present HEV. Meanwhile, Li-ion battery applications are mostly limited at present to smaller electronics devices due to its superior power density where cost is not as much of a factor. Li-ion batteries, as a promising technology for vehicle applications in the future, start to see applications in high-end low speed vehicles. A study to optimize the cost and performance of batteries, considering three

different vehicles, three types of batteries, and three powertrains was carried by [12]. As an energy storage device, batteries have a number of drawbacks, including large size, limited power density, thermal impact, low efficiency, long charging time and relatively short life. A summary of battery characteristics for EV applications is shown in Table 2-7. The data was gathered from a number of sources [18-20].

2.3.1. Sealed Lead Acid Battery (SLA)

The sealed lead acid battery is the most common battery currently been used to power electric bicycles, mainly due to its low cost per watt-hour. The SLA battery is also very robust and durable when used properly. The self-discharge rate of the SLA battery is also low, only losing ~5% of its charge per month if not used. The SLA battery does not have a memory effect like the NiCad battery. Problems with the SLA battery include low power and energy densities, and potential environmental impact, where the lead electrodes and electrolyte can cause environmental harm if not disposed properly at a recycling facility.

2.3.2. Nickel Metal Hydride Battery (Ni-MH)

The Ni-MH battery is the most widely used battery to power electric automobiles at present. The Ni-MH battery has a higher energy density than a SLA battery. Its specific energy (Wh/kg) can be up to four times that of a SLA battery; and 40% higher than Ni-Cad battery. The battery is also relatively environmentally friendly, as it contains very mild toxic materials that can be easily recycled. The main problem with the Ni-MH battery pack is its higher cost than a SLA battery pack. It also takes longer time to charge a Ni-MH than a SLA or NiCad battery and generates a large amount of heat during charging. It is also more difficult to determine when the Ni-MH battery is fully charged than with a SLA or NiCad battery, resulting in the need for more complicated and expensive chargers.

The recent effort of improving Ni-MH for HEV applications has been focused on reducing the

resistance and increasing the power capability. The trade-off will likely be a lower energy density than those used on an EV [14].

2.3.3. Lithium Ion Battery (Li-ion)

Many automotive companies are in the process of developing advanced Li-ion battery technologies for vehicle related applications. Much interest is focused on high power batteries for HEV and high energy batteries for EV. For example, a lithium-ion battery for EV will have a specific energy up to 150 *Wh/kg* and that of a Ni-MH battery will be 70 *Wh/kg*. The major concern of using Li-ion battery on a hybrid vehicle is the over-heating problem during recharging [21].

Table 2-7 Battery Performance Characterizes for HEV and EV

| Battery Technology | App. Type | Capacity Ah | Voltage (V) | Spec. Energy Wh/kg | Resis. Ohm | Spec. Pwr W/kg | Useable SOC |
|-----------------------------|------------------|--------------------|---------------------|---------------------------|-------------------|-----------------------|--------------------|
| <u>Lead-acid</u> | | | | | | | |
| Panasonic | HEV | 25 | 12 | 26.3 | 7.8 | 389 | 28% |
| Panasonic | EV | 60 | 12 | 34.2 | 6.9 | 250 | |
| <u>Nickel Metal Hydride</u> | | | | | | | |
| Panasonic | HEV | 6.5 | 7.2 | 46 | 11.4 | 1093 | 40% |
| | EV | 65 | 12 | 68 | 8.7 | 240 | |
| Ovonic | HEV | 12 | 12 | 45 | 10 | 1000 | 30% |
| | EV | 85 | 13 | 68 | 10 | 200 | |
| Saft | HEV | 14 | 1.2 | 47 | 1.1 | 900 | 30% |
| <u>Lithium-ion</u> | | | | | | | |
| Saft | HEV | 12 | 4 | 77 | 7.0 | 1550 | 20% |
| | EV | 41 | 4 | 140 | 8.0 | 476 | |
| Shun-Kobe | HEV | 4 | 4 | 56 | 3.4 | 3920 | 18% |
| | EV | 90 | 4 | 105 | 0.93 | 1344 | |
| <u>Ultracapacitor</u> | | | | | | | |
| | V rated | C (F) | Resis. (Ohm) | | | | |
| Maxwell | 2.7 | 2800 | 0.48 | | | | |

2.3.4. Ultracapacitors

Ultracapacitors are electrochemical capacitors. Energy is stored in the double layer formed at a solid/electrolyte interface [22]. Advances in new materials and new ultracapacitor designs have considerably improved the energy storage capability and cost of this emerging electrical energy storage device. Compared with the conventional capacitors, ultracapacitors allow for more energy storage for a factor of 20 times [23]. Other unique characteristics of ultracapacitors include maintenance-free operation, longer operation cycle life, and insensitivity to environment temperature variation. The energy density of ultracapacitors is still limited compared with batteries. The goal for ultracapacitor development is a specific energy of 5 Wh/kg for high power discharge [24]. Carbon-carbon ultracapacitor devices are commercially available from several companies, including Maxwell, Ness, and EPCOS. The capacitance of their products ranges from 1000-5000 F.

An experimental test was carried out on a series hybrid Ford Escort with and without ultracapacitors as load-levelling devices for the batteries [25]. Simulations of a series hybrid bus on the same test were also carried out on PSAT using data validated from the tests. Both experimental and simulation results suggest significant reduction to the RMS and peak battery currents.

A method for determining the size of batteries and ultracapacitors on a fuel cell powered SUV was presented in [26]. The peak-to-average ratio was introduced as the sizing criteria. An optimization tool in ADVISOR is used to obtain the results. Cost analysis was also carried out. Life cycle was not considered in the study.

2.3.5. Hydrogen Fuel Cells

A fuel cell system is an electric power-generating device based on controlled electrochemical reaction of hydrogen fuel and oxidant air [6]. In principle, fuel cells are more efficient in energy conversion and much cleaner than ICE. Due to many attractive features, such as low operation temperature, compact structure, less corrosion concern and quick start time, the Proton Exchange

Membrane (PEM) fuel cells serve as an ideal power plant for automotive applications. Dozens of fuel cells are bundled together to form a modular power unit, the fuel cells stack. To satisfy the need of power on a vehicle, multiple fuel cells stacks are connected in series. Together with various ancillary devices, fuel cells stacks form a fuel cell power system. Over the last decades, extensive efforts have been devoted to improve the performance of fuel cell system and to lower its costs. There is also an interest in using fuel cells to build uninterrupted power systems (UPS). Since a fuel cell system is a capable energy conversion device, rather than an energy storage device as battery and ultracapacitor, it can continuously provide electric power as long as the hydrogen fuel is provided, either in the form of pure hydrogen, or reformed natural gas. This unique capability, plus its quiet operation, zero emission and high efficiency, makes it a promising alternative to the ICE.

One weakness of a fuel cell system is its slow dynamic response to power demand. According to an experiment[27], at the initial start-up, it takes 90 seconds for the fuel cells to reach a steady state; thereafter whenever there is a change of electric power demand, it take 60 seconds for the fuel cells to readjust and reach a new steady state. A fuel cells power system alone is not capable of dealing with the rapid power demand change to serve as the sore power plant in the UPS system. At present, most research applying PEM fuel cells to electric backup power systems are limited to smaller, mobile UPS systems for computers and communication equipments with built-in battery units to fill the need of dynamic power demands. Several other barriers exist to the widespread use of fuel cells as the electric power plant for an electric vehicle or backup power system. The most obvious one among them is cost. As with any new technology, fuel cells are expensive to develop and manufacture. The magnitude of the cost problem for vehicles and backup power systems is exacerbated by the low cost of the incumbent ICE and battery technologies. In order to improve the viability of fuel cells as an alternative power plant, some method of either reducing their cost or the cost of the total backup power system over life time is required.

CHAPTER 3 Review on Vehicle Simulation Tools

3.1. Vehicle Simulation Tools

Simulation based analysis on vehicle performance is crucial to the development of hybrid powertrain since design validation using costly prototype is impractical. Due to the inconvenience of the many separated modeling methods, integrated modeling tools are required to speed up the modeling process and to improve the accuracy. Vehicle simulation is a method for fast and systematic investigations of different design options (fuel choice, battery, transmission, fuel cell, fuel reformer, etc.) in vehicle design and development. At present, several simulation tools based on different modeling platforms are available, although none of them is sufficient to model all design options. These tools always focus on a specific application with focused concerns. After years of continuing improvements, a fast, accurate and flexible simulation tool is still under development. Among the most widely used vehicle modeling and analysis platforms are MatLab/Simulink and Modelica/Dymola. In this section, two vehicle simulation packages, ADVISOR and Dymola, were discussed. ADVISOR was used extensively in this thesis to model two typical vehicles. Dymola, a newer and more flexible modeling tool, was used at the later stage of the study to overcome the limitation of ADVISOR.

3.2. ADvanced VehIcle SimulatOR (ADVISOR)

3.2.1. ADVISOR Background

ADvanced VehIcle SimulatOR (ADVISOR) was developed by the National Renewable Energy Laboratory of US in late 1990s. It was first developed to support US Department of Energy in the hybrid propulsion research. The model was set up in a backward modeling approach, although it was labelled as both forward and backward in the official documents. ADVISOR is

widely used by auto manufacturers and university and institute researchers worldwide. Many users contributed new components and data to the ADVISOR library. With a friendly user interface, ADVISOR was created in MatLab/Simulink[®] which is a software module in MatLab for modeling, simulating and analyzing dynamic systems. It supports both linear and nonlinear systems, modeled in continuous time, sampled time, or a hybrid of the two. Systems can also be MultiMate, e.g. having different parts that are sampled or updated at different rates.

3.2.2. ADVISOR Modeling Approaches

ADVISOR employs both backward and forward modeling approaches [28]. A backward approach starts from a given driving cycle at the wheels, and traces back the needed power flow through the powertrain model to find how much each involved component has to perform. A control flow chart of a backward model is shown in Figure 3-1. No driver behaviour model is required in such a model. Instead, the power required at the wheels of the vehicle through the time step is calculated directly from the required speed trace (drive cycles). The required power is then translated into torque and speed that go up stream to find the power required at the power source, an ICE, for instance. Component by component, this power flow is calculated backward through the drivetrain, considering losses. At the end, the use of fuel or electric energy is computed for the given speed trace or drive cycle.

Vehicle simulations that use a forward-facing approach include a driver model and a similar powertrain model. A driver model compares the required speed and the present speed to decide appropriate throttle and braking commands (using a PI controller). The throttle command is then translated into a torque demand at the power source (engine or motors). While the brake commands will be translated to friction torque at the wheels. The torque provided by the power source goes through the whole drivetrain to the wheels. Vehicle speed will be calculated and sends back to driver model as the present speed.

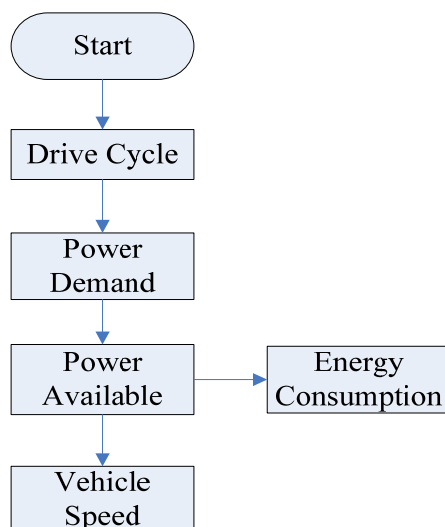


Figure 3-1 Flow Chart of an Backward Modeling Approach

Figure 3-2 shows the Simulink diagram of a two-mode hybrid vehicle model. The simplified function of this diagram is explained using the flow chart shown in Figure 3-1, as a so-called backward computer model.

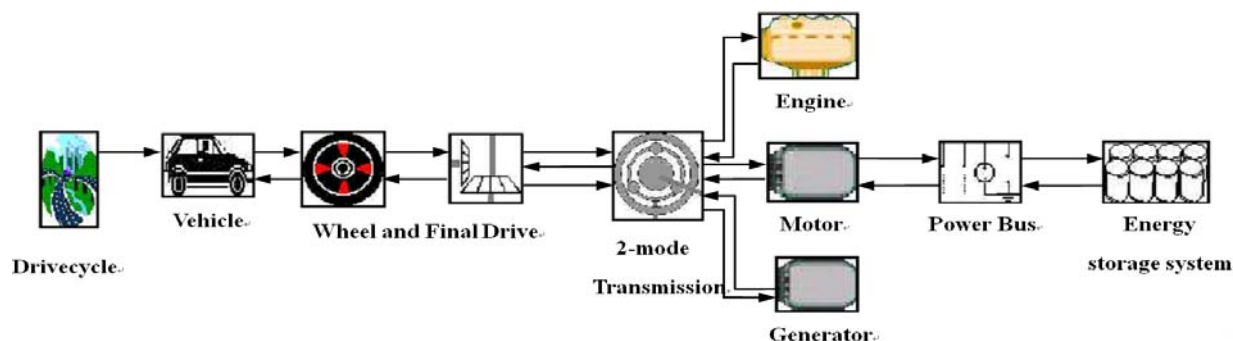


Figure 3-2 ADVISOR/Simulink Block Diagram of a Two-mode Truck

3.2.3. ADVISOR Interface

ADVISOR provides easy access and quick results to a trained user in vehicles modeling through a GUI interface. Three windows would guide users from the initial setting up toward the final results. The first window is used to enter data related to the vehicle initial setup. The second window provides several simulation options one can select from. The last window shows

selected simulation results.

In the ADVISOR vehicle input window Figure 3-3, the vehicle drivetrain configurations (e.g. series, parallel, conventional, etc.) is specified as well as the other key drivetrain components[29]. Characteristic performance maps for various drivetrain components are accessible using the associated menus. The size of a component (*i.e.* peak power capability and number of modules) can be modified by editing the characteristic values displayed in the boxes. Due to its straightforward backward approach, ADVISOR is 2.5 to 8 time faster than forward looking approach[30]. Any scalar parameter can be modified using the edit variable menu in the lower right portion of the window. All vehicle configuration parameters can be saved for future use. After these vehicle input characteristics are specified, the next GUI interface is the simulation setup window.

In the ADVISOR simulation setup window as shown in Figure 3-4, a user defines the event over which the vehicle is to be simulated. Some of the events are driving cycle, acceleration test and other special test procedures. For example, when a single driving cycle is selected, the speed trace can be viewed in the upper left portion of the window and a statistical analysis of the cycle on the lower left portion. With simulation parameters configured, simulation can be run and results will be presented upon completion.

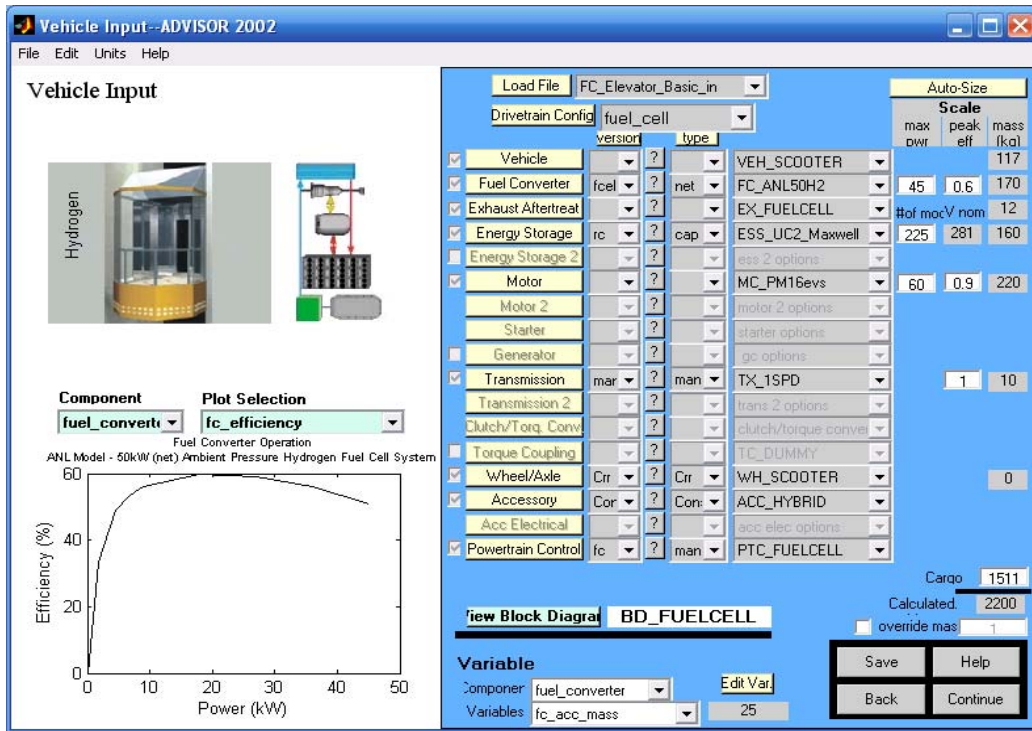


Figure 3-3 ADVISOR Vehicle Input Interface

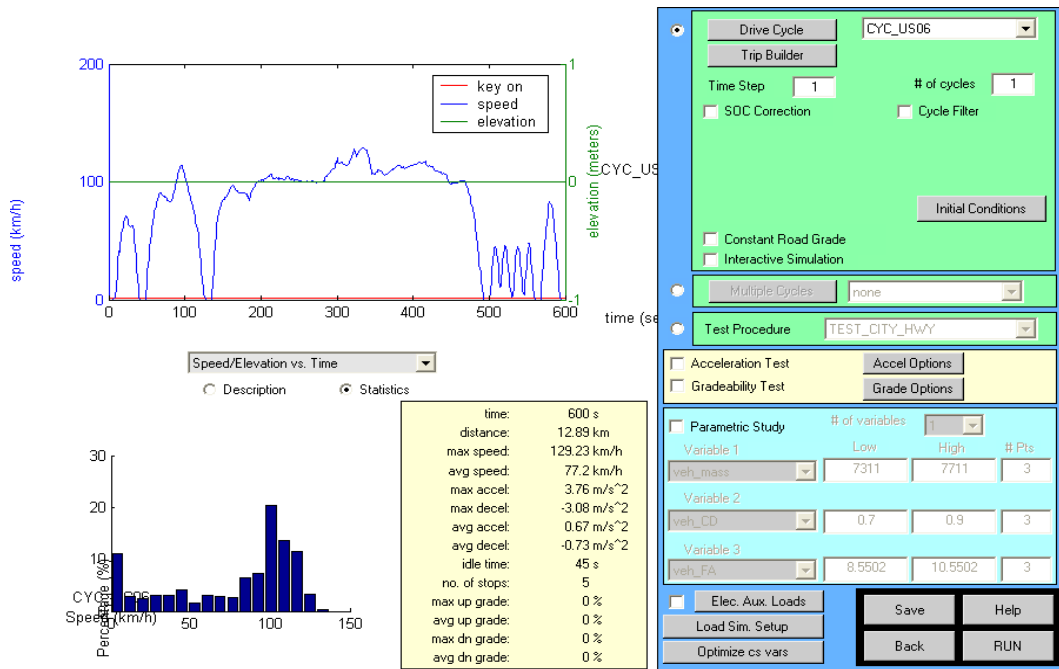


Figure 3-4 Simulation Setup Interface

The ADVISOR results window, shown in Figure 3-5, displays the review of vehicle performance,

both integrated over a cycle and instantaneously at any point in the cycle. The results include vehicle performance, both integrated over a cycle and instantaneously at any point in the cycle, fuel economy, and emissions. Detailed time-dependent results can be plotted with options on different level of details (e.g. engine speed, engine torque, battery voltage, etc.)[31]. On the right portion of the window, summary results such as fuel economy and emissions are given. On the left, the detailed time-dependent results are plotted. These results can be dynamically changed to show other details (e.g. engine speed, engine torque, battery voltage, etc.) using the menus on the upper right portion of the window [28].

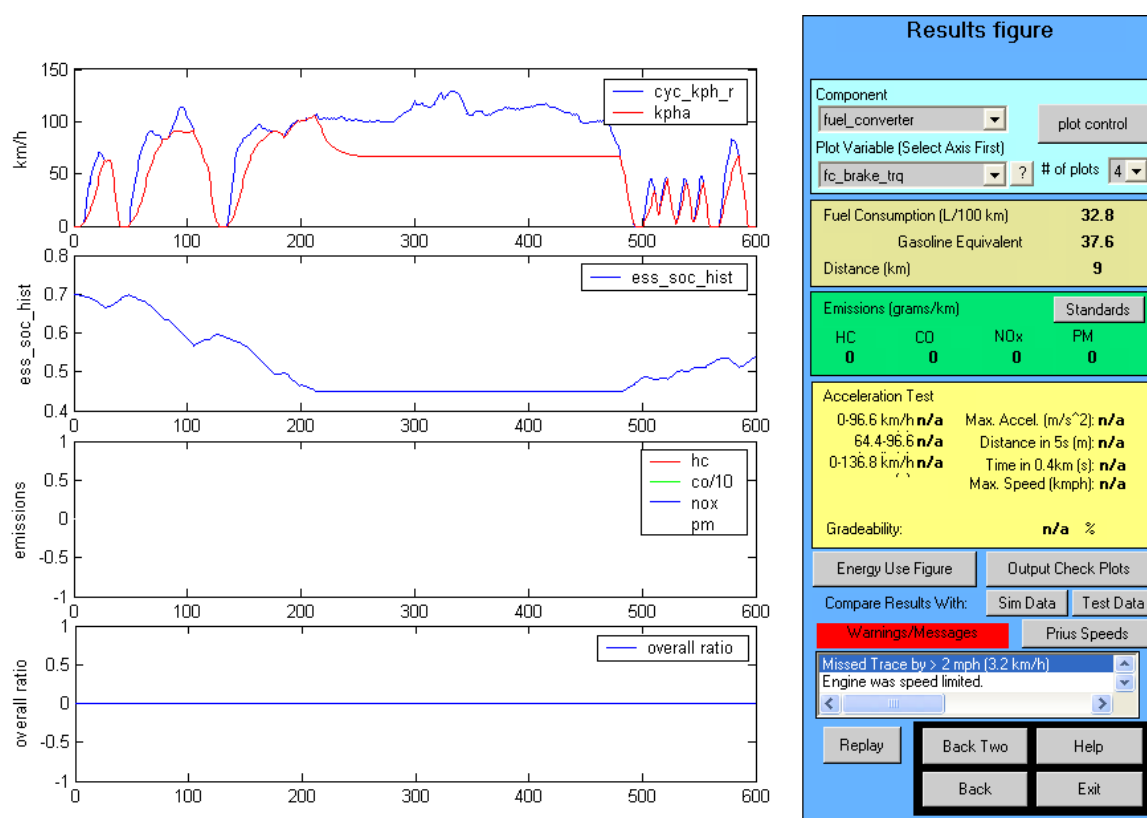


Figure 3-5 Simulation Result Window

3.2.4. Models in ADVISOR

Internal Combustion Engines and PEM Fuel Cells Models

A fuel converter is used in ADVISOR to convert indirect energy from fuel into direct energy such as electricity or kinetic energy to power the vehicle. The fuel converter for a motorized vehicle will be an ICE or fuel cells.

There are two categories of empirical, steady-state fuel cells models in ADVISOR. One simulates the performance of fuel cell system by mapping the system efficiency as a function of net power output. The other represents fuel cells performance based on a given polarization curve. Both models exclude thermal considerations and water management. Reformer and gas compressor are not included. The ICE model in ADVISOR is explained in CHAPTER 5.

Energy Storage Model

There are several energy storage devices as build-in component models in ADVISOR library, including lead acid batteries, nickel metal hydride batteries, Li-ion batteries and ultracapacitors.

Electric Motor and Motor Controller Models

Several commonly used electric motors are preloaded in ADVISOR including induction motors, permanent magnet brushless DC motors, and switched reluctance motors. In terms of motor modeling for a vehicular drivetrain, two different approaches are used. One is the theoretical model based on physical principles. For a given motor geometry, material parameters and power electronics, the torque and speed of the motor are calculated. For example, the motor model for a brushless DC motor will be fundamentally different from the model of an induction motor. The other modeling approach is more empirical data-driven, simply based on the static map of the drivetrain efficiency as a function of motor torque, speed and voltage, as used at NREL. The empirical input data are obtained using a motor test stand. The latter cannot explain how the

motor functions, but present more accurate motor performance behaviours and require much less computation, serving the system design task better. In this work, the latter approach was used.

3.3. Modelica and Dymola

3.3.1. Modelica

Modelica is a relatively new programming language, introduced in Europe to model a broad scope of physical systems. The language is object-oriented, non-causal and the models are mathematically described by differential algebraic equations (DAE). The language suits modeling of large and complex systems and supports a development of libraries and exchange of models. With Modelica it is possible to model both at high levels by composition (use icons that represent models of the components, connect them with connectors and set parameter values in dialogue boxes) and at a much more detailed level by introducing new library component that describe the physical behaviours of the modeled element using DAE. The development of Modelica started in 1996 by a small group of people who had experience of modeling languages and DAE models. A year later the first version of Modelica was released, but the first language definition came in December 1998. Modelica version 2.0 was released in December 2000 and was developed by the non-profit organization Modelica Association in Linköpings, Sweden.

3.3.2. Dymola

Dymola is developed by Dynasim in Lund, Sweden, and the name is an abbreviation for Dynamic Modeling Laboratory. The tool is designed to generate efficient code and it can handle variable structure Modelica models. It finds the different operating modes automatically and a user does not have to model each mode of operation separately. Dymola is based upon the use of Modelica models, which are saved as files. The tool contains a symbolic translator for the Modelica equations and a compiler that generates C-codes for simulation. When needed, the codes can also be exported to MatLab Simulink. The main features of Dymola are

experimentation, plotting and animation.

Dymola has two different modes, modeling and simulation. In the modeling mode the models and model components are created by “drag and drop” from the Modelica libraries and equations and declarations are edited with the built-in text editor. The simulation mode makes it possible to do experiments on the model, plot results and animate the model behaviours. In order to simulate the model, Dymola uses Dymosim, Dynamic Model Simulator. It is an executable, which is generated by Dymola and used to perform simulations and compute initial values. Dymosim also contains the codes that are required for continuous simulation and handling of events. Model descriptions are transformed into state space descriptions by Dymola and solved by the integrators in Dymosim. The result of the simulation can in turn be plotted or animated by Dymoview. Dymosim can be used in other environments too, though it is especially suited in combination with Dymola.

3.3.3. Vehicle Modeling and Simulation Libraries

To facilitate vehicle related simulations, several vehicle modeling and simulation packages were developed with different focuses in Dymola. Powertrain library developed at Germany has a complete mechanical powertrain to carry out speed and torque simulation. Smart electric drive by Arsenal in Austria is a library with electric components. Modelon developed a dynamic package dealing with kinetic movement such as vehicle stability. Descriptions on some of the other libraries are listed in Table 3-1.

Table 3-1 Vehicle Modeling Packages in Modelica

| Library name | Developer | Description | Availability |
|----------------------|-----------------------------------|---|--------------------------------|
| Powertrain | German Aerospace Center (DLR)[32] | A commercial library to model vehicle power trains as well as various planetary gearboxes with speed and torque dependent losses | Through Dymola, Others unknown |
| Smart Electric Drive | Arsenal Research/Austria [33] | A commercial library to model hybrid electric vehicles and new alternative concepts with electrical auxiliaries (from Arsenal research) | |
| Alternative Vehicles | German Aerospace Center [32] | Simulations on hybrid or fuel cells vehicles [34], Little details is available | Under Development |
| Transmission | Ricardo/UK[35][35] [35] | | Dymola |
| Vehicle Dynamics | Modelon AB | A Commercial library to model hybrid electric vehicles and new alternative concepts with electrical auxiliaries | From Dymola or SimualtionX |
| Fuel cells | Open | A Free library to model fuel cells | Free |
| Vehicle Interface | Collaborated work | Promoted compatibility among different automotive libraries | Free |

CHAPTER 4 Modeling of a Fuel Cells Hybrid Power System for Elevator Power Backup Using ADVISOR

4.1. Modeling High Speed Elevators as Electric Vehicles

An elevator is a vertically travelling vehicle designed and used to transport people and goods from given to targeted locations, following unique driving patterns. High speed elevators are commonly used in various high-rise buildings today. An elevator resembles to an electric vehicle in many ways, both in terms of their power source and functionality. The relatively maturing technology for modeling and simulating the operations of pure electric and/or fuel cell - battery hybrid electric vehicles can be used to better understand the operation of the less well studied high-speed elevators. However, there are also differences between these two types of “vehicles”. Different from a regular vehicle, an elevator overcomes gravity of both the passenger compartment and the passengers. The power sources of an elevator, including the source of electric power and motor are attached to the building, rather than carried in the vehicle, and the torque from electric motor is transported to the elevator car by cables and gear boxes.

In this work, these unique characteristics of elevators are modeled using a special “vehicle” drivetrain model by modifying the conventional vehicle drivetrain model according to the stated differences. The drivetrain model of an elevator powered by a hydrogen fuel cell backup power system is introduced by modifying existing fuel cells vehicle powertrain model in ADVISOR 2002, as shown in Figure 4-4. Four different powertrain architectures of the elevator backup power system were studied, including a fuel cells only system (FC), fuel cells-battery hybrid (FC-BA), fuel cells-ultracapacitor hybrid (FC-UC) and fuel cells-battery-ultracapacitor hybrid

(FC-BA-UC). Due to the similarity of these models, only the FC-BA-UC hybrid is explained in this section. The objective of this work is to utilize the existing fuel cell vehicle modeling and simulation tool to help the design and optimization the fuel cell backup power system, targeted to specific elevator type and specific needed operation patterns.

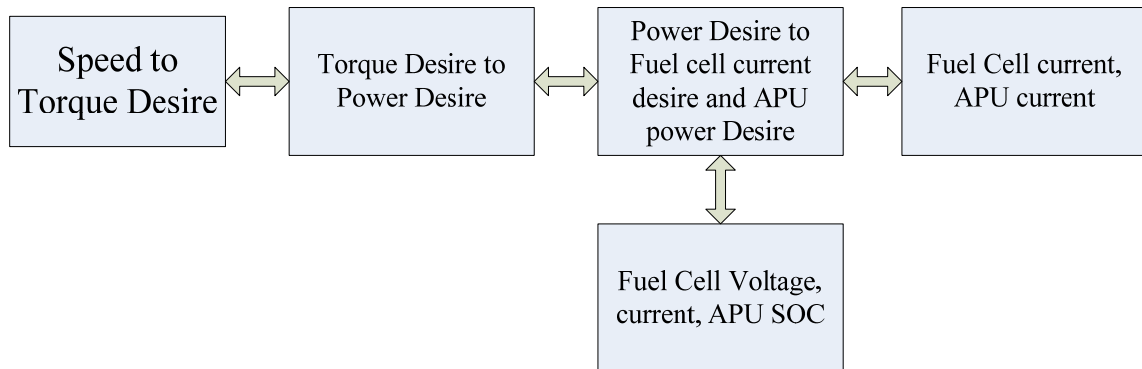


Figure 4-1 Elevator Powertrain Model

4.2. Power Failures of Elevators in High-rise Buildings

Serving as a vertically moving platform for transporting people or freight, elevators have been proved to be a great convenience and necessity for both industrial and residential applications. Since its invention by Erhard Weigel in 1670 as a flying chair for people [36], elevators were used widely in multi-storey, high-rise residential buildings and multi-level industrial structure to meet the thirty of industry in productivity.

With limited available space in the city and increasing land cost, multi-storey and high-rise buildings now dominate most urban areas of the world. The irresistible trend to build taller and taller buildings to leverage the increasing land cost turns elevator from a tool of convenience to a necessity of life. The dependence of elevator in multi-storey and high-rise buildings further requires its continuous function in spite of power failure caused by many reasons. A no operational elevator during power failure may lead to catastrophic consequences, such as the 911 tragedy. Reliable and effective elevator power backup system is an urgent need today.

The possibilities of power failures are many, including temporary power shutdown, unexpected failures of the power grid, fire accident in the building or neighbourhood, or even a terrorist attack. Traditionally, an elevator completely depends on commercial power grid. Any power failure will result in the besiegement of passengers in the elevator. This problem is extremely serious for high-rise buildings, and buildings with health-related or other crucial functions, such as hospitals and senior homes. To manually descend the elevator to the nearest floor and release the trapped passengers are normally done by maintenance personals with substantial delay. In the case of natural disaster or terrorist attack, the help will be too little and too late. It is also infeasible for people to retreat by walking down the stairs in a high-rise building that is hundreds of meters above the ground, and for fire and rescue crews to reach the troubled floor using the shared stairs at the same time. The 911 tragedy at the World Trade Center taught us an important lesson.

4.3. Backup Power Solutions

Elevator load cycles are characterized by a poor power balance between ascending and descending. A high power demand arises during acceleration in the upward movement, while high power restitution appears during stopping in downward movement [37], resulting a low average and high pulse power requirements. The power density of present batteries is so low that they cannot provide the peak power. While ultracapacitors with a higher power density can meet the power demand, they cannot last long enough due to the limited energy density. A fuel cell system is able to provide high power demand continuously as long as the fuel gas is provided. However, the slow dynamic response of fuel cell system prohibits it to work alone. In addition, the investment cost of fuel cells remains high and the size of the fuel cell system must be reduced. Electric power backup systems for multi-storey and high-rise buildings are emerging, although the technologies that serve this crucial function seem to be still crude at present. These technologies include energy conversion devices, such as ICE, and energy storage devices, such as

battery, ultracapacitor and flywheels.

4.3.1. Batteries for Power Backup

Traditionally, batteries have been most widely used in electric backup power systems on computers, protecting the potential loss of important data during abrupt power failure. An Uninterrupted Power System (UPS) has a fast response and provide high quality power backup over a short period to allow the proper shut down of the computer. Due to the limited capacity demand, high quality and maintenance free batteries such as nickel metal hydride can be used. Battery backup power is also in place for some multi-storey and high-rise buildings. To reduce the investment costs and to achieve the large energy capacity required, low cost lead-acid battery banks are used. However, the limited current density of batteries means that their maximum power discharging rate is fairly limited. Study on battery-based and battery-assisted elevator power supply indicates that the operation of an elevator can be continued by reducing the speed of travel when the power demand exceeds the battery current limit [38]. Compared with the conventional emergency landing device that just lands the elevator onto the nearest floor, battery backup power system provides much better service during power failure. Even though the battery-based elevator power supply is a great improvement, the much reduced speed is unacceptable for high-rise buildings. Meeting the current density of super high speed elevators will require high energy density as well a high current density. In addition, these lead-acid battery banks require constant maintenance and care, and have a limited life.

4.3.2. Ultracapacitors for Power Backup

Capacitors have only been used as short time power keeper in electronic devices during battery replacement. Applying ultracapacitors as the only ESS or together with battery on vehicles has attracted considerable attentions in literatures. A power-based computer model of an ultracapacitor hybrid pickup truck has developed in [39]. It employs a backward modeling

approach[28] to predict fuel economy on a series hybrid truck based on Ford Explorer. The result shows 18% fuel economy improvement over non-hybrid counterpart on an UDDS drive cycle. The nature of ultracapacitor with high density discharge and charge has potential to manage power with large peak to average ratio. The limited energy density according to Table 2-7 prevents the use of ultracapacitor to provide continuous power.

4.3.3. ICE Generator for Power Backup

ICE, either diesel or gasoline engines, have been widely used to provide backup power to large businesses and hospitals. As a low-cost electric backup power supporting tool, the technology and products have reached their maturity. However, the system has a number of inherent drawbacks, including slow response, extensive maintenance needed and the unavoidable noise and pollution. These factors make it a less desirable for multi-storey and high-rise buildings.

4.4. A Fuel Cells Hybrid Power Backup Solution

4.4.1. A Hybrid Energy Storage System

Meeting the load variations is a significant challenge for current technology. To minimize cost and maximize performance, an integrated elevator backup power system, consisting of PEM fuel cells, ultracapacitors and batteries, is proposed. A fuel cells – ultracapacitor – battery hybrid forms an ideal architecture for the elevator backup power system. As an efficient and clean power conversion device and the only one among the three, a PEM fuel cell system is chosen to continuously supply electric power. The ultracapacitor module is the second most important component of the system, due to its high power density, extremely long life, excellent charge and discharge efficiency, and its unique capability for providing large transient power instantly to deal with the load surge of the elevator during upward acceleration. A battery bank is also used to supply auxiliary power due to its better energy density and much lower cost. DC-DC converters and power electronics integrate these three key components.

The intention of combining ultracapacitor and batteries to form a hybrid energy storage device on vehicles dates back to a decade ago [40]. Energy density and cost of ultracapacitors has been an obstacle preventing further developments leading to its commercial application [41]. The improved energy density and overwhelming development of HEV shows hybrid ultracapacitor/battery energy storage device very promising in recent future [14].

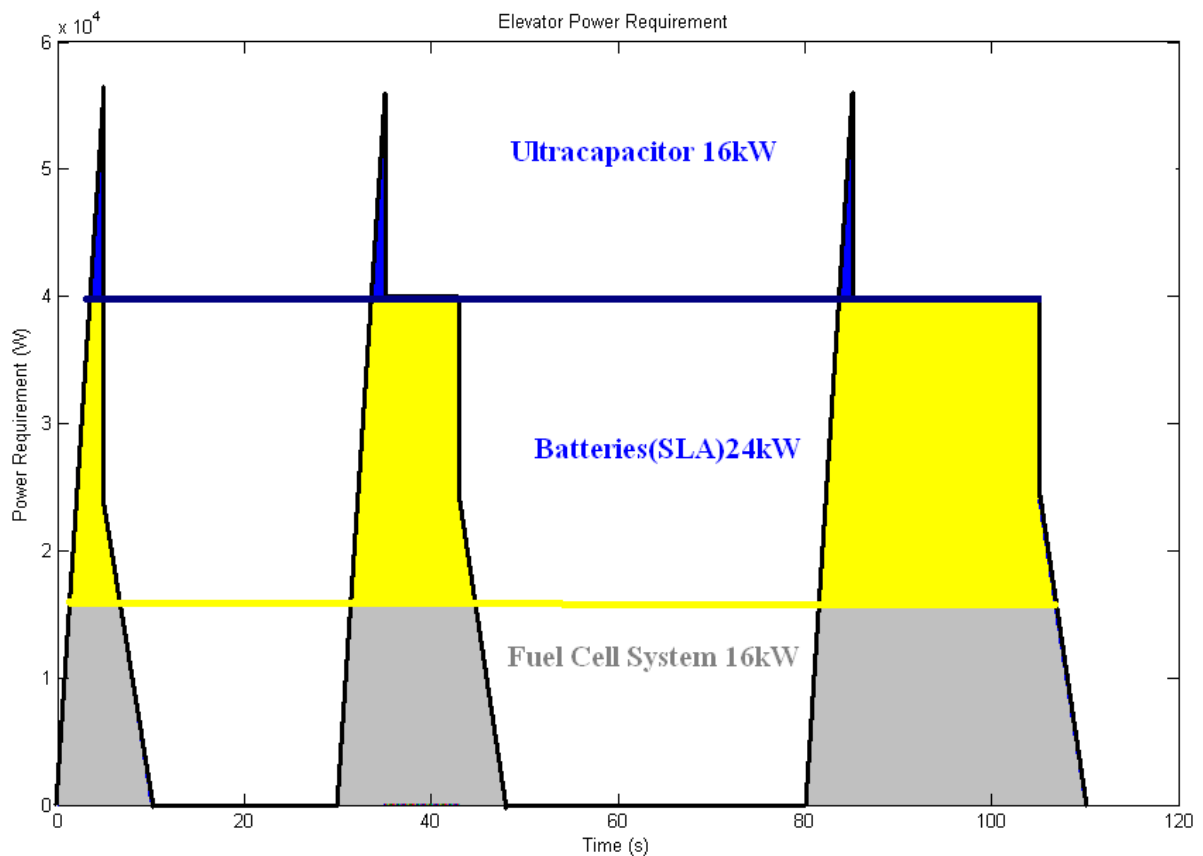


Figure 4-2 a Fuel cells Super Hybrid Power System

Figure 4-2 shows the power contribution of an idealized fuel cells, battery and ultracapacitor hybrid (also called fuel cells super hybrid). Fuel cells operate in a continuous manner to provide the average power flow. Battery, which has a higher energy density, manages the power at medium range. Ultracapacitors would be responsible for providing high but transient power demand.

4.4.2. Operation of Battery Ultracapacitor Hybrid

Most early study tries to connect ultracapacitors to batteries through direct parallel connection [42, 43]. Some other study shows that improved performance would be achieved by using power converters to actively control the power sources [44, 45]. The type of batteries used to achieve the hybrid is also case dependent, depending power and physical requirements. [46] uses a lead-acid batteries and ultracapacitors as hybrid, while [43] studied a hybrid system using Ni-MH and ultracapacitors.

When power supply is normal, the batteries and ultracapacitors are charged by the power grid and fuel cells are ready to work. When power failure is detected, the ultracapacitor module with fast dynamic response immediately supplies electric power to the elevator motor. The fuel cell system will start to work while it takes a couple minutes to adjust fuel flow before reaching the steady state[38]. The batteries charge ultracapacitors as well as supplying power to the elevator motor. The power flow is controlled by a DC-DC converter and power electronics that also consume a small amount of energy. Recently some research efforts have been devoted to more effective and efficient power electronics and converters for ultracapacitor applications [38, 47-49]. At steady state, fuel cells generators supplies the average power whereas the ultracapacitors and batteries serve as power buffers to satisfy the surge power need and to recover brake power of the elevator.

4.5. Modeling of High-rise Building Elevator

In this study, an elevator model is created to simulate power demand for the fuel cells hybrid backup power system. The modeling and simulation will provide guidelines for selecting energy storage and conversion devices and for determining the key parameters of the backup power system. Based on its resemblance to an electric vehicle traveling vertically, the elevator model is built on ADVISOR platform which was introduced previously.

4.5.1. Elevator Model

The prototype elevator considered in this study is a gearless traction elevator. The design essentials are referenced from [50]. The detailed design parameters are listed in Table 4-1.

Figure 4-3 shows the schematic structure of the elevator, featuring single wrap ratio of 1:1. The elevator car is pulled by a motor located at the top of the building. A counterweight is placed beside the elevator to offset the average weight of the elevator car and its passengers. The Elevator ascends and descends vertically. It overcomes the gravity difference between the elevator and its cargo, and the balance weight. The rolling resistance on the pulleys is relatively small. Both the elevator and counterweight have to overcome air drag.

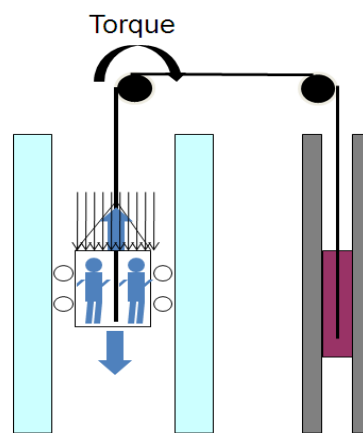


Figure 4-3 Physical Model of an Elevator

The kinematics of an elevator includes velocity, acceleration and jerk. Modeling and reduction of jerk is largely related to passengers' comfort [51]. The study, like many others, was geared toward the understanding on the kinematics and dynamics of the elevator's mechanical system, not on the elevator's electric drive which is the major concern for the modeling and design of the elevator electrical backup power system.

4.5.2. Powertrain Model

Most commonly known as an electric vehicle simulator [28], ADVISOR provides great flexibility

in introducing new architectures for the vehicle drivetrain.

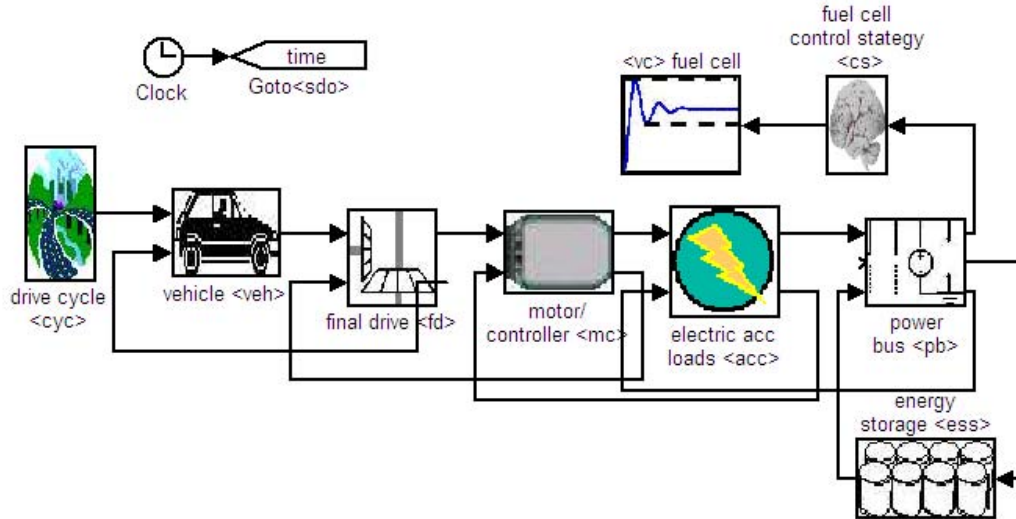


Figure 4-4 Modeling a Fuel Cell Hybrid Vehicle/Elevator in ADVISOR

Figure 4-1 is an explanation of how an elevator powertrain was modeled in ADVISOR. The simulation starts from a predefined driving cycle (see section 4.7.1). The vehicle model receives the speed demand from the driving cycle and interprets it as a power demand (torque and speed) using kinetic relations from the elevator dynamic model in 4.5.1. The torque and speed demand then go to the final drive block in which direct torque and speed for electric motor is calculated. Motor block receives the power demand from final drive and decides how much power to deliver. Four independent forces were considered, forces for ascending, acceleration, overcoming aerodynamic drag, and overcoming rolling resistance between the rope and pulleys. In addition, change of travelling speed would introduce an additional torque to overcome the momentum of the pulleys. The power demand for the motion of an elevator car is thus expressed in Eq. (2.5):

$$\begin{aligned}
 P_{wheel} &= \sum Force \times v = (F_{acceleration} + F_{ascend} + F_{rr} + F_{drag}) \times v \\
 &= (ma + mg \sin A + mgC_{rr} \cos A + \frac{1}{2} \rho_{air} C_D A_F v_{aero}^2) \times v
 \end{aligned}
 \tag{2.5}$$

where m is the total mass of vehicle, a is the vehicle acceleration, v is the vehicle velocity, A is the

angle of slope (90° for a elevator), C_{rr} is the coefficient of tire rolling resistance, C_D is the drag coefficient, ρ is the density of air, A_F is the frontal cross-section area, and v_{aero} is the velocity of the vehicle plus the headwind (m/s).

Table 4-1 Parameters of a Prototype Elevator

| Parameters | Description | Value |
|-------------|----------------------------|------------------------|
| m_e | Mass of the elevator car | 1260 kg |
| m_c | Mass of the counterweight | 1600 kg |
| m_p | Maximum passengers load | 1200 kg |
| A | Width of the elevator car | 2 m |
| B | Length of the elevator car | 3 m |
| H | Height of the elevator car | 2 m |
| g | Gravitational acceleration | 9.81 m/s ² |
| N_f | Numbers of floors | 50 |
| C_l | Clearance between floors | 3 m |
| C_r | Rolling Resistance | 0.009 |
| R_{final} | Final Drive ratio | 3.55 |
| A | Surface slope | 90° |
| ρ | Air density | 1.21 kg/m ³ |
| C_D | Air Drag Co-efficiency | 0.8 |
| A_F | Elevator section area | 6 m ² |

4.5.3. Modeling of PEM Fuel Cell system

Much effort has been put forth to understand the parameters and issues affecting the performance of fuel cell systems. There are many approaches of modeling a PEM fuel cells performance, which may be classified as: a) theoretical, or mechanistic, b) Computational Fuel Cells Dynamics (CFCD) simulation, c) semi-empirical, and d) empirical, depending on the level of modeling sophistication. Each approach has advantages and disadvantages, as discussed in details in[52].

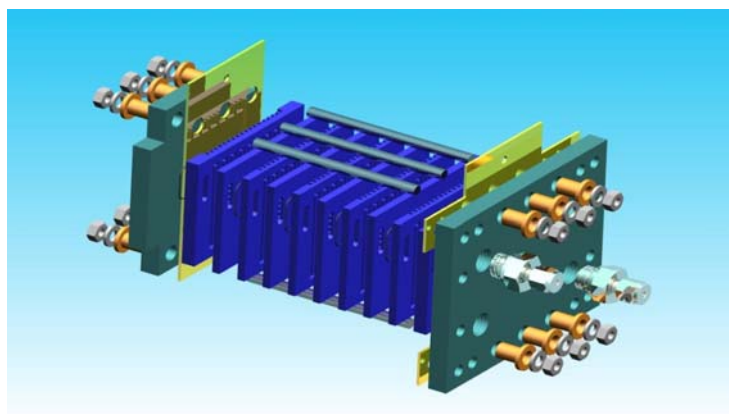


Figure 4-5 A PEM Fuel Cells Stack

Since the main interest of this work is not to design the fuel cell system itself, a simple and computationally inexpensive semi-empirical model was used to model the fuel cells hybrid elevator backup power system. The robust and flexible semi-empirical model considered primarily steady-state behaviours with simplified transient effects [53, 54]. The model has been used by members of industry, where Ballard Power Systems is the most notable example [55], and by other research groups that have incorporated early versions of the model and used experimentation to validate its veracity[56]. Recently, this model was used in the authors' research group to model the performance of a PEM fuel cell system and to optimize the system design [55, 57]. In this work, a build-in semi-empirical fuel cells model in ADVISOR was used to test the backup power system model. More accurate PEM fuel cell system sub-model, based on the group's recent work [57] is to be incorporated at later stage of the research.

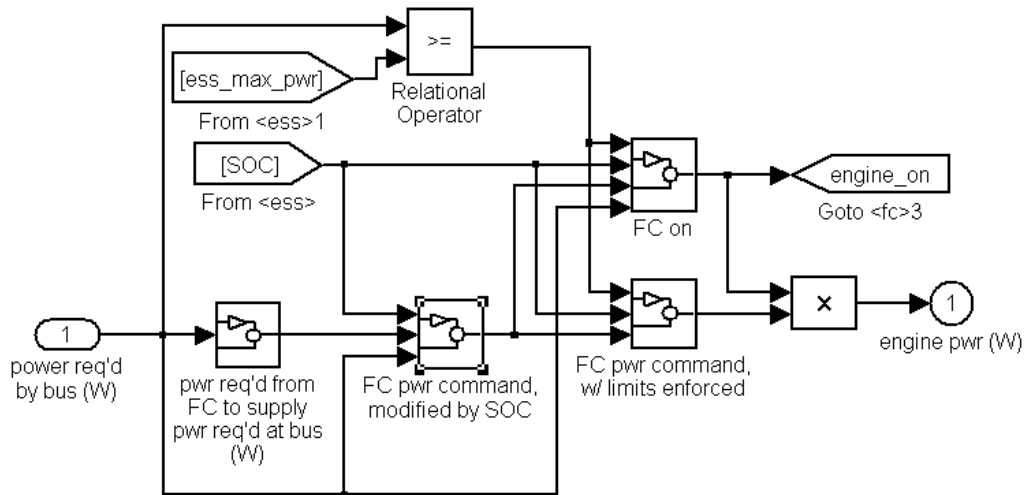


Figure 4-6 a Fuel cell system Model in ADVISOR

The empirical fuel cells power model was built on test data. The test data was hydrogen flow rate indexed by voltage and current. According to power actually delivered at fuel cells, hydrogen flow rate at each time step was calculated. Therefore, the total hydrogen consumption was calculated. The power efficiency map of the fuel cells model is shown in Figure 4-7.

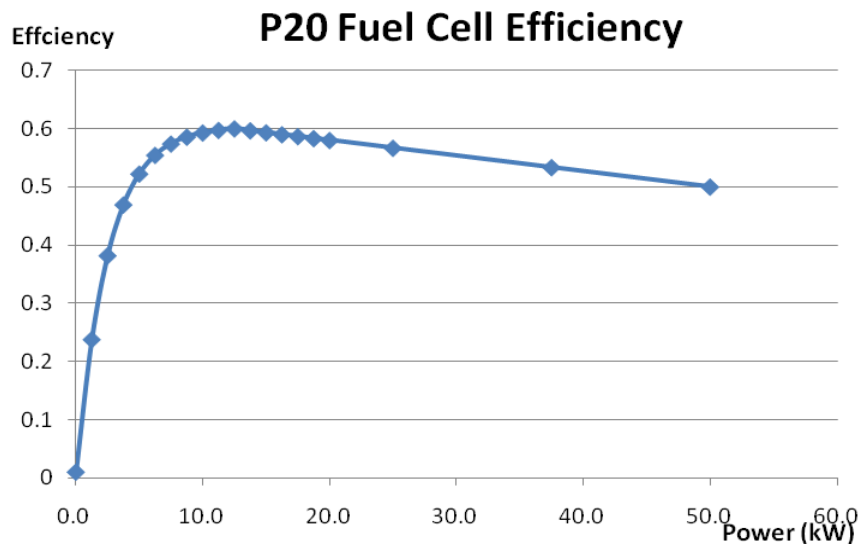


Figure 4-7 a Fuel cells Power Efficiency Map

4.5.4. Modeling of Motors

The motor model was created on the similar basis of fuel cells. It mainly decides the torque and speed to be delivered at the output shaft. At the same time, the energy consumption (electricity) is calculated. Figure 4-9 is a motor model in ADVISOR. The simplified explanation is shown in Figure 4-8. A motor model receives torque and speed request from final drive and decides torque and speed available to be delivered. Using a DC/DC converter, the motor voltage in this study remains constant. The experimental data was based on current demand indexed by motor torque and speed.

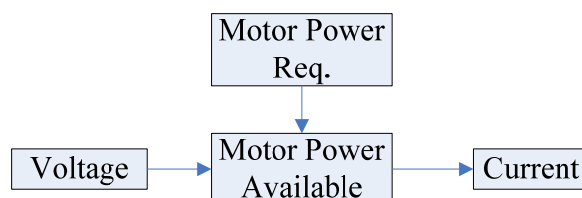


Figure 4-8 Motor Model Power Flow

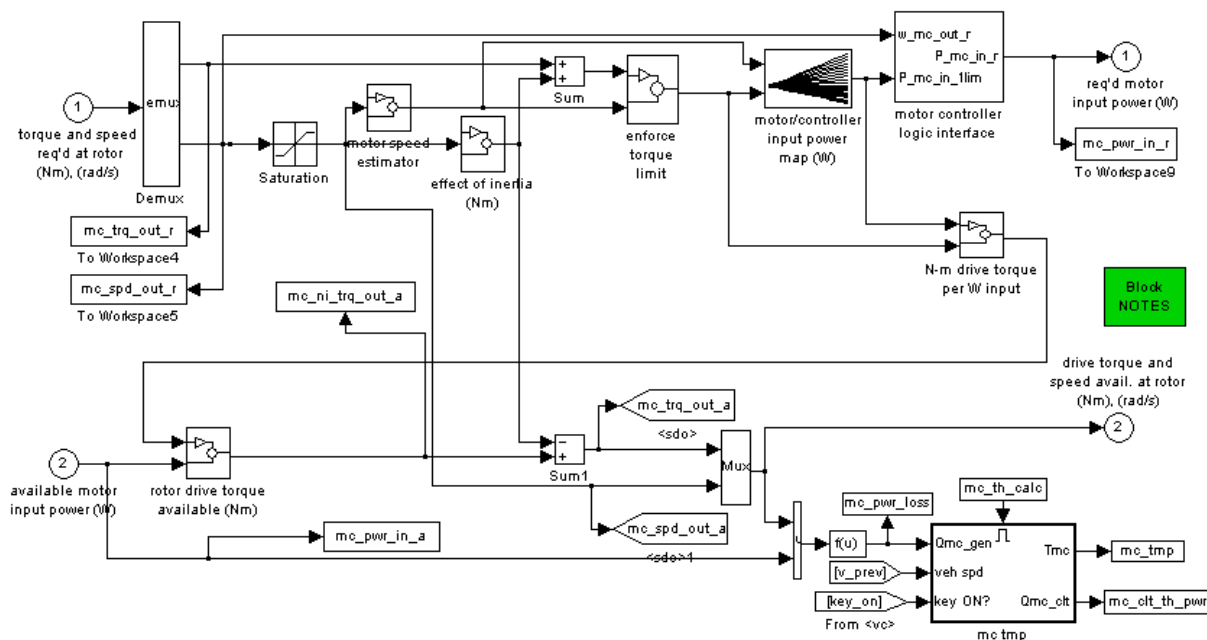


Figure 4-9 Motor Model in ADVISOR

Figure 4-10 shows experimental data of the motor efficiency. The tested motor is a 30 kW

Siemens motor operates at 216 V. The motor had a steady high efficiency of 80% during most of test conditions. The efficiency would drop in low speed or low torque operation.

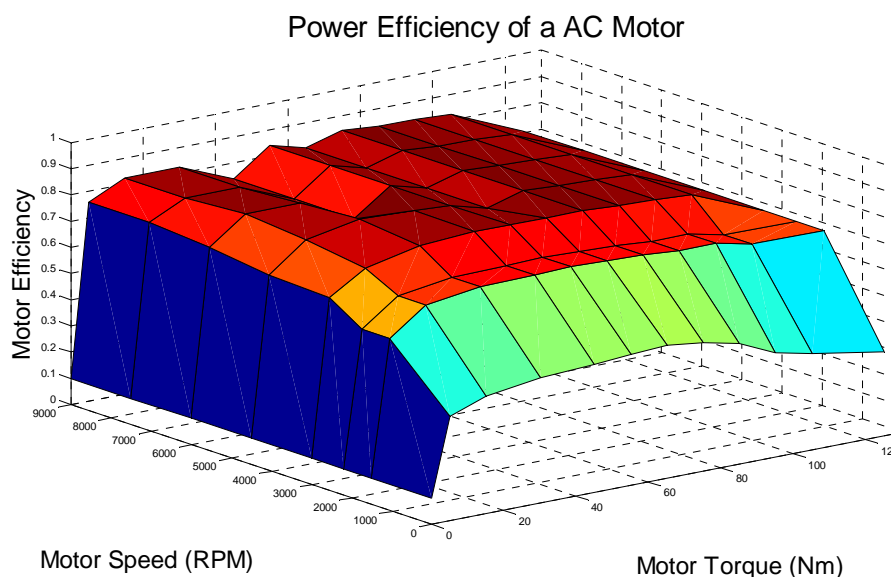


Figure 4-10 AC30 Motor Power Efficiency

4.5.5. Modeling of Energy Storage System

As a power leveraging device to assist fuel cells, an energy storage system (ESS) was designed based on power demand. In a computer model of an energy storage system, power capability and operating status of the representing physical devices were decided. The selection of energy storage devices was largely based on the energy density, power density and costs of the device. Battery and ultracapacitor were considered in this study.

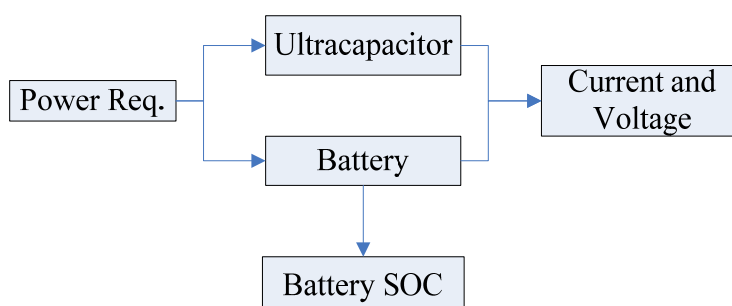


Figure 4-11 Energy Storage System Model

4.6. Elevator Power Management

With various electric and hybrid drivetrains, the primary function of power management was to prioritize the real time power request from load and allocate the power source in an optimized manner for system life and efficiency. A good power management can reduce the weight, size, and cost of the system, and improve system performance.

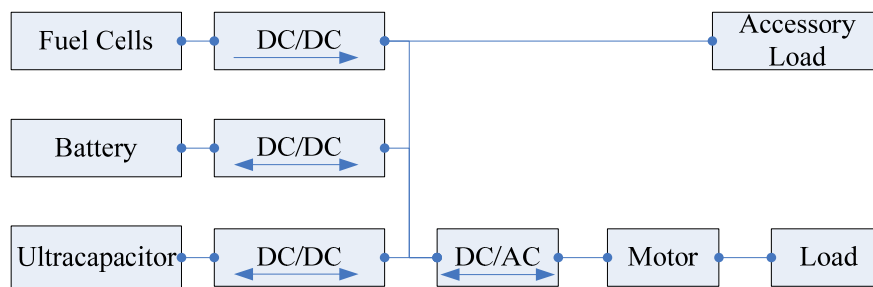


Figure 4-13 Power Management System of a Fuel Cells Hybrid Powertrain

Figure 4-13 is a sketch of the entire powertrain. Several power converter/inverters were used to coordinate the voltage. In this work, a fuel cells optimization oriented scheme was used in energy management. The objective is to reduce fuel cells power variation with a reasonable size of energy storage system.

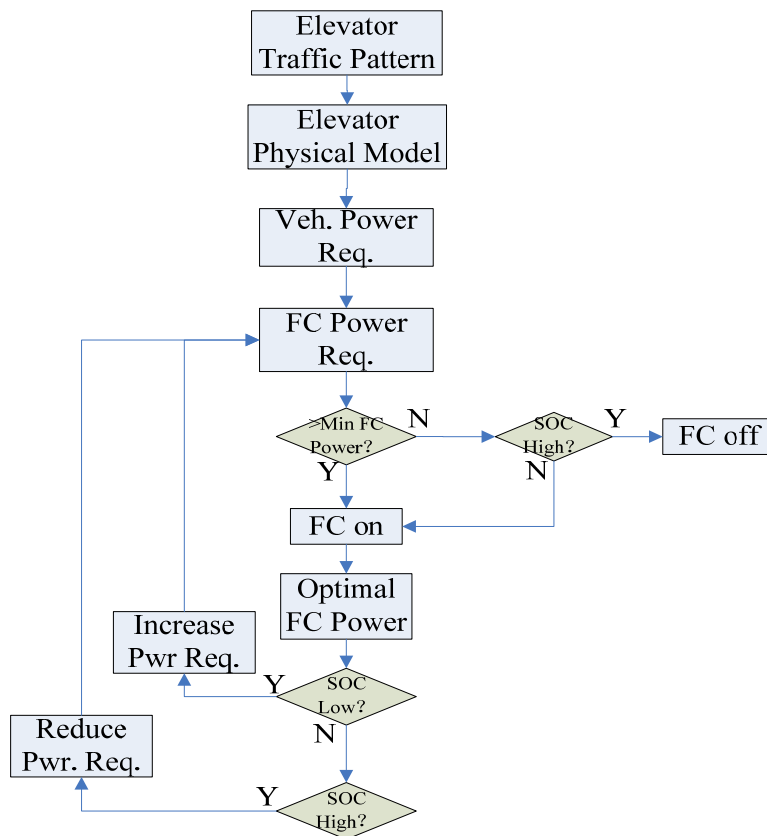


Figure 4-14 Fuel cell system Power Management Flow Chart

Figure 4-14 shows flow chart of fuel cell power management. According to predefined traffic pattern and motor model, a real time power request is calculated. The system first evaluates status of energy storage system. Then the fuel cells model decides the fuel cells operating power based on power request and SOC from the energy storage system. Fuel cells are switched off when power demand is lower than a pre-set value. When the fuel cells are on, it coordinates the power flow so that the SOC maintain at an economic range. It is therefore easy to understand the importance of fuel cells being affected by energy storage systems. A larger and more efficient energy storage system would reduce the fluctuation of fuel cells power demand. The efficiency and life of fuel cells could be further improved. Some of the control parameters are listed in Table 4-2.

Table 4-2 Power Control Parameters

| Parameters | Description | Value |
|-----------------------------|------------------------------------|--------------|
| <i>Cs_hi_soc</i> | Highest desired battery SOC | 0.8 |
| <i>Cs_lo_soc</i> | Lowest desired battery SOC | 0.4 |
| <i>Cs_ini_SOC</i> | Initial SOC | 0.7 |
| <i>Cs_min-pwr</i> | Fuel cells min operating power | 3 kW |
| <i>Cs_charge_pwr</i> | Minimum time for FC remain off | 100 s |
| <i>Cs_max_pwr_rise_rate</i> | Maximum ratio of increase of power | 2 kW |
| <i>Cs_max_pwr_fall_rate</i> | Maximum ratio of decrease of power | -3 kW |

4.7. Computer Simulation

4.7.1. Elevator Traffic Patterns (Drive Cycles)

After the system model was built, the traffic pattern over which elevator performs must be specified. The traffic patterns of an elevator are always case dependent. In a preliminary review, very few standard elevator operation cycles were developed. To evaluate the performance of elevator's power drive, two elevator driving patterns were randomly picked using guidelines based on engineering intuition. One scenario was to maintain elevators at normal operation during power failure. The other scenario was a low power mode which was only used for emergency purposes. In a normal mode, an elevator operated at a moderate speed and performed up and down movement until power grid resumed. On the other hand, a half hour cycle was developed for the low power mode, which is aimed at evacuating people at higher levels of the building as well as people with disability at lower levels. In the low power mode, an elevator would only stop at 10th floor or higher during most of the cycles, with few stops at lower level. Features of these two driving cycles are shown in Table 4-3. More realistic driving cycles can be obtained from real world elevator operation.

Table 4-3 Description of Two Driving Cycles

| | Travel Schedule (floor) | Max Acceleration | Max Speed | Average Speed |
|------------------|----------------------------------|----------------------|-----------|---------------|
| High Power cycle | 0-10-5-25-0-40 | 1 m/s ² | 5 m/s | 0.93 m/s |
| Low Power cycle | 0-50-45-0-40-35-0-30-5-0-25-20-0 | 0.5 m/s ² | 2.5 m/s | 0.46 m/s |

4.7.2. Low Power Mode Simulation

To perform an initial simulation, the sizes of power source units were as specified in Table 4-4.

Table 4-4 Power Source Unit Sizes on Initial Simulation Test

| Power Source | Size |
|--------------------|---------------------|
| Fuel cells | 20 kW |
| Battery | 15 units of 12V26Ah |
| Maxwell Ultra-cap. | 100 units PC2500 |
| Motor | AC 40 kW |

Figure 4-15 shows the performance the elevator regarding to the low power cycle. The elevator was able to meet the cycle with little nominal speed variations.

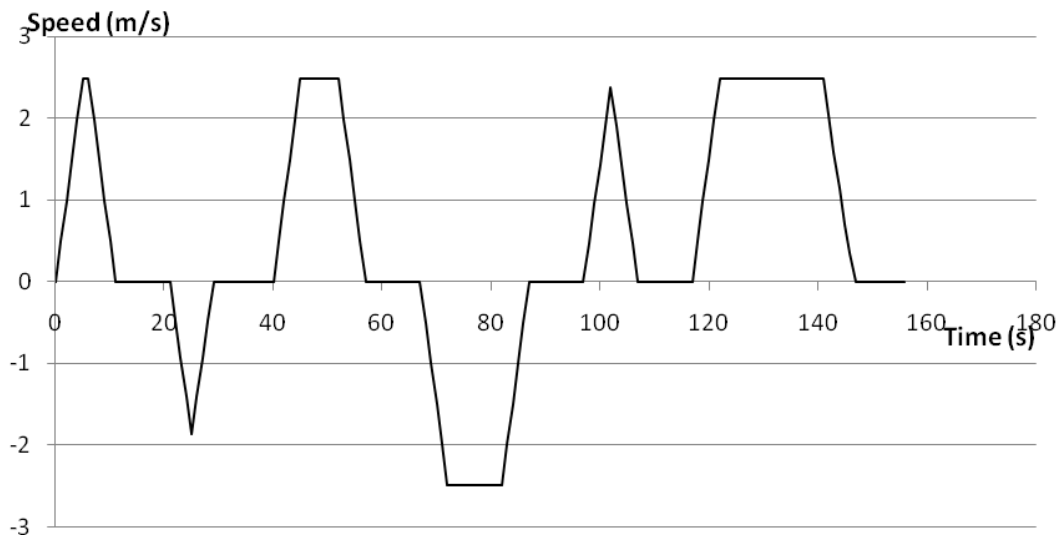
**Figure 4-15 Simulation of Low Power Cycle**

Figure 4-16 shows the real time power demand from electric motor while Figure 4-17 is the

power supply from fuel cells. With power aid from energy storage system, the power draw from fuel cell will be much smoother.

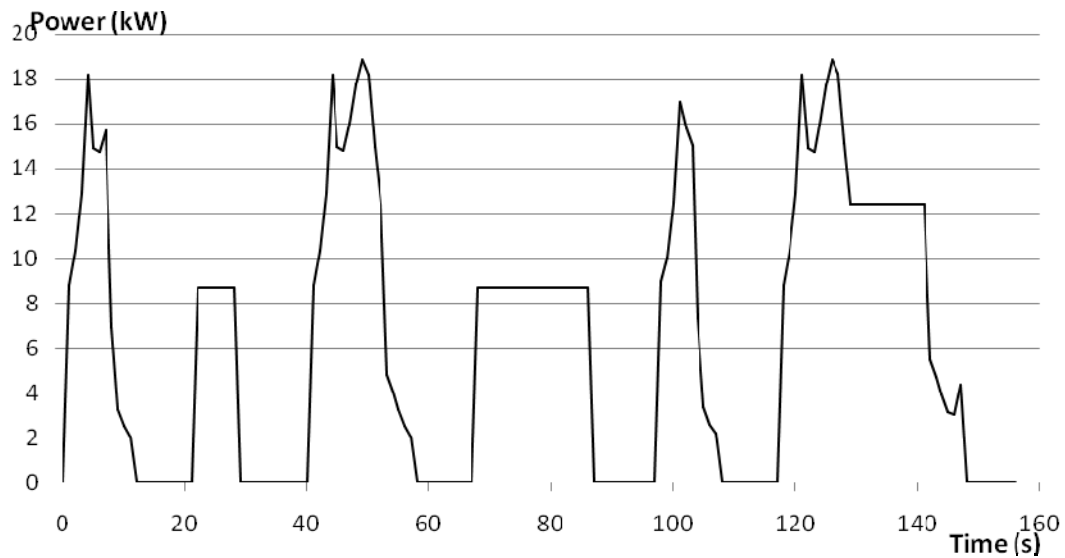


Figure 4-16 System Power Demand-Low Power Cycle

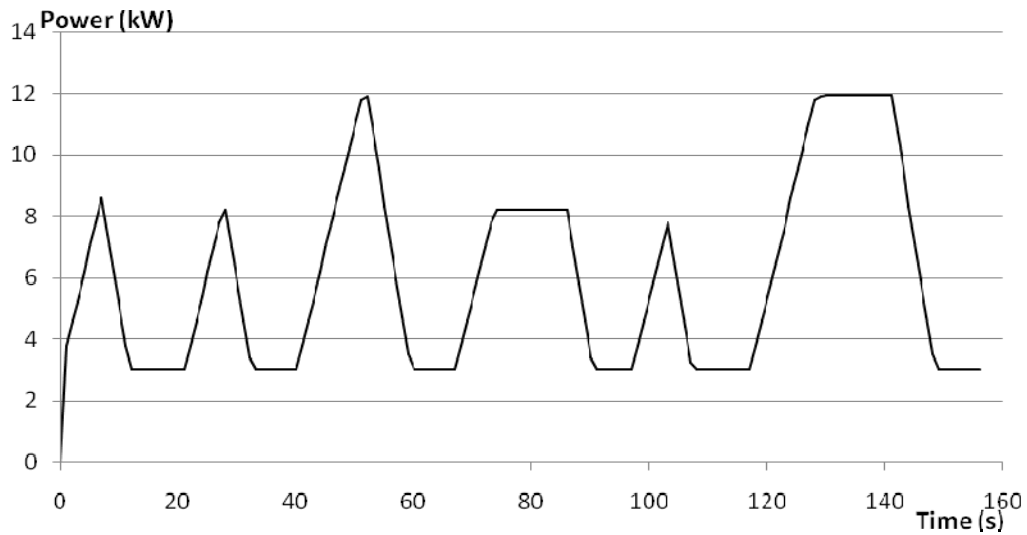


Figure 4-17 Fuel cells Power Demand-Low Power Cycle

Figure 4-18 shows the battery SOC change during the low power cycle simulation. The battery SOC fluctuated between 0.66-0.73. The batteries were through 6 discharging and charging cycles during the 160 seconds of simulation.

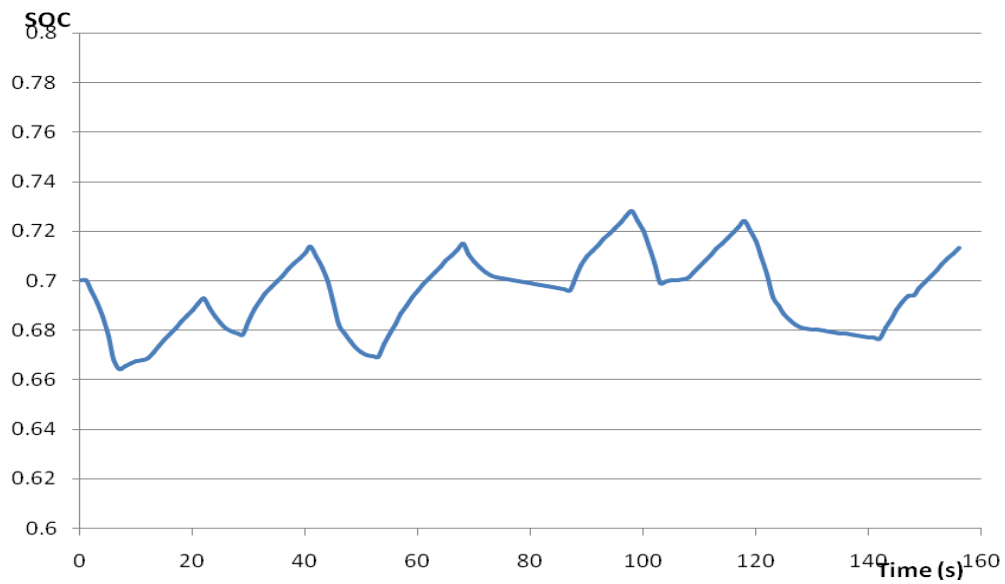


Figure 4-18 Battery SOC-Low Power Cycle

In the ultracapacitor based ESS, the SOC fluctuated at a range broader than that of the battery based ESS, from 0.62 to 0.74, as shown in Figure 4-19.

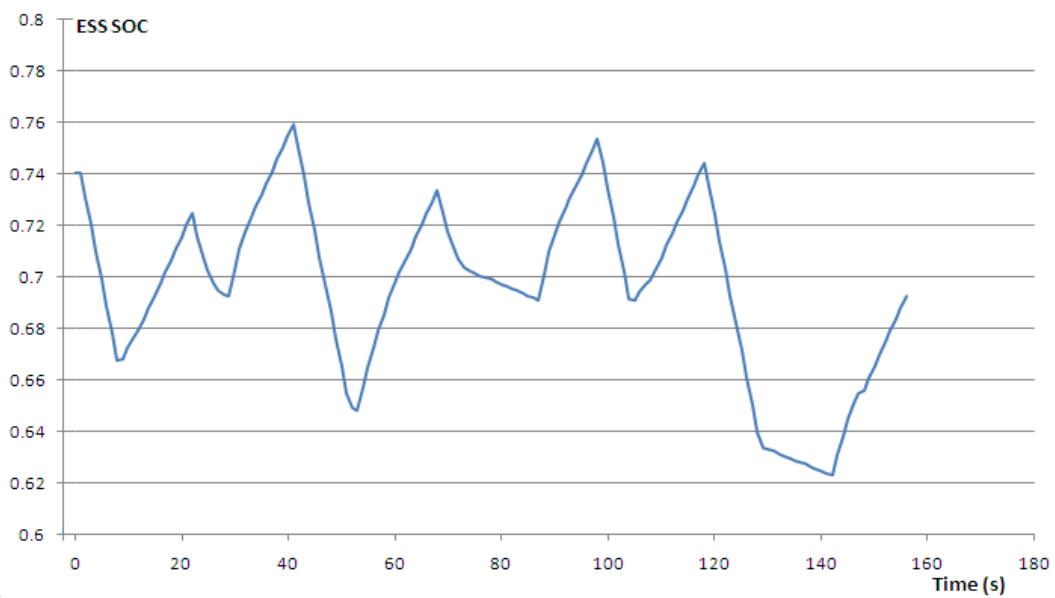


Figure 4-19 Ultracapacitor SOC-Low Power Cycle

4.7.3. High Power Mode Simulation

Figure 4-20 shows the performance the evaluator regarding to the high power cycle. The elevator is able to satisfy most cycle with slight miss at peak speed as circled.



Figure 4-20 Performance Simulation of High Power Cycle

Figure 4-21 shows the real time power demand at electric motor while Figure 4-22 shows power demand at fuel cells.

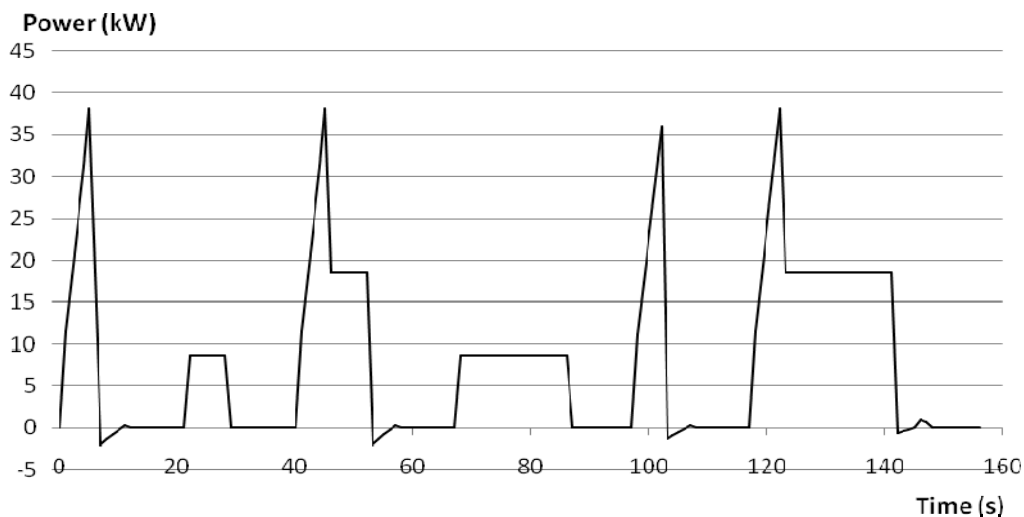


Figure 4-21 System Power Demand-High Power Cycle

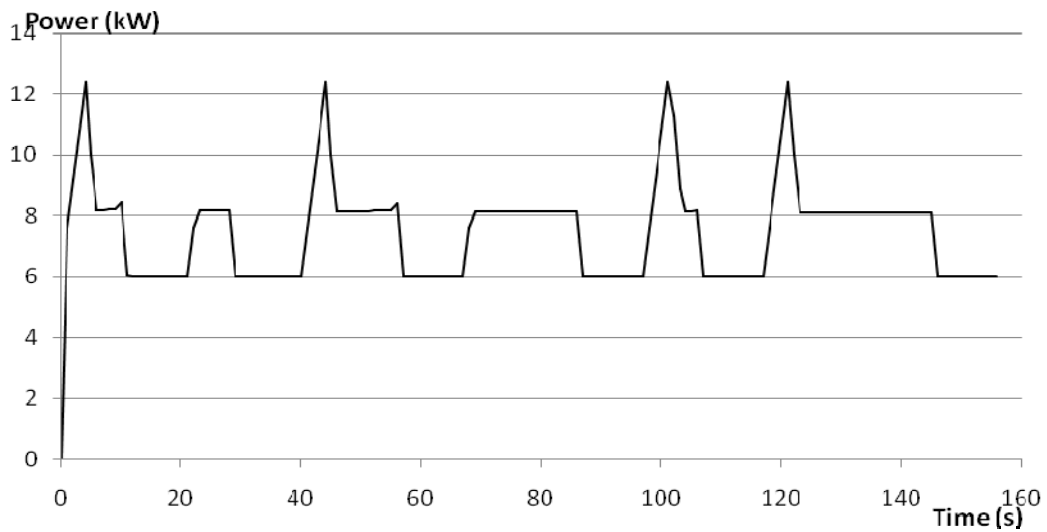


Figure 4-22 Fuel cells Power Demand-High Power Cycle

The 12.5kW peak power demand at fuel cells was used to size the fuel cells stack. A 20 kW fuel cells stack were chosen based on the high efficiency of this stack when operating at 10 kW to 15 kW range.

During the 160 seconds of high power operation, the battery SOC was reduced from 0.76 to 0.62.

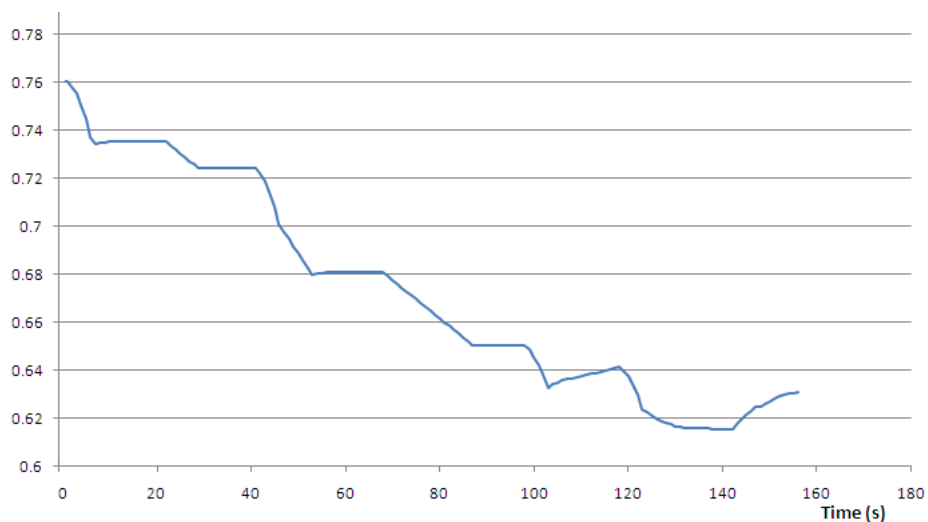


Figure 4-23 Battery SOC-High Power Cycle

On a fuel cells ultracapacitor hybrid, ultracapacitor operated at a much broader SOC range.

Figure 4-24 shows the ultracapacitor SOC varied from approximately from 0.2 to 0.8.

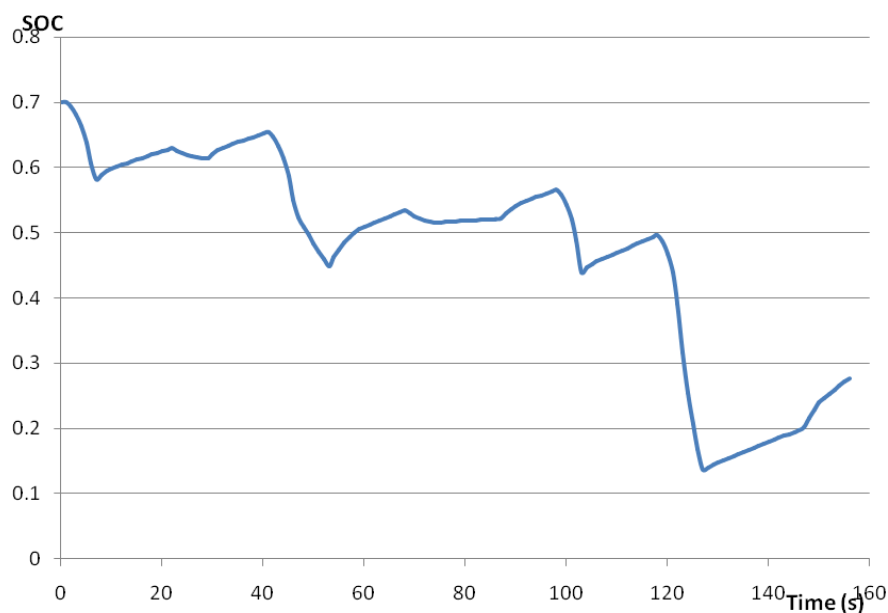


Figure 4-24 Ultracapacitor SOC-High Power Cycle

4.8. Optimal Battery and Ultracapacitor Units

The size of energy storage system affects the overall efficiency. The minimum size of the battery depends on the peak power demand. In order to find the optimal number of battery unit for best power efficiency, the number of battery unit was treated as a variable. This work determined the optimal battery size that was needed to meet the high power drive cycle as introduced previously. By setting the start units at 10, an increment of one was used to identify the optimal battery units. According to the system efficiency map shown in Figure 4-25, the system reached optimized power efficiency with 17 battery units.

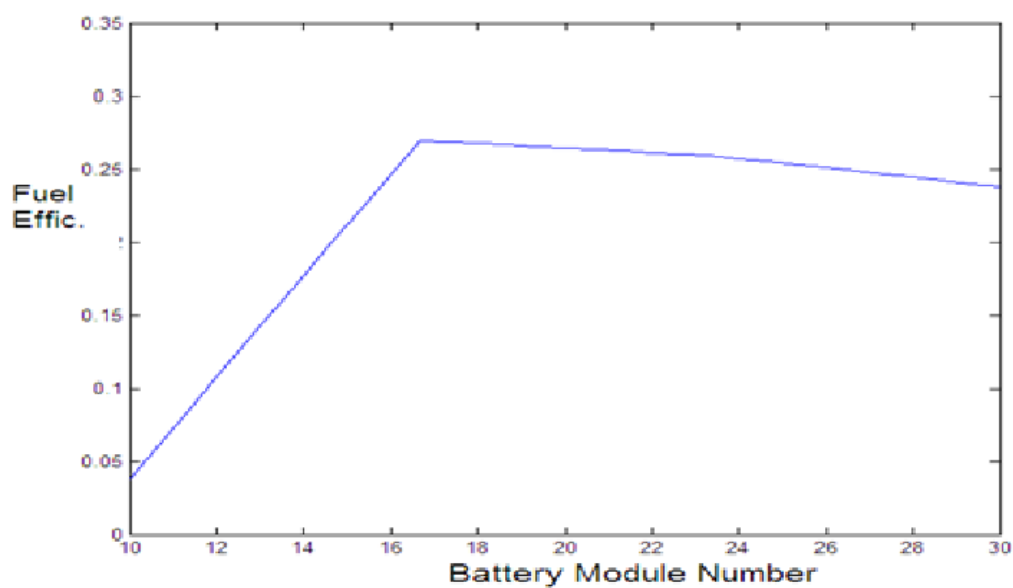


Figure 4-25 Optimal Battery Units

A slightly different method was used to search for the optimal ultracapacitor units. With search point start from 100 units and a step size of 5, hydrogen consumption decreases until 125 units was selected. Therefore, the improved ultracapacitor module was selected as 125.

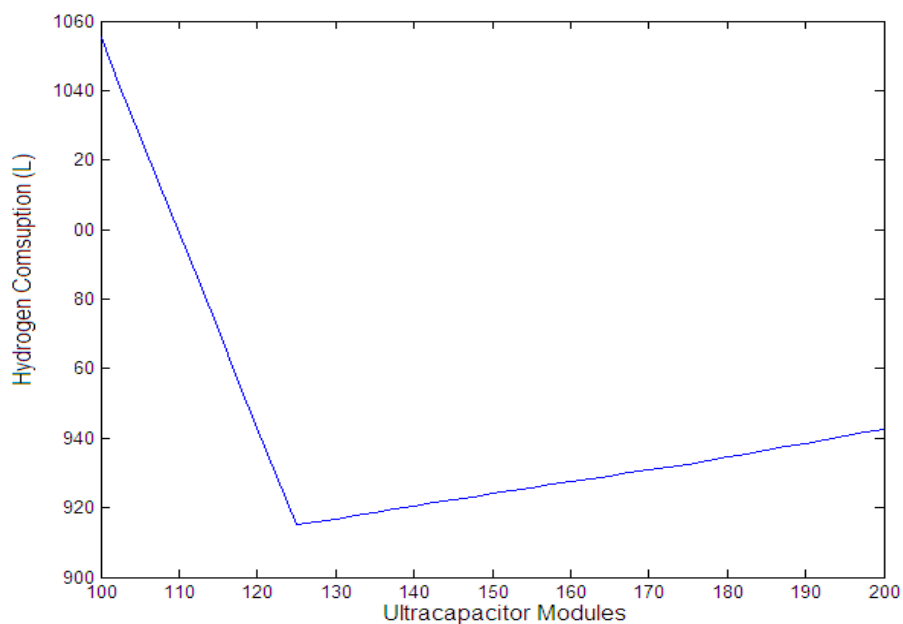


Figure 4-26 Optimal Ultracapacitor Units

The optimized power train is summarized at Table 4-5.

Table 4-5 Specification of Optimized Powertrain

| Power Source | Initial | Optimized |
|---------------------------|----------------|------------------|
| Fuel cells | 20 <i>kW</i> | 20 <i>kW</i> |
| Battery (12V26Ah) | 15 Units | 17 Units |
| Ultracapa. Maxwell PC2500 | 100 Units | 125 Units |

The hydrogen consumption test was based on 15 repeating cycles of each traffic pattern. The increased battery size improved the hydrogen consumption by 35% as listed in Table 4-6.

Table 4-6 Specification of Battery Based Elevator Backup Power System

| | Initial | | Optimized | |
|------------------|----------------|--------------|------------------|--------------|
| | FC-BA | FC-UC | FC-BA | FC-UC |
| Low Power Cycle | 194.5g | 205g | 144g | 151g |
| High Power Cycle | 314.5g | 331g | 223g | 231g |

4.9. Cost Analysis

The operational performance of the elevator only presents half of the considerations. The investment, operation and maintenance cost of the backup power system over life time is another important aspect in determining the design of the elevator backup power system.

4.9.1. Cost of PEM Fuel Cell System

The primary cost of the hybrid backup power system is the initial investment cost of the PEM fuel cell system. The cost of fuel cells stack, in reasonably sized mass production, is to be reduced to \$67/*kW*, and cost of balance of plant (BOP) apparatus and assembly is \$41/*kW* on average [6]. The investment cost of a 30 *kW* fuel cell system then becomes \$2,160. Based on data over the past a few years [58], the price of PEM fuel cells is likely to come down even more, further reducing the cost of the system. However, before PEM fuel cells enter mass production, a prototype fuel cell system tends to cost as high as \$500/*kW* to \$1000 /*kW*. With active braking

and effective of recovery of brake power, the ultracapacitor can be frequently charged, reducing the size of the need fuel cell system and the cost of the power backup system.

4.9.2. Costs of Batteries and Ultracapacitors

As a mature product, the cost of lead acid battery is quite low. The unit price of Leopard 12 *V*-12 *Ah* SLA battery is \$30. One of the leading ultracapacitor manufacturers is Maxwell. A most recent ultracapacitor model developed by Maxwell, MC2600, costs \$92 in low volume and \$54 in mid-range volumes. The BMOD2600-48 ultracapacitor module is encased in a rugged, splash-proof, aluminium chassis, weighting 13.5 *kg* and having 13.4 litres in volume (420 mm x 200 mm x 160 mm). These durable “smart boxes” include temperature and voltage monitoring and internal cell balancing that give designers a “plug and play” solution. Available module-to-module balancing makes these ultracapacitor modules versatile building blocks for systems with higher voltage requirements. The ultracapacitor module is priced at \$613 each for low volumes and \$366 at midrange[59].

4.9.3. Power Converter and Controller

Power converter and power electronics play a key role in the backup power system. They control the effective and optimal power flow from the battery pack, ultracapacitor module, and fuel cell system to the drive motor and the flow of recovery power under power enhancement. These control system and power electronics is not a simple DC-DC converter, much more research and development efforts have devoted to this area [60, 61] and a variety of less sophisticated and less capable commercially products are available. For instance, the experiment system with a 60 *kW* power capability in well fits the power demand of this elevator application[47].

Table 4-7 Overall System Cost Prediction

| | Prototype | Mass Produced |
|-------------------------|---------------------|--------------------|
| Fuel Cells Single Stack | \$20000 (\$1000/kW) | \$1340 (\$67/kW) |
| Fuel Cells BOP | --- | \$820 (\$41/kW) |
| Ultracapacitors | \$6750 (\$54/Unit) | \$6750 (\$54/Unit) |
| Lead Acid batteries | \$3000 (\$30/Unit) | \$3000 (\$30/Unit) |
| Power Converters | \$3000-5000 | |
| Over All | \$30,000-\$35,000 | |

4.10. Discussion and Conclusions

The results of simulation shown in Table 4-6 indicate that FC-BA and FC-UC architectures had comparable power efficiency. The lead acid battery hybrid yielded good power efficiency, satisfied the driving cycle with lower investment costs. However, the battery had a much shorter cycle life, required regular inspection and maintenance. These shortcomings and higher operation costs of the batteries were not reflected in our preliminary model as presented. According to the SOC histories of battery and ultracapacitor shown in the previous section, the battery SOC maintained at a relatively stable level, while the ultracapacitor SOC changed dramatically. Since the efficiency of ultracapacitors drops with their operation voltage, an increase in the size of the ultracapacitor module leads to an improvement of the power system efficiency, as shown in Figure 4-26. The system efficiency drops with a decrease of battery units according to Figure 4-25. This reveals the difference of batteries and ultracapacitors in nature. Ultracapacitor is good to provide high peak power, but its energy density is low. Battery has a higher energy density, but its power density is lower. A further study to find the optimal balance of batteries and ultracapacitors in the ESS of the FC-BA-UC hybrid backup power system is the focus of on-going research. A FC-BA-UC hybrid backup power system will lead better

operation conditions for both fuel cells and batteries, of which the life and efficiency are sensitive to the operation conditions.

The cost of the system is also in a reasonable range. Even with immature fuel cells commercialization, the overall system cost would be within \$35,000 US. There is also a potential of dramatic cost cut with the promising mass production of fuel cells.

CHAPTER 5 Modeling of a ICE Hybrid Powertrain for Two-mode Hybrid Trucks Using ADVISOR

Medium and heavy duty trucks serve an important role in modern society. More than 80% of the freights transported in the US were carried by medium and heavy duty trucks. In this work, fuel efficiency improvement of a heavy duty truck using different hybrid technologies was studied.

The architecture of an advanced hybrid electric truck, called two-mode, as mentioned in the previous section, showed more flexibility on power delivery than Toyota THS. In order to compare the detailed performance of this powertrain architecture, a two-mode model was introduced in this study. In the following sections, modeling of each powertrain component is introduced, as well as the control for the power management.

5.1. Planetary Gear Based Power Transmission

5.1.1. Speed, Torque and Power of the Planetary Gears

Planetary gears are used widely in many HEV transmissions. It features a compact structure, high load ability and a high efficiency. Figure 5-1 shows the section drawing of a single planetary gear. It includes three parts, a sun gear, a ring gear and several planet gears connected by a gear carrier. The sun gear, the ring gear and the carrier gear are the three shafts a planetary gear set connects to the outside. The complexity of the system brings difficulty to the speed, torque and power calculation. In this section, a method was summarized to compute and evaluate the drive ratios, torque and power.

The speed equation of the planetary gear is defined as in Eq. (5.1), where ω_c , ω_s , ω_r is the angular velocity of gear carrier, sun gear and ring gear respectively. k is defined as the basic ratio which

equals to the radius of ring gear divided by the radius of sun gear. i_{sr}^c is the relative drive ratio between sun gear and ring gear.

$$\frac{\omega_s - \omega_c}{\omega_r - \omega_c} = -k = i_{sr}^c \quad (5.1)$$

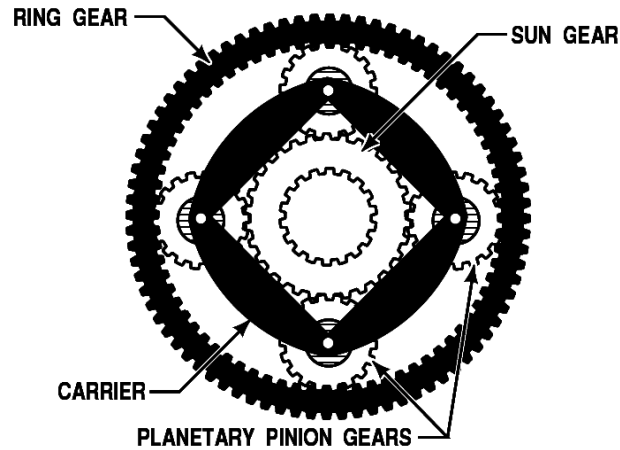


Figure 5-1 A General Planetary Gear

Similarly, drive ratio relations are found among other gears in Eq. (5.2). The relative drive ratios

i_{sr}^c , i_{cs}^r , i_{cr}^s are terms only associated with k .

$$\left. \begin{aligned} \frac{\omega_c - \omega_r}{\omega_s - \omega_r} &= \frac{1}{1+k} = i_{cs}^r \\ \frac{\omega_c - \omega_s}{\omega_r - \omega_s} &= \frac{k}{1+k} = i_{cr}^s \end{aligned} \right\} \quad (5.2)$$

Define absolute drive ratios as $R_{sr} = \frac{\omega_s}{\omega_r}$, $R_{rc} = \frac{\omega_r}{\omega_c}$, $R_{cs} = \frac{\omega_c}{\omega_s}$. From Eq. (5.1) and Eq. (5.2),

absolute drive ratio is found in Eq. (5.3). The absolute drive ratios are determined by k and the other absolute drive ratio R .

$$\left. \begin{aligned} R_{sr} &= \frac{\omega_s}{\omega_r} = (1+k)R_{cr} - k \\ R_{rc} &= \frac{\omega_r}{\omega_c} = (1+k - R_{sc})/k \\ R_{cs} &= \frac{\omega_c}{\omega_s} = (1+kR_{rs})/(1+k) \end{aligned} \right\} \quad (5.3)$$

For the three axles connected to the outside of a planetary gear, either one or two axles act as input. The other one acts as output. T_r, T_s, T_c represent torques at ring, sun and gear carrier respectively. To simplify the problem, gear friction is not included. For a stabilized status, the external torques was balanced as shown in Eq. (5.4) [62].

$$T_s + T_r + T_c = 0 \quad (5.4)$$

The input power is defined as positive while the output power is defined as negative. When angular acceleration α is zero on all gears, there is no gain or lose of potential energy considered on the planetary gears. The power is also balanced where P_s, P_r, P_c are inputs or output power on sun, ring and the gear carrier as shown in Eq. (5.5).

$$P_s + P_r + P_c = T_s \omega_s + T_r \omega_r + T_c \omega_c = 0 \quad (5.5)$$

From Eqs. (5.1), (5.4) and (5.5), torque relations are found Eq. (5.6)

$$\left. \begin{aligned} T_s &= -\frac{1}{k+1} T_c \\ T_r &= -\frac{k}{k+1} T_c \\ T_s &= \frac{1}{k} T_r \end{aligned} \right\} \quad (5.6)$$

The ratio of power flow is found in Eq. (5.7), in which R is absolute drive ratio as defined in Eq. (5.3).

$$\left. \begin{aligned} \frac{P_r}{P_s} &= \frac{T_r \omega_r}{T_s \omega_s} = k R_{rs} \\ \frac{P_r}{P_c} &= \frac{T_r \omega_r}{T_c \omega_c} = -\frac{k}{k+1} R_{rc} \\ \frac{P_c}{P_s} &= \frac{T_c \omega_c}{T_s \omega_s} = -(k+1) R_{cs} \end{aligned} \right\} \quad (5.7)$$

To study the power flow direction in and out, θ was defined as a power flow factor (PF) represented in Eq. (5.8). If $\theta=1$, both gears provide or withdraw power to the planetary gears. There is no power flows from one gear to another. If $\theta=-1$, power flows on those two gears are in opposite directions. If $\theta=0$, there is no flow of power on the node.

$$\left. \begin{aligned} \theta_{rs} &= \frac{R_{rs}}{|R_{rs}|} \\ \theta_{rc} &= -\frac{R_{rc}}{|R_{rc}|} \\ \theta_{cs} &= -\frac{R_{cs}}{|R_{cs}|} \end{aligned} \right\} \quad (5.8)$$

The power flow can be expressed using power flow chart once gear directions are decided. According to Eq. (5.8), $\theta_{rc}=-1$, $\theta_{rs}=-1$, $\theta_{cs}=1$. A '+1' results in the same direction of power flow while a '-1' results in the opposite direction of power flow. For $\theta_{cs}=1$, arrows at carrier gear and sun gear either both point to the center or both point to node. For θ_{rc} and θ_{rs} are both '-1', the power flows are different. The power flow chart is shown in Figure 5-2, the arrow points out power flow direction.

The power transfer efficiency on a planetary gear is defined as the ratio of power out by power in. Power input is considered as positive and power output is negative. The efficiency is shown in Eq. (5.9),

$$\eta = \frac{\text{output_power}}{\text{input_power}} = \left| \frac{-\omega_{out} T_{out}}{\omega_{in} T_{in}} \right| \quad (5.9)$$

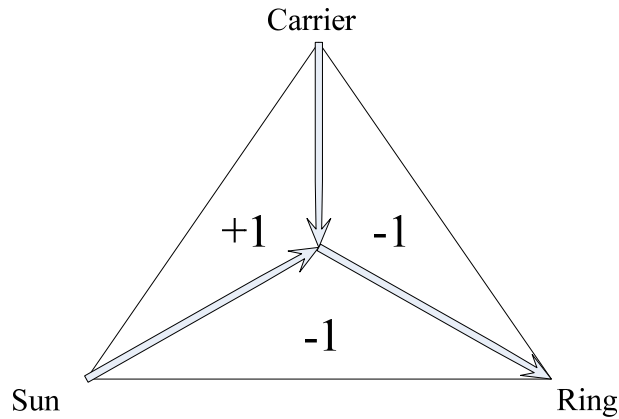


Figure 5-2 Power Flow Chart of Planetary Gear

For planetary gear systems with multiple input or output, efficiency is defined as in Eq. (5.10),

$$\eta = \frac{\sum_{i=1}^m -\omega_{out_i} T_{out_i}}{\sum_{j=1}^n \omega_{in_j} T_{in_j}} \quad (5.10)$$

where i, j are the number of input and output axle. $\omega_{out}, \omega_{in}$ are speed of the output axle and the input axle, and T_{out}, T_{in} are the torque output and input.

5.1.2. Toyota Hybrid System

Figure 5-3 shows the drivetrain configuration used in a Toyota hybrid system (THS). There are three shafts connected to the planetary gear, engine, two motors and output shaft to the wheel. Eq. (5.11) and Eq. (5.12) are the absolute drive ratios between output shaft and engine shaft, where ω is the angular velocity defined previously. This gear train has two degrees of freedom, the motor speed $\omega_{M/G1}, \omega_{M/G2}$ are determined by the engine speed and output speed as shown in Eq. (5.16).

$$R_{rc} = \frac{\omega_{out}}{\omega_{engine}} = \frac{\omega_r}{\omega_c} = \frac{1+k-R_{sc}}{k} \quad (5.11)$$

$$\left. \begin{aligned} \omega_{M/G1} &= (k+1)\omega_{Engine} - k\omega_{Out} \\ \omega_{M/G2} &= \omega_{out} \end{aligned} \right\} \quad (5.12)$$

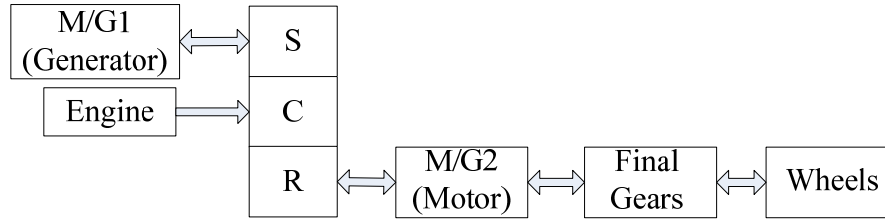


Figure 5-3 Toyota THS Configuration

The torque relations are found in Eq. (5.6). No transient condition is considered. No potential energy gained or lost was considered at planetary gears.

$$\left. \begin{aligned} T_{M/G1} &= -\frac{1}{k+1}T_{Engine} \\ T_{M/G2} &= \frac{k}{k+1}T_{Engine} - T_{out} \end{aligned} \right\} \quad (5.13)$$

To understand the power flow of the THS architecture, a plot was drawn with assumed constant engine speed as shown in Figure 5-4. From Figure 5-4, the direction of M/G2 and engine didn't change when vehicle was moving forward. The direction of M/G1 changed at speed V1 and V2. As a result, there were three groups of power flow factors (PF) of both planetary gears are shown in Eq. (5.14) according to Eq. (5.8) and relations shown in Figure 5-4.

$$\left. \begin{aligned} \theta_{rs} = -1 \\ \theta_{rc} = 0 \\ \theta_{cs} = 0 \end{aligned} \right\} \rightarrow \left. \begin{aligned} \theta_{rs} = -1 \\ \theta_{rc} = -1 \\ \theta_{cs} = 1 \end{aligned} \right\} \rightarrow \left. \begin{aligned} \theta_{rs} = 1 \\ \theta_{rc} = -1 \\ \theta_{cs} = -1 \end{aligned} \right\} \quad (5.14)$$

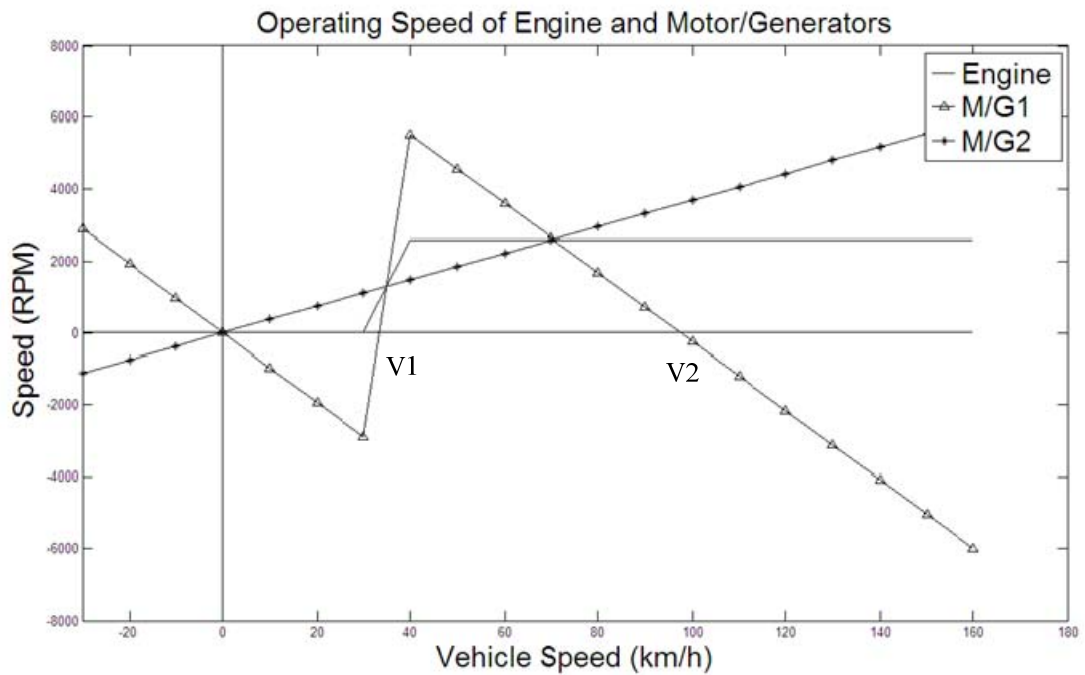


Figure 5-4 Engine, M/G1 and M/G2 Speed of THS

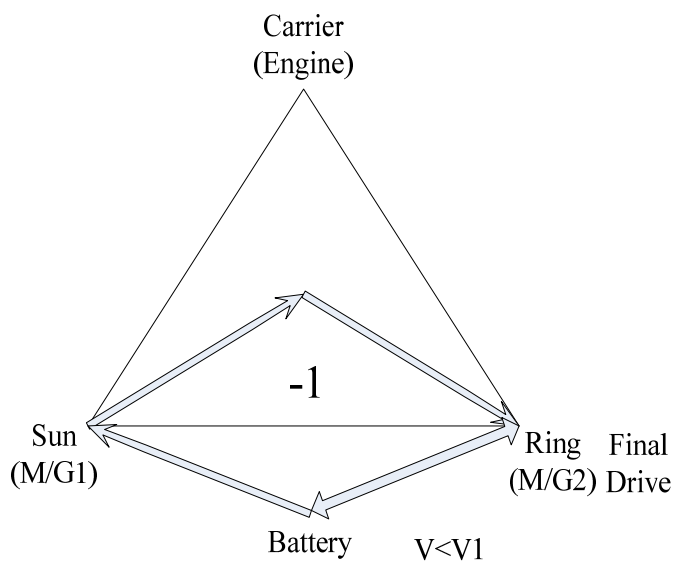


Figure 5-5 THS Power Flow Chart Engine Off

The preset engine launching speed is around 30 *km/h*. It also depends on battery SOC. Engine

is not turned on until certain conditions are satisfied due to the low engine efficiency at low power demand. According to Figure 5-5, at the engine off mode, M/G2 withdraws power from ESS and provides most of the torque to the wheel. If additional torque is needed, there is a possibility to switch M/G1 on. However, it may be impractical to switch M/G1 on the low speed mode due to the low power demand nature at low speed. During braking, the regenerative energy would be captured by M/G2 and charged back to the battery. Because of the small battery size on a THS, the engine off range is limited. Engine would kick in when the battery SOC reached a low point.

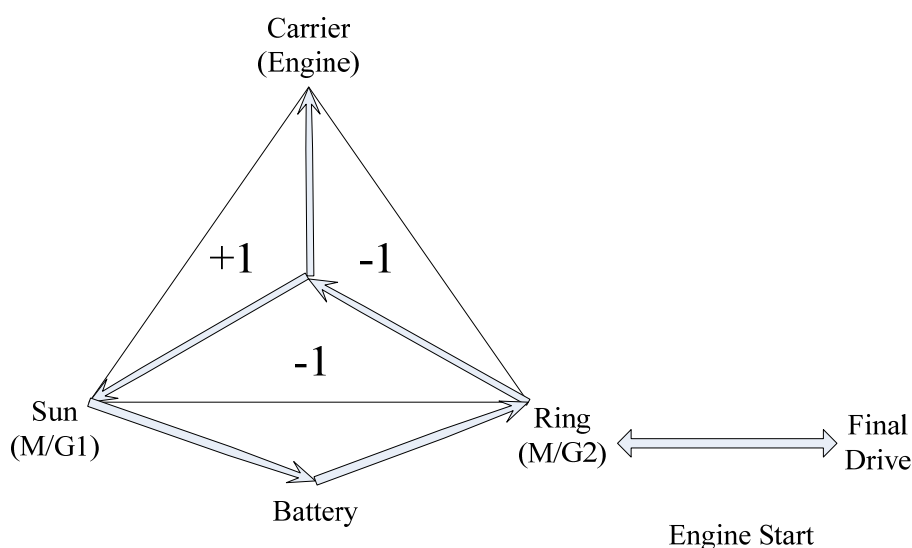


Figure 5-6 THS Power Flow Chart Engine Start

In a THS, there is no starter motor equipped to start the engine. Instead, M/G2 is used to provide the starting torque. Figure 5-6 shows the power flow direction during the engine start. Both engine and M/G1 receives power from M/G2. After this transient condition, the vehicle switched to a power split mode.

Power split mode is the most often operation mode in a THS vehicle. The power flow chart of this mode is shown in Figure 5-7. The speed range V1-V2 covers speed range at most urban city and part highway conditions. To notice engine braking is not considered as motor braking would be much more economically efficient.

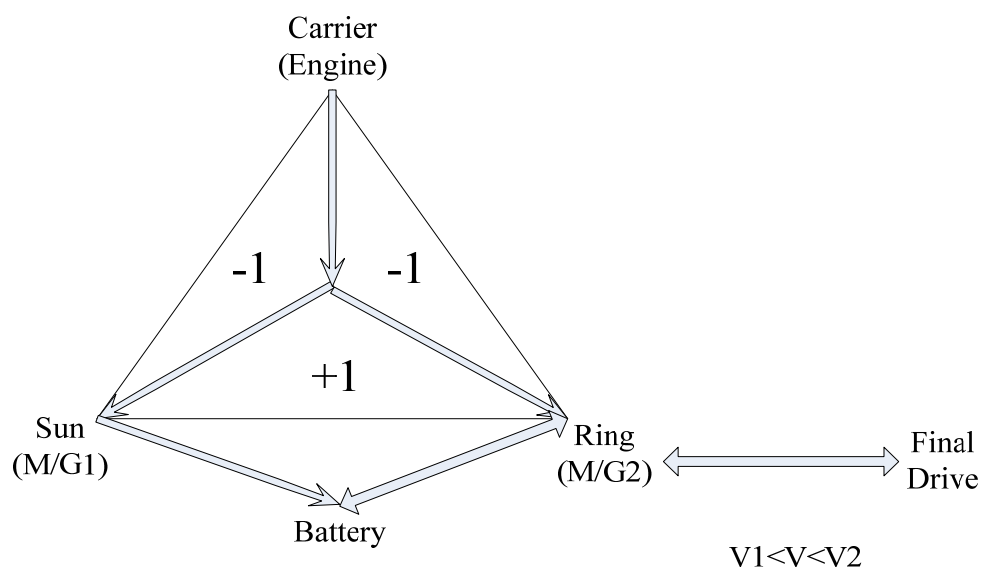


Figure 5-7 THS Power Flow Chart $V_1 < V < V_2$

During the power split mode, engine torque is split into two ways. One way goes through M/G1 and the other way goes through M/G2. M/G2 produces additional torque plus torque split from the engine to satisfy the wheel torque demand. The power generated at M/G1 is used to maintain the battery SOC while the motor is drawing power. M/G2 is also used to capture braking energy to regenerate electricity.

As vehicle speed increased, the spinning direction of M/G1 switches again (around 100 km/h according to Figure 5-4). As the direction changed, M/G1 switched from a generator to a motor. In this speed range, M/G2 could operate as either a motor or a generator. At this point, if both motors are withdrawing power from battery, the battery SOC is no longer sustainable. As a result, M/G2 would be used as a generator to keep the SOC balance. To notice a power circulation happened when M/G2 operates as a generator. Power circulation is an energy flow of the same form circulating among the system. It usually brings in energy loss and generates more heat. From Figure 5-8 at node of ring gear, part of torque received from engine and M/G1 was used to generate electricity at M/G2. The electric energy was then used to supply power demand

at M/G1. And the torque generated at M/G1 went back to M/G2. As a result, there was an energy flow circulating among M/G2, M/G1 and Battery. It would significantly reduce the system efficiency which partly explained the poor fuel economy of Prius on a highway condition.

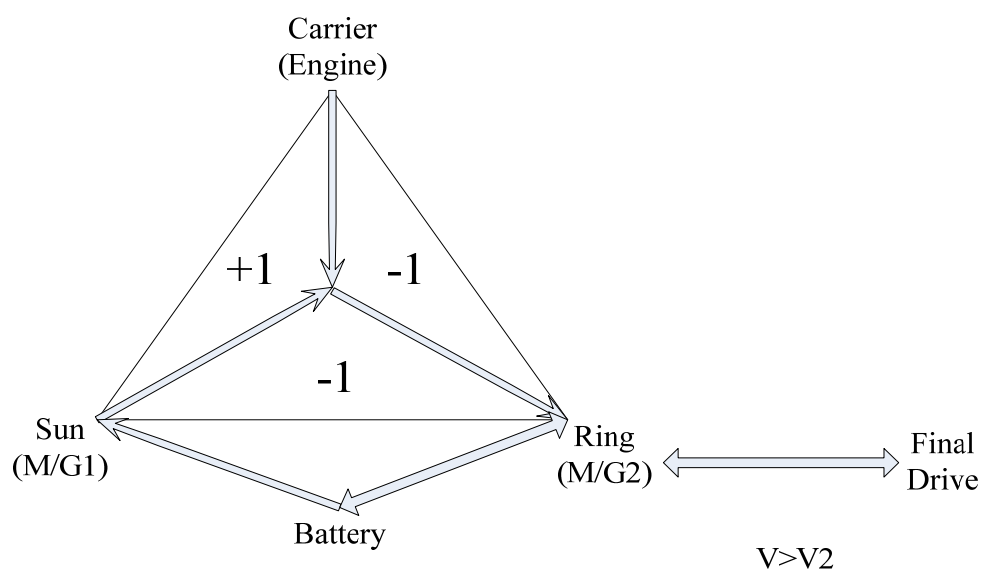


Figure 5-8 THS Power Flow Chart $V > V2$

Table 5-1 summarized operating mode of engine and motors at all speed range. M/G1 could be switched on as a motor during the engine off mode but it's not necessarily the case. The power circulation only takes place when vehicle speed is over $V2$ continuously.

Table 5-1 Engine and Motor Operating Condition of THS

| | Engine | M/G 1 | M/G 2 | Power Circulation |
|----------------------------------|--------|-------------|-----------|-------------------|
| Backward | Off | Off/Motor* | Motor | No |
| Forward low speed ($V < V1$) | Off | Off/Motor** | Motor | No |
| Engine Start | On | Generator | Motor | No |
| Forward Normal ($V1 < V < V2$) | On | Generator | Motor | No |
| Forward Over speed ($V > V2$) | On | Motor | Generator | Yes |

*, ** : If M/G1 is switched on

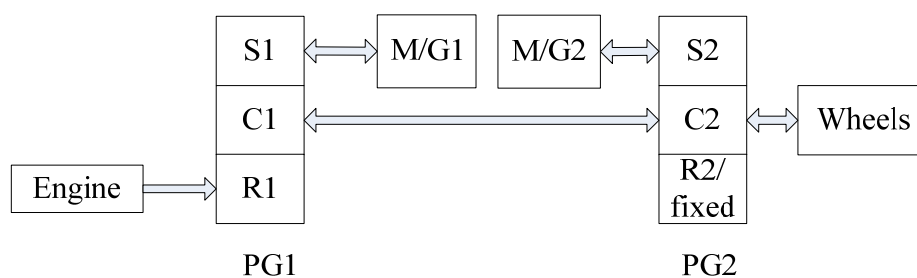
Table 5-2 further explained the power flow path in details. Energy converts from mechanical form to electrical form and then back to mechanical form.

Table 5-2 Power Flow Summary of THS

| | Backward/Low speed | Engine Start | Mid-speed | Over Speed |
|--------------|---------------------------------|-------------------------------|-------------------------|----------------------|
| Power Flow 1 | Battery-M/G2-Out | Battery-M/G2-Out | Battery-M/G2-Out | Engine-C-R-M/G2 |
| Power Flow 2 | Battery-M/G1-S-R-Out (optional) | Battery-M/G2-R-S-M/G1-Battery | Engine-C-R-Out | Engine-C-R-Out |
| Power Flow 3 | | Battery-M/G2-R-C-Engine | Engine-C-S-M/G1-Battery | Battery-M/G1-S-R-Out |

5.1.3. The First Mode of a Two-mode Transmission

Due to the different mechanical configurations of the two modes, each mode was discussed separately. On first mode, there are four shafts connected to the planetary gear transmission, an engine shaft, two motor shafts and an output shaft to the wheel. Eq. (5.15) described the absolute drive ratio between the output shaft and the engine shaft. This gear train has two degrees of freedom, the speed of both electric motors $\omega_{M/G1}, \omega_{M/G2}$ are determined by engine speed and output speed in Eq. (5.16). Figure 5-10 shows the speed profile of motors and engine during speed was constantly accelerating.

**Figure 5-9 First Mode Drivetrain Configuration**

$$R_{c1r1} = \frac{\omega_{out}}{\omega_{engine}} = \frac{\omega_{c1}}{\omega_{r1}} = \frac{k}{1+k-R_{sc}} \quad (5.15)$$

$$\left. \begin{aligned} \omega_{M/G1} &= (k_1 + 1)\omega_{out} - k_1\omega_{Engine} \\ \omega_{M/G2} &= (k_2 + 1)\omega_{out} \end{aligned} \right\} \quad (5.16)$$

According to Eq. (5.6), torque relations in first mode were found in Eq. (5.17)

$$\left. \begin{aligned} T_{M/G1} &= \frac{1}{k_1} T_{engine} \\ T_{M/G2} &= -\frac{1}{k_2 + 1} T_{out} - \frac{k_1 + 1}{k_1(k_2 + 1)} T_{engine} \end{aligned} \right\} \quad (5.17)$$

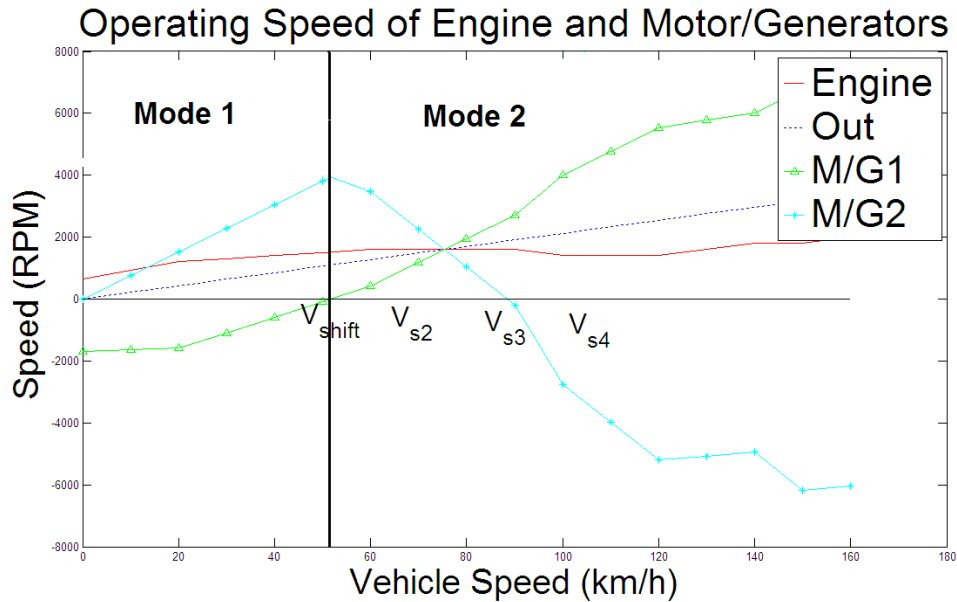


Figure 5-10 Speed of Engine, M/G 1, M/G2 and Output Shaft

Both forward and backward movement of the vehicle was considered. The simulation section to be presented in the following section will not consider the backward movement. For the forward movement of the vehicle, the power flow factors (PF) of both planetary gears were shown in Eq. (5.18) using Eq. (5.8) and relations shown in Figure 5-10.

$$\left. \begin{aligned} \theta_{r1s1} &= -1, \theta_{r2s2} = 0 \\ \theta_{r1c1} &= -1, \theta_{r2c2} = 0 \\ \theta_{c1s1} &= 1, \theta_{c2s2} = -1 \end{aligned} \right\} \quad (5.18)$$

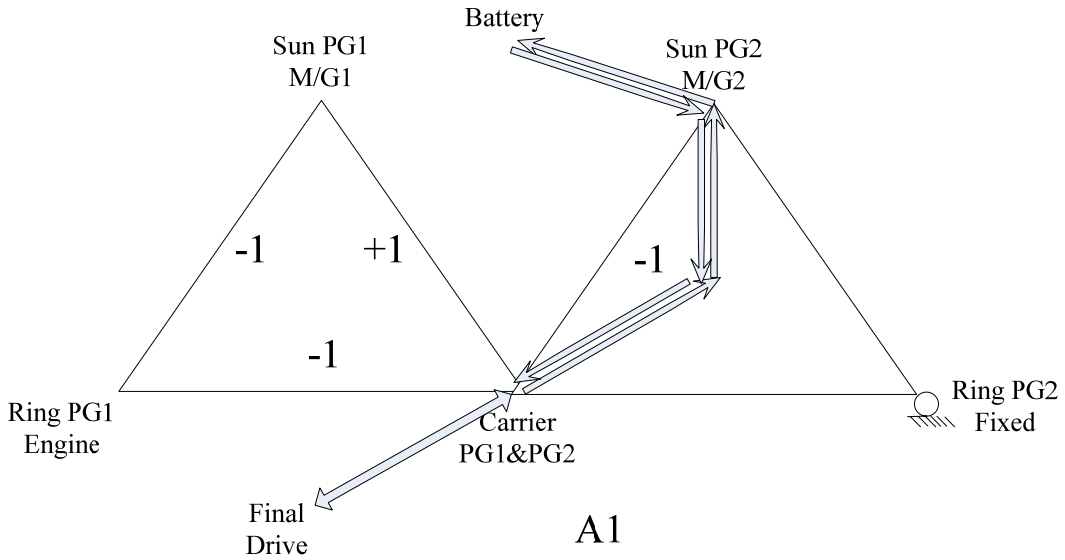
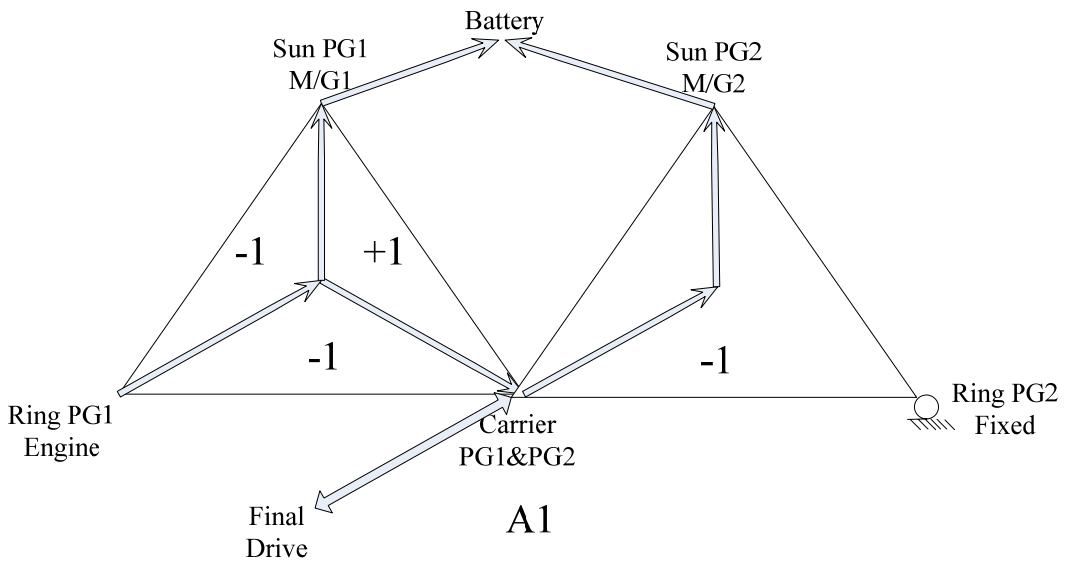


Figure 5-11 First-mode Power Flow Chart-Engine Off

Figure 5-11 shows the power flow of the two-mode transmission when engine is off. M/G2 would withdraw the power and catch braking power through the regenerative braking.



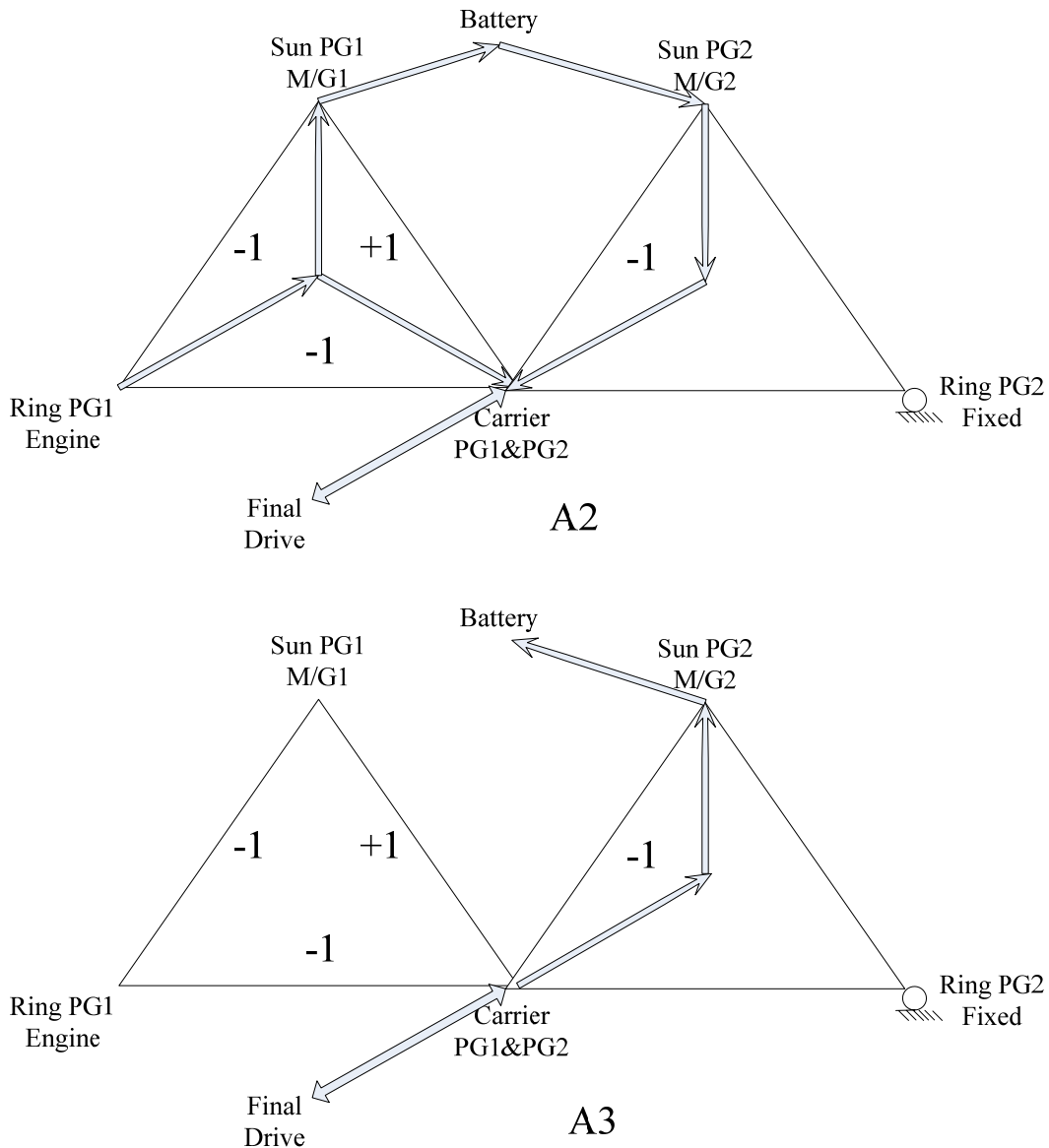


Figure 5-12 Power Flow Chart of Forward Movement in the First Mode

A1 in Figure 5-12 shows power flow when vehicle is idling or at very low power demand. If the vehicle is idling, the power flow follows the solid line transforming from the engine to the M/G1. When vehicle is moving but at low power demand, engine provides adequate power to the wheel through carrier gear and to the M/G1 at the same time. The excess power from the engine could be captured by the motor/generator 2 (M/G2) through the carrier and the sun gear on planetary gear 2 as shown.

A2 shows power flow of the most common operating condition in the first mode. There are two ways power transferring from the engine to the wheel. One way is directly through the ring 1 to the carrier 1. No energy transformation takes place. The other way is through M/G1 as a generator to M/G2 as a motor. Here the mechanical energy would be transformed into electrical form and back to mechanical form by electric motors. ESS is charged if more power provided by M/G1 than requested by M/G2. ESS would be discharged otherwise. A3 shows power flow when the vehicle is decelerating or braking. Most of the power would be captured by M/G2 and charged back to ESS shown as dot line. Mechanical brake disks or drums play an important part during an emergent brake. There is also a possibility of using engine brake. First mode is also used when vehicle moves backward. The PF is then calculated in(5.19).

$$\left. \begin{aligned} \theta_{r1s1} &= -1, \theta_{r2s2} = 0 \\ \theta_{r1c1} &= 1, \theta_{r2c2} = 0 \\ \theta_{c1s1} &= -1, \theta_{c2s2} = -1 \end{aligned} \right\} \quad (5.19)$$

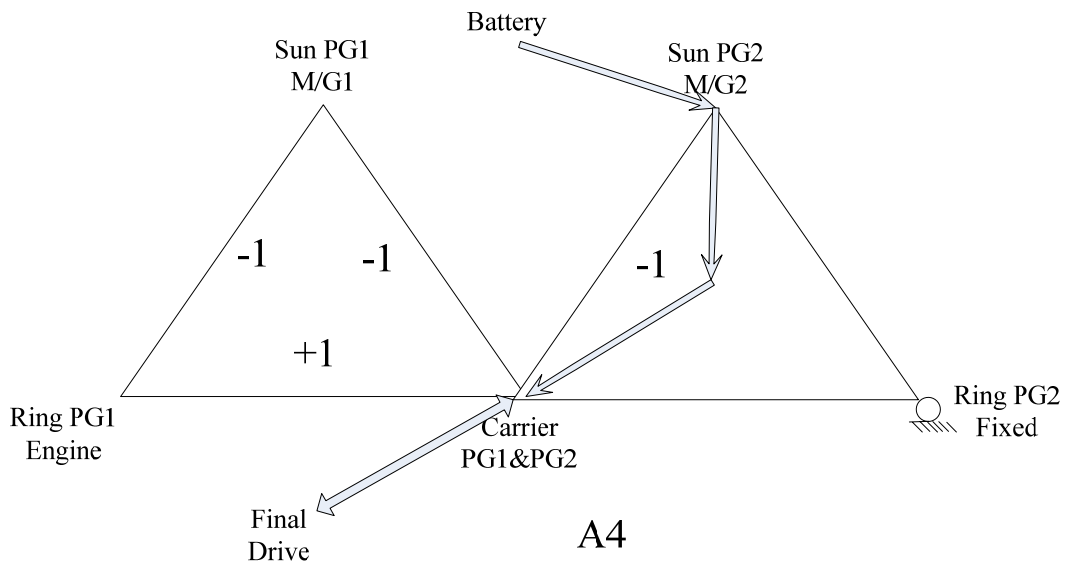


Figure 5-13 Power Flow Chart of Backward Movement in the First Mode

During the backward movement, only M/G2 is activated. The power flow is shown in Figure 5-13. Table 5-3 and Table 5-4 summarized the engine and the motor operation for the first mode.

There is no power circulation takes place except for backward movement.

Table 5-3 Summary of Engine, M/G1 and M/G2 in First Mode

| | Engine | M/G1 1 | M/G2 | Power Circulation |
|--------------------|----------|--------------|--------------|-------------------|
| Idle | On | As Generator | Off | No |
| Forward Power Low* | On | As Generator | As Generator | No |
| Forward Normal | On | As Generator | As Motor | No |
| Forward Brake | On | As Motor | As Generator | No |
| Backward | On/Off** | As Generator | As Motor | Yes* |

* Can be eliminated by accurate engine control

**Can turn off if battery SOC is high enough

Table 5-4 Power Flow Summary of First Mode

| Idle | Forward Power Low | Forward Normal | Forward Brake | Backward |
|-------------------|----------------------|-------------------|----------------|--|
| Engine-R1-S1-M/G1 | Engine-R1-S1-M/G1 | Engine-R1-S1-M/G1 | Out-C2-S2-M/G2 | Engine-R1-S1-M/G1 |
| | Engine-C1-Out | Engine-C1-Out | | M/G2-S2-C2-Out |
| | Engine-C1-C2-S2-M/G2 | M/G2-S2-C2-Out | | M/G2-S2-C2-C1-S1-M/G1(power circulation) |

5.1.4. The Second Mode of a Two-mode Transmission

Figure 5-14 is the drivetrain configuration of the second mode. In the second mode, the ring gear on PG2 is connected to the sun gear 1 instead of being grounded.

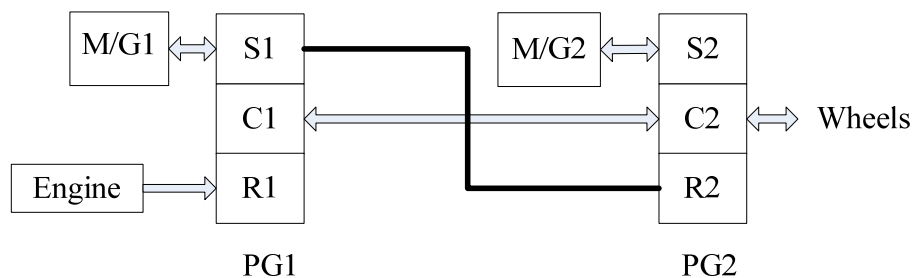


Figure 5-14 Second Mode Drivetrain Configuration

There are also four shafts connected to the planetary gears transmission. Eq. (5.20) is the absolute drive ratio between the output shaft and engine shaft, where ω the angular velocity as is defined previously. This gear train has two degrees of freedom, speed of both motors $\omega_{M/G1}, \omega_{M/G2}$ are determined by the engine speed and output speed in Eq. (5.21).

$$R_{c1r1} = \frac{\omega_{out}}{\omega_{engine}} = \frac{\omega_{c1}}{\omega_{r1}} = \frac{k}{1+k-R_{sc}} \quad (5.20)$$

$$\left. \begin{aligned} \omega_{M/G1} &= (k_1 + 1)\omega_{out} - k_1\omega_{Engine} \\ \omega_{M/G2} &= (1 - k_1k_2)\omega_{out} + k_1k_2\omega_{Engine} \end{aligned} \right\} \quad (5.21)$$

Using Eq. (5.6), torque relations are found in Eq. (5.22)

$$\left. \begin{aligned} T_{M/G1} &= -\frac{k_2}{k_2 + 1}T_{out} + \frac{1 - k_1k_2}{(1 + k_2)k_1}T_{Engine} \\ T_{M/G2} &= -\frac{1}{k_2 + 1}T_{out} - \frac{k_1 + 1}{(k_2 + 1)k_1}T_{Engine} \end{aligned} \right\} \quad (5.22)$$

At a vehicle speed lower than Vs3, the power flows factors (PF) of both planetary gears are shown in(5.18) using(5.8) and relations in Figure 5-10.

$$\left. \begin{aligned} \theta_{r1s1} &= 1, \theta_{r2s2} = 1 \\ \theta_{r1c1} &= -1, \theta_{r2c2} = -1 \\ \theta_{c1s1} &= -1, \theta_{c2s2} = -1 \end{aligned} \right\} \quad (5.23)$$

There are two possible power flows transformations at the vehicle speed of V3 or lower. The first one is shown in Figure 5-15 A1. Both M/G1 and M/G2 withdraw power from the ESS. The mechanical power provided by M/G1 is split into two paths to the wheel. One way goes through S1 to C1; the other way goes through R2 to C2. This power flow mode is favourable when vehicle speed is between V_shift and Vs2, as shown in Figure 5-10. The reason for it is the low speed of M/G1 between V_shift and Vs2, which provides relative low power to the wheel. M/G2 acts as a motor to provide additional torque.

The second power flow direction is shown in Figure 5-15 A2. As the speed of M/G1 increases, power output at M/G1 increases. At certain speed V_{s2} when M/G1 and engine provides more power than the wheel required, M/G2 switches from motor to generator.

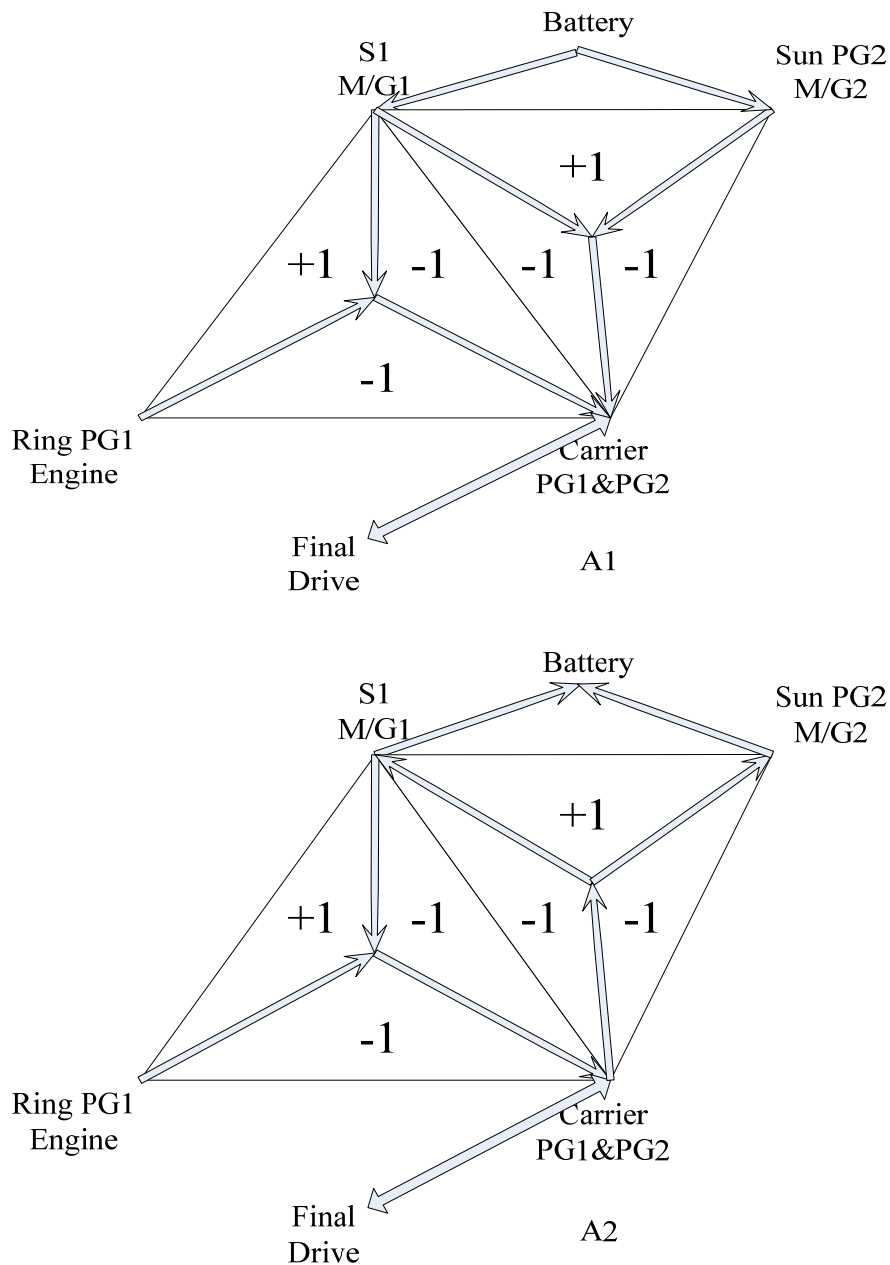


Figure 5-15 Power Flow of Second Mode at Vehicle Speed of V_{s3} or Lower

Node S1 receives power from both M/G1 and ring 2 through internal power circulation. As

vehicle speed increases, M/G1 switches to generator if power from ring 2 is adequate for node S1. This speed is defined as Vs4. In this study, the speed Vs4 greater than Vs3 was assumed. As a result, M/G1 is always a motor when the vehicle speed is below Vs3. While the vehicle is decelerating or braking at this speed range, the power is split between M/G1 and M/G2 to generate power. The second mode also enables the system to recapture more power than in the first mode, as both electrical machines could be activated. This feature is also beneficial to capture the higher braking power at higher speed. The shaft to engine is also disconnected by a clutch while braking as a result of opposite direction torque provided to the engine. The power flow of braking is shown in Figure 5-16.

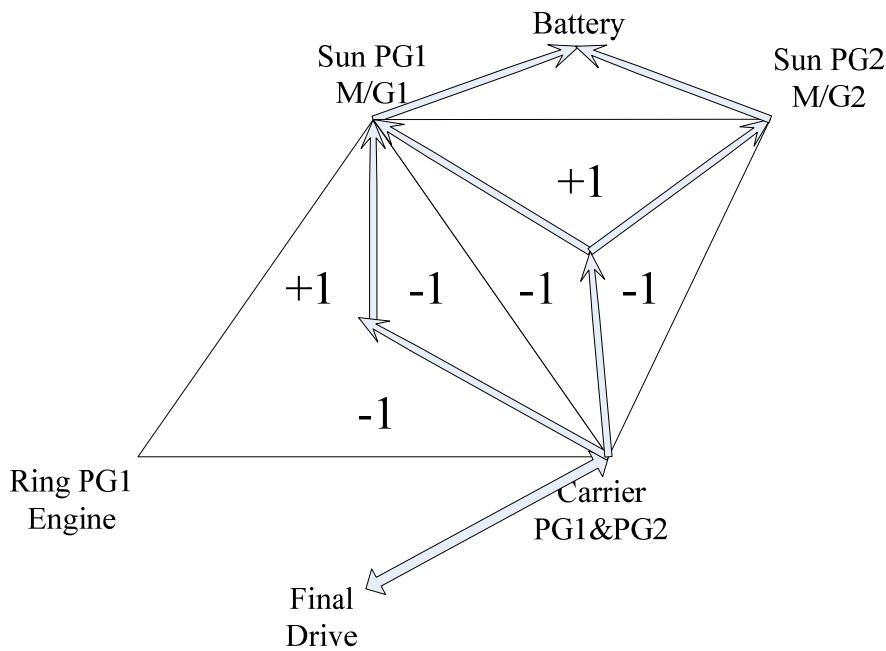


Figure 5-16 Power Flow of Second Mode during Brake at a Vehicle Speed of Vs3 or Lower

After the vehicle speed reaches higher than Vs3, the direction of M/G2 changes as in Figure 5-10. The FP is changed accordingly in Eq. (5.24).

$$\left. \begin{aligned} \theta_{r1s1} = 1, \theta_{r2s2} = -1 \\ \theta_{r1c1} = -1, \theta_{r2c2} = -1 \\ \theta_{c1s1} = -1, \theta_{c2s2} = 1 \end{aligned} \right\} \quad (5.24)$$

The power flow transformation at a vehicle speed higher than V_{s3} is shown in Figure 5-17.

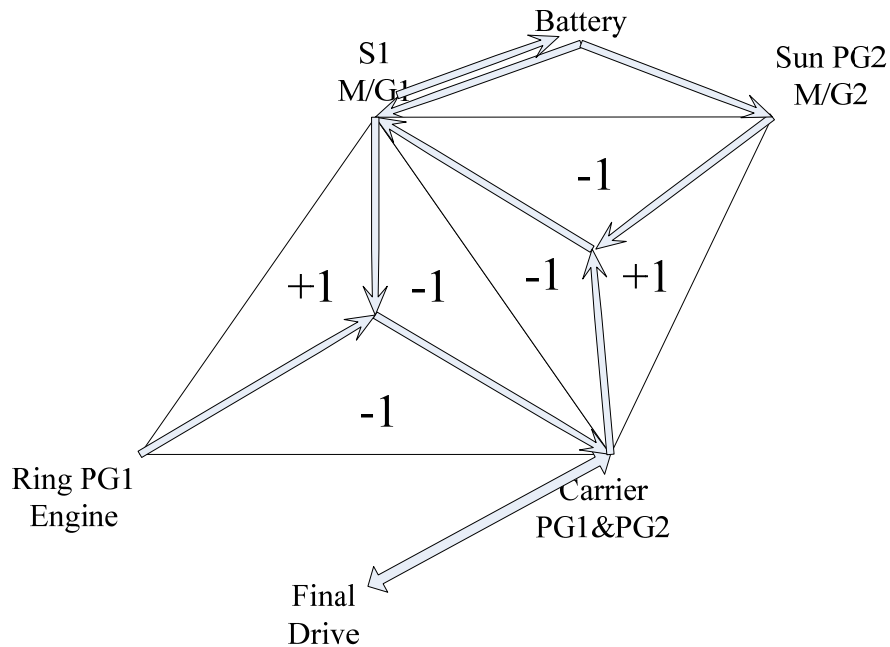


Figure 5-17 Power Flow of Second Mode at a Vehicle Speed Greater than V_{s3}

Node S1 receives power from both M/G1 and ring 2. At a vehicle speed between V_3 and V_4 , M/G1 acts as a motor since power received from ring 2 is lower than power demanded at S1. Power from engine is added to power from node S1 and sent to carrier 1. Output power from M/G2 is split into two paths. One way goes directly to the wheel and the other way goes through S1. While the vehicle speed is greater than V_{s4} , M/G1 switches from a motor to a generator. In this case, part of the power would circulate from M/G2 back to M/G1. The power flow at node S1 changes to charge battery.

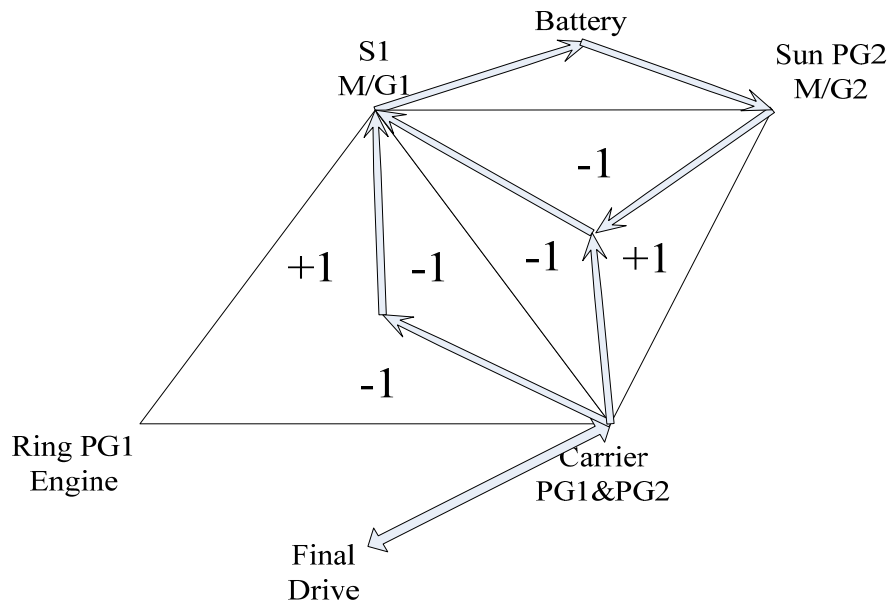


Figure 5-18 Power Flow of Second Mode Brake at Speed over V_{s3}

Figure 5-18 is the power flow of second mode while braking. The braking energy is regenerated by M/G1. There are two paths of power flow. One way goes through PG1 to S1. The other way goes through PG2. In the second path, torque from M/G2 is added and sent to M/G1. Compared with braking at lower speed in Figure 5-16, less power could be captured as only M/G1 could be active. More braking power aid from friction brake would be needed.

The operation of engine and motors were summarized in Table 5-5. Power circulation took place at several operation conditions. The circulated paths were summarized at

Table 5-6.

Table 5-5 Summary of Engine, M/G1 and M/G2 in Second Mode

| Speed Range | Engine | M/G1 | M/G 2 | Power Circulation |
|----------------------------|------------|-----------|-----------|-------------------|
| $V_{_}$ shift to V_{s2} | On | Motor | Motor | No |
| V_{s2} - V_{s3} | On | Motor | Generator | Yes |
| Brake < V_{s3} | Disengaged | Generator | Generator | No |
| V_{s3} - V_{s4} | On | Motor | Motor | Yes |

| | | | | |
|-----------|------------|-----------|-------|-----|
| Vs4- | On | Generator | Motor | Yes |
| Brake>Vs3 | Disengaged | Generator | Motor | |

Table 5-6 Power Flow Summary of Second Mode

| V_shift to Vs2 | Vs2-Vs3 | Brake<Vs3 | Vs3-Vs4 | Vs4- | Brake>Vs3 |
|-----------------------|-----------------------|---------------------|-----------------------|----------------------------|---------------------|
| Engine-R1-C1-Out | Engine-R1-C1-Out | Out-C2-R2-M/G1 | Engine-R1-C1-Out | Engine-R1-C1-Out | Out-C2-R2-M/G1 |
| M/G1-S1-C1-Out | M/G1-S1-C1-Out | Out-C2-S1-M/G2 | M/G1-S1-C1-Out | M/G2-S2-R2-S1-C1-Out | M/G2-S2-R2-M/G1 |
| M/G1-R2-C2-Out | M/G1-S1-C1-C2-R2-M/G1 | | M/G2-S2-R2-S1-C1-out | M/G2-S2-R2-S1-M/G1 | |
| M/G2-S2-C2-Out | M/G1-S1-C1-C2-S2-M/G2 | | M/G1-S1-C1-C2-R2-M/G1 | Engine-R1-C1-C2-R2-S1-M/G1 | |

5.2. Vehicle Modeling in ADVISOR

The power source of a two-mode hybrid electric vehicle consists of an ICE and two electric motors. The principal theory is to improve the ICE operation efficiency during the vehicle operation with the assists from both electric motors as well as ESS. Two electric motors served as either motor or generator depending on mode and speed to coordinate power flow between the vehicle demand and ICE output. The excess power generated or consumed was charged or discharged by the ESS. The ICE operation was determined by the vehicle power demand and SOC of ESS. Therefore, SOC of ESS was maintained at a predetermined range for optimal charge/discharge capability, efficiency and longer cycle life.

The advantage with two-mode was that the ICE ran at its optimal combination of speed and torque at all the time. The engine fuel consumption is therefore much lower. However, part of the power goes through two conventions during the transportation of the energy between the ICE and the wheels (ICE-Generator-Motor-Wheel) which creates power loss on electrics. Energy

lost because of the ESS inner resistance, friction and planetary gears are also worth consideration.

5.2.1. Modeling of Drivetrain

The modeling of a drivetrain in a two-mode hybrid vehicle shares lots of similarity with the powertrain modeling in the elevator model. The “power at the wheels” P_{wheel} , which is a sum of the total mechanical power demanded, is calculated according to vehicle speed and acceleration. The power at the wheels model, calculated as the dot product of the vehicle velocity and the various forces acting upon the vehicle, considers the following determining factors as shown in Figure 5-19. The four resistances a vehicle facing were force for acceleration, force to overcome gravity, rolling resistance of the wheels, aerodynamic resistance or drag.

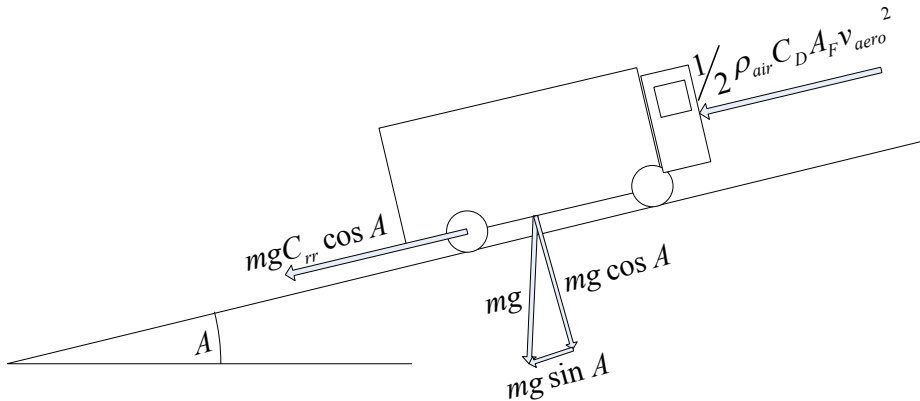


Figure 5-19 Free Body Diagram of a Truck

The power at the wheels model is given by:

$$\begin{aligned}
 P_{wheel} &= \sum Force \times v = (F_{acceleration} + F_{incline} + F_{rr} + F_{drag}) \times v \\
 &= (ma + mg \sin A + mg C_{rr} \cos A + \frac{1}{2} \rho_{air} C_D A_F v_{aero}^2) \times v
 \end{aligned} \tag{5.25}$$

where m is the total mass of vehicle, a is the vehicle acceleration, v is the vehicle velocity, A is the angle of slope, C_{rr} is the coefficient of tire rolling resistance, C_D is the drag coefficient, ρ is the density of air, A_F is the frontal cross-section area, and v_{aero} is the velocity of the vehicle plus the

headwind (m/s). The coefficient of rolling resistance (C_{rr}) was experimentally obtained. It was a function of many factors including the deformation of the tire, weight of the vehicle, tire pressure, roughness of the surface and radius of the wheel. It was the ratio of the rolling resistance force to the load on the tires. It was fairly constant for a given tire and road surface. In the aerodynamic drag term, the drag coefficient C_D was a dimensionless constant that attempted to capture the resistance caused by the relative motion of the vehicle and the air. The C_D can vary from as high as 1.2 for a bicycle with an erect rider to 0.7 for a truck, and to 0.20 for a very aerodynamically styled sport car. Although the equation used to determine the drag power was a simplification, it avoided complex airflow simulation while preserved the general behaviours of the drag force with respect to velocity. The frontal cross-section area was measured on the truck by projecting a bright light directly onto the front of the truck and then measuring the area of the shadow on a wall behind to obtain the cross-sectional area. The density of air ρ is approximately 1.23 kg/m^3 . Vehicle modeling parameters for a trust of interest are listed in Table 5-7.

Table 5-7 Modeling Parameters

| Vehicle | C_D | C_{rr} | $A_F (\text{m}^2)$ | Curb Weight (kg) | Auxiliary Power (W) |
|------------------|-------|----------|--------------------|----------------------|---------------------|
| Class 7 Truck | 0.7 | 0.009 | 8.55 | 5818 | 7450 |
| Mid-size Sedan | 0.3 | 0.009 | 1.7 | 1500 | 700 |
| Electric Scooter | 0.9 | 0.014 | 0.6 | 105 | 60 |

The truck coefficient of tire rolling resistance was estimated to be 0.009 by NREL research group. The drag coefficient and frontal area were obtained Based on a Kenworth T400 truck. The velocity dependence of the rolling resistance coefficient was likewise neglected.

5.2.2. Modeling of Engine

An ICE is a complex assembly a variety of components that are designed on the basis of aerodynamic laws. A mathematical engine model with individual components is complicated.

Also, the engines designed by different manufacturers can be significant different in material and structure. Therefore, it is difficult to quantified modeling parameters which are also confidential.

In the vehicle simulation, engine model was used to represent the accuracy of fuel consumption and emission calculation. An empirical model based on test data of existing engine served as a choice for this particular need. In this study, the engine test data was based on a 7.3L diesel engine and implemented in ADVISOR model. Figure 5-20 is a schematic diagram of engine model in ADVISOR. The required torque and speed was calculated from externally as an input signal to this block. The engine model decided the torque and speed available to delivery and calculated fuel and emission accordingly.

The existing engine data was obtained from a Detroit diesel 7.3L engine. Two look-up maps were in this model, engine torque and fuel consumption. Engine torque map decided engine torque limit at each speed, while fuel consumption table decide fuel rate (g/s) of engine speed and torque.

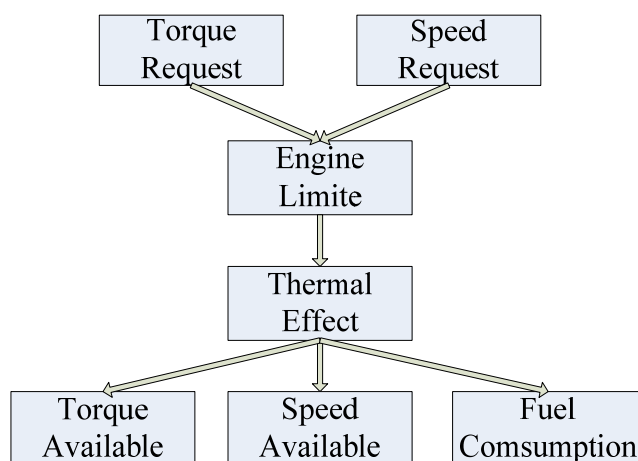


Figure 5-20 Engine Model Schematic Diagram

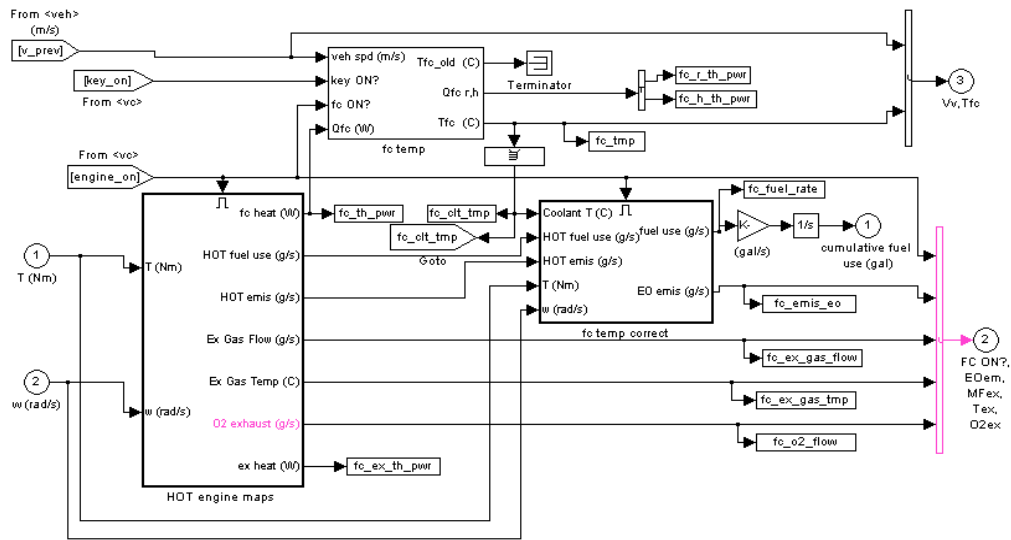


Figure 5-21 Simulink Block Diagram of Engine Thermal and Fuel Model

Figure 5-21 shows the Simulink diagram of engine thermal model in ADVISOR. Engine temperature was calculated based on engine friction, material conductivity and coolant temperature. Due to availability of test data, thermal effect was not considered. A more accurate result of fuel and emission data could be obtained if thermal test data becomes available.

5.2.3. Modeling of a Two-mode Transmission

The need for the higher highway fuel economy and higher power output leads to further mechanical development of the two-mode transmission. A two-mode transmission includes an input split mode and a compound split mode. Several mechanical clutches were used for mode switch. The powertrain of a two-mode HEV is shown in Figure 5-22.

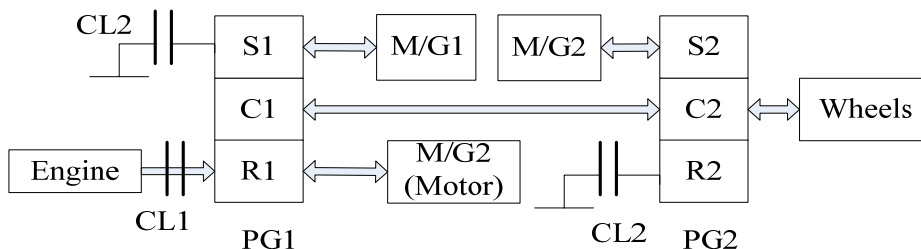


Figure 5-22 A Schematic Diagram of Two-mode HEV

The first mode of the two-mode transmission was activated when clutches CL1=1, CL2=0, CL3=1, as shown earlier in Figure 5-9. Engine was engaged with ring gear 1. The ring gear of PG2 was fixed through clutch 3. In first mode, the system operated as input split. M/G1 operated as generator and M/G2 operated as a motor. The drivetrain configuration of first mode is shown in Figure 5-9. The input torque of engine from ring gear 1 was split between carrier 1 and sun gear 1. The torque received at M/G1 and carrier 1 use Eq. (5.26) and Eq. (5.27),

$$T_{M/G1} = \frac{1}{k_1}(T_{Engine} - J_{ring1}\dot{\omega}_{ring1} - J_{sun1}\dot{\omega}_{sun1}) \quad (5.26)$$

$$T_{out1} = T_{C1} = \frac{k_1+1}{k_1}(T_{Engine} - J_{ring1}\dot{\omega}_{ring1} - J_{carrier}\dot{\omega}_{carrier}) \quad (5.27)$$

PG2 at this mode was in fact a torque multiplier. As ring gear on PG2 was grounded, the motor torque is then transfer to the final shaft as in Eq. (5.28),

$$T_{out2} = -(k_2+1)(T_{M/G2} - J_{sun2}\dot{\omega}_{sun2} - J_{carrier}\dot{\omega}_{carrier}) \quad (5.28)$$

That final torque available to the final shaft is Eq. (5.29)

$$\begin{aligned} T_{out} = T_{out1} + T_{out2} = & \frac{k_1+1}{k_1}T_{Engine} - \frac{k_1+1}{k_1}(J_{ring1}\dot{\omega}_{ring1} + J_{carrier}\dot{\omega}_{carrier}) \\ & -(k_2+1)T_{M/G2} - (k_2+1)(J_{sun2}(k_2+1)\dot{\omega}_{carrier} + J_{carrier}\dot{\omega}_{carrier}) \end{aligned} \quad (5.29)$$

As k_1 equals to k_2 in this study, the final torque is further simplified as Eq. (5.30)

$$T_{out} = (1 + \frac{1}{k})T_{Engine} - (1+k)T_{M/G2} - \dot{\omega}_{carrier}((2 + \frac{1}{k} + k)J_{carrier} + (k+1)^2 J_{sun2}) - \dot{\omega}_{ring1}(1 + \frac{1}{k})J_{ring1} \quad (5.30)$$

The second mode of the two-mode transmission was activated when clutches CL=1, CL2=1, CL3=0. The engine was engaged with ring gear 1 to provide the power instead of being fixed. The ring gear of PG2 was connected to M/G1. The system then operated as both input and

output split. In this mode, the input torque of engine from ring gear 1 was split between carrier 1 and sun gear 1. The received Torque at M/G1 and carrier 1 are using Eq. (5.31) and(5.32),

$$T_{M/G1} = \frac{1}{k_1}(T_{Engine} - J_{ring1}\dot{\omega}_{ring1} - J_{sun1}\dot{\omega}_{sun1}) \quad (5.31)$$

$$T_{out1} = T_{C1} = \frac{k_1+1}{k_1}(T_{Engine} - J_{ring1}\dot{\omega}_{ring1} - J_{carrier}\dot{\omega}_{carrier}) \quad (5.32)$$

PG2 at this mode was also a torque splitter. As ring gear on PG2 connected to M/G1, the motor torque was transferred to the final shaft as in Eq. (5.33).

$$T_{out} = -(k_2+1)T_{M/G2} - \frac{k_1+1}{k_1}T_{Engine} \quad (5.33)$$

That final torque available to the final shaft was decided. As k_1 equals to k_2 in this study, the result was simplified as the following equation,

$$T_{out} = -(1+\frac{1}{k})T_{Engine} - (1+k)T_{M/G2} - \dot{\omega}_{carrier}((2+\frac{1}{k}+k)J_{carrier} + (k+1)^2J_{sun2}) - \dot{\omega}_{ring1}(1+\frac{1}{k})J_{ring1} \quad (5.34)$$

Based on speed and torque relations explained in chapter 5.1 and section 5.2.3, a two-mode transmission model was built in Simulink to incorporate with the rest of ADVISOR models. Figure 5-23 is the top level of a two-mode transmission model built in Simulink. This model received 5 inputs externally and sent out 4 outputs. These inputs and outputs decide the torque and speed for a specific powertrain components based on demand from one other. The functionalities of the input and output ports are explain in Table 5-8.

Table 5-8 Signal Interface Explanation of a Two-mode Transmission Model

| Inputs | | Outputs | |
|--------|---|---------|--|
| Input1 | Torque and speed required from output shaft | Out1 | Torque and speed available at output shaft |
| Input2 | Torque and speed available at engine | Out2 | Torque and speed required from engine |
| Input3 | Torque and speed available at M/G1 | Out3 | Torque and speed required from M/G1 |
| Input4 | Torque and speed available at M/G2 | Out4 | Torque and speed required from M/G2 |
| Input5 | Mode Shifting Signal | | |

The model contains three blocks, a first mode block, a second mode block and a mode selector as shown in Figure 5-23. When one mode is activated, the other mode block is bypassed. The mode selection is decided by input 5 which contains engine speed to be used with vehicle speed.

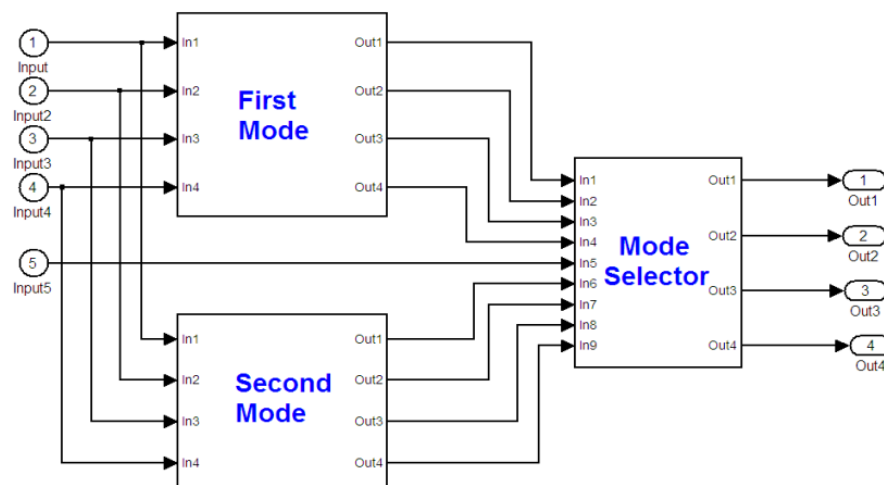
**Figure 5-23 Two-mode Transmission Model and its Controller**

Figure 5-24 is the detailed diagram in first mode block. The torque and speed on each gear were calculated according to relations explained previously. The second mode block was constructed on a similar basis, which is not explained in detail.

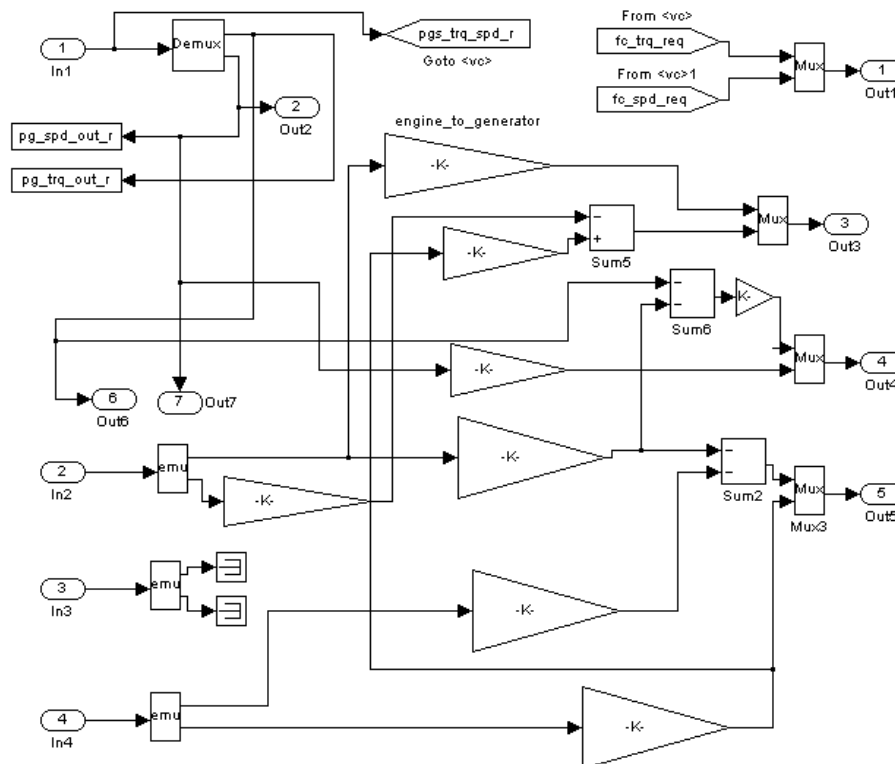


Figure 5-24 First Mode Block in Transmission Model

5.3. Control Strategy of a Two-mode Hybrid Vehicle

5.3.1. Review on HEV Control Development

The control strategies of hybrid electric are in an area of high interest due to the complex nature of hybrid electric vehicles. Engineering intuitions based control strategies frequently fail to achieve the optimal of overall system efficiency. An optimal control strategy for a parallel hybrid truck using dynamic programming methods was introduced in [63, 64]. Other researchers explored different ways leading to an optimal control to minimize fuel consumption of parallel hybrid vehicles in general [9, 65-68]. An approach to control powertrain of series hybrid electric vehicles from the aspect of excitation of motor winding control was presented in [69]. Power management logics for fuel cells hybrid electric vehicles were given in [70, 71].

The study of two-mode hybrid vehicles control strategy was not available in literature. The review and modeling of two-mode hybrid electric were studied in detail by the author's research group [11]. The control theory in this simulation is explained in the following section.

5.3.2. Mode Selection

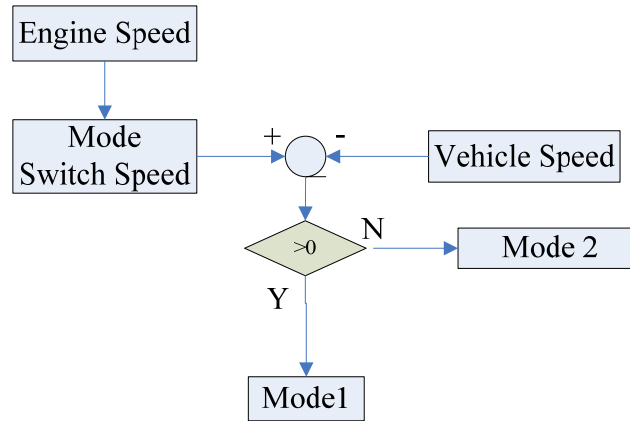


Figure 5-25 Mode Switch Control

Figure 5-25 shows the basis on how the mode is selected. The mode switch speed is determined by the engine speed. With an engine speed range between 2000 rpm and 3000 rpm, the mode switch speed changes from 40 km/hr to 60 km/hr. If the current vehicles become greater than the mode switch speed, mode 2 will be chosen. Otherwise, mode 1 will be selected. In a two-mode configuration, the mode was switched when both ends of the clutch reached the same speed. It also guaranteed the smooth operation of the vehicle. During the mode switch according to Figure 5-26, the engagement of clutch 2/3 was switched from fixtue to sun gear 1 when M/G1 reaches stationary point (direction change). The switch speed (in *km/h*) was decided using the following equation.

$$V_{switch} = \left(\frac{k_1}{1+k_1} \right) \omega_{engine} \div R_{final} \times r_{wheel} \times 3.6 \quad (5.35)$$

5.3.3. Power Management of First Mode

Due to the difference of mechanic configurations on each of the two modes, power management strategies were studied differently. On first mode, as the configuration shown in Figure 5-9, ring gear of PG2 was fixed.

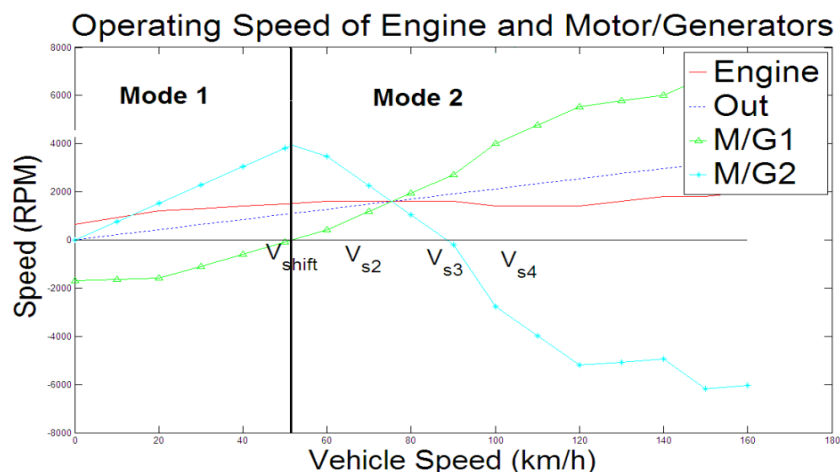


Figure 5-26 Speed Profile of All Shafts (Engine Speed predefined)

The control strategy of mode 1 is explained in Figure 5-27. As in a backward mode, the power demand from the transmission output can be calculated according to speed profile of drivecycle and the vehicle dynamic model. Instead of producing the exact power at each time instance, such as on a non-hybrid vehicle, the engine on a hybrid vehicle only produced the average power demand based on last 14 seconds power demand average. The speed of both motors discussed in section 5.1.3 was calculated from the engine speed and vehicle speed. The torque of M/G1 was decided by engine, to ensure the transmission operating at relative steady status. M/G2 produced the supplementary torque to the final drive.

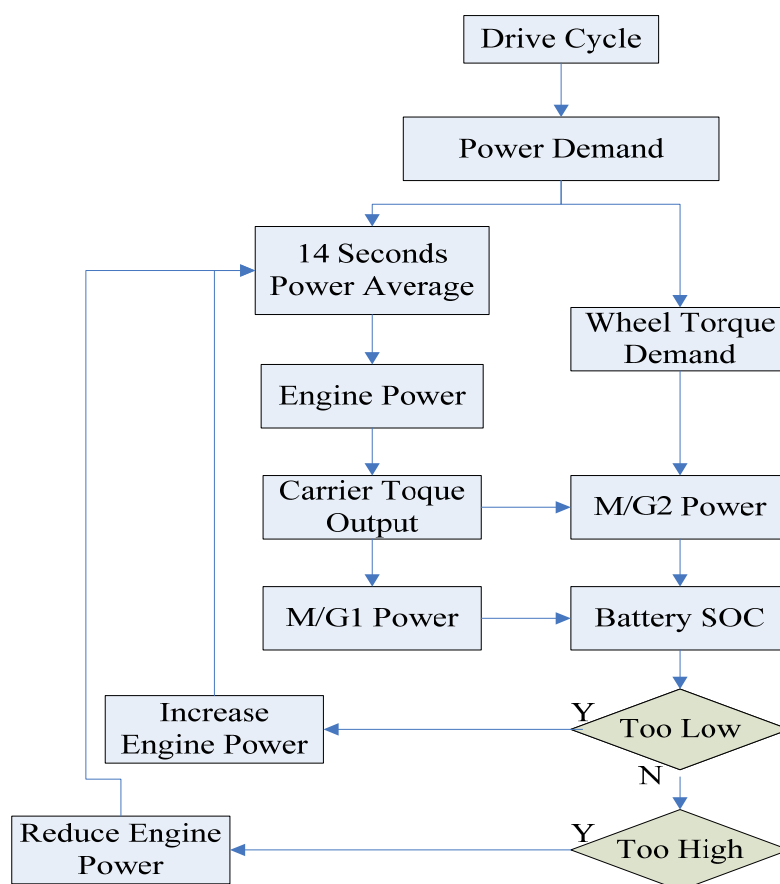


Figure 5-27 Power Management Chart Mode 1

The main objective of this control theory was to maintain the battery SOC within a predefined range. Table 5-9 showed the value of SOC target and range in this simulation. In order to catch regenerative braking power, the SOC range was decided at between 0.45 and 0.75, with a target at 0.6. While the battery operated with the predefined SOC range, a control signal was generated either to increase or reduce the engine power so that the target SOC could be achieved. While operating beyond the range, as a reason of battery inefficiency or low capability, a penalty value was added to ensure the battery operating within the range.

Table 5-9 ESS SOC Management

| Initial | Target | Low | High |
|---------|--------|------|------|
| 0.7 | 0.6 | 0.45 | 0.75 |

5.3.4. Power Management of Second Mode

The power management chart of second mode is as shown in Figure 5-28. The only difference between first and second mode is how M/G1 power was decided. In second mode, M/G1 was connected to both sun gear on PG1 and ring gear on PG2. Therefore, power of M/G1 was decided by both the output wheels.

The ESS SOC management for this mode was same as that in first mode. Therefore, the same control theory was used as discussed previously.

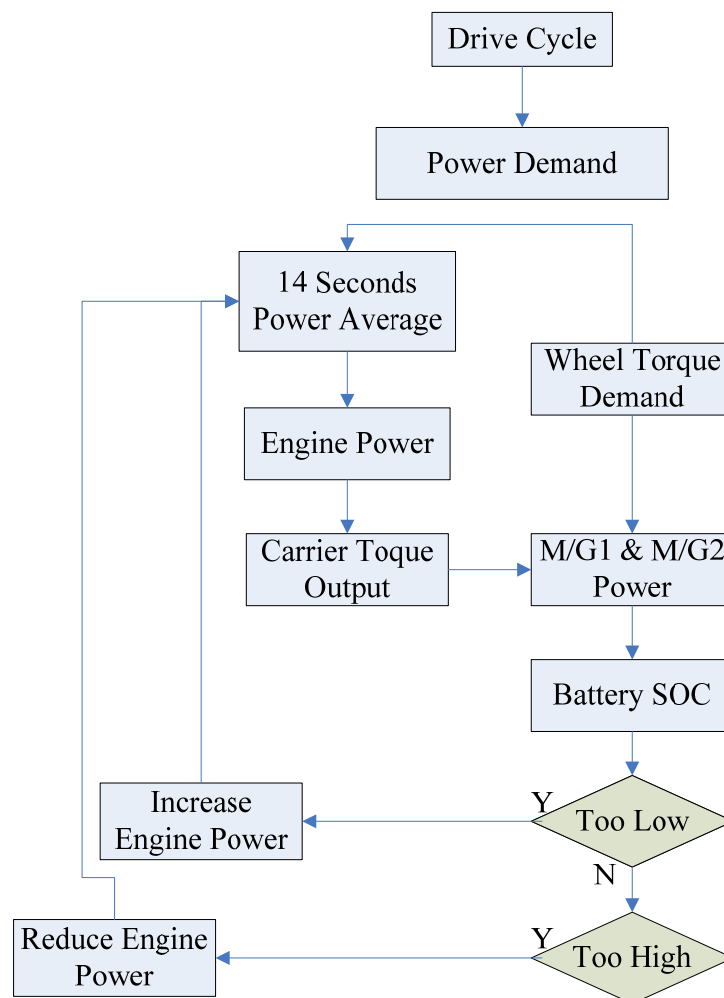


Figure 5-28 Power Management Chart Mode 2

5.4. Computer Simulation

To evaluate the performance of a two-mode hybrid vehicle, a conventional vehicle model was used as a guideline. The modeling of the conventional vehicle was described by [28]. The vehicle weight reflected the vehicle in a loaded condition. The specification of the vehicle simulated is shown in Table 5-10.

Table 5-10 Simulation Vehicles Specification

| | | |
|---------------------|-----------------------|------------------------------|
| Two-mode | Engine | 171 <i>kW</i> Diesel |
| | Motor/Generator 1 | GE-AC83 |
| | Motor/Generator 2 | GE-AC83 |
| | Energy Storage System | 200 Units of Ni-MH 6Ah/7.2V |
| | Transmission | 2 Planetary Gears |
| | Weight | 12311 <i>kg</i> |
| Conventional | Engine | 246 <i>kW</i> Cummins Diesel |
| | Transmission | Eaton Fuller 10-Speed |
| | Weight | 12311 <i>kg</i> |

5.4.1. Drive Cycles

Drive cycles for real life vehicles are well developed. These velocity profiles can be valuable in exploring and comparing the performance of different vehicles, as they can closely reflect real-world driving patterns. Many of these driving cycles are standardized for particular purposes by various international bodies. For example determining the city and highway mileage figures for new cars is accomplished by using two different standard velocity profiles. Other driving cycles had been obtained experimentally from driving in various regions, including New York City during a daily commute, or on the highway in Madras, India. After the simulation was completed, results can be obtained including values from the vehicle as a whole or of individual sub-systems. Information from individual time periods during the simulation or aggregate results can be collected and compared. The model showed the difference between the achieved speed and the desired speed, as well as how much power was required to reach the

driving cycle. Four drive cycles were chosen for the simulations. These drive cycles represent drive schedules for all types of conditions.

Urban Dynamometer Driving Schedule for Heavy Duty Vehicles (UDDSHEV)

UDDSHEV represents a less busy traffic urban drive condition for heavy duty vehicles. It is an 8.94 *km* cycle last 1060 seconds. The average speed is 30.3 *km/h* while the max speed is as high as 92 *km/h*. The peak acceleration is 2m/s². There are 14 stops during the cycle. The total idling time is 353 seconds.

New York City Truck Driving Schedule (NYCTRUCK)

NYCTRUCK represents a busier traffic urban drive condition for heavy duty vehicles based on New York City. It is a 3.43 *km* cycle last 1016 seconds. The average speed is 12.16 *km/h* while the max speed is as high as 54.7 *km/h*. The peak acceleration is 2m/s². There are 20 stops during the cycle. The total idling time is 529 seconds.

City Suburban Heavy Vehicle Route (CSHVR)

CSHVR represents a composite drive cycle of various macro trip pulled from on-road test data. It represents typical city suburban driving for a heavy vehicle. It is a 10.81 *km* cycle last 1780 seconds. The average speed is 21.86 *km/h* while the max speed is as high as 70.49 *km/h*. The peak acceleration is 1.16m/s². There are 18 stops during the cycle. The total idling time is 385 seconds.

Highway Fuel Economy Test (HWFET)

Highway Fuel Economy Test (HWFET) driving cycle used by the US EPA for Corporate Average Fuel Economy certification of passenger vehicles in the US. It is a 16.51 *km* cycle last 765 seconds. The average speed is 77.58 *km/h* while the max speed is as high as 96.4 *km/h*. The peak acceleration is 1.43m/s². There is only 1 stop during the cycle. The total idling time is 6 seconds.

5.4.2. Road Performance

In this section, the road performance of the two-mode vehicle model was presented based on four drive cycles. The simulation results on these speed profiles were first compared with speed requested (drive cycle). Then an acceleration test and a grade ability test were carried out.

Figure 5-29 shows the simulation result of vehicle speed following the UDDSHEV drivecycle. The dashed line is cycle speed requested while the solid line is vehicle speed achieved. There were barely noticeable differences between the two which are circled in the figure.

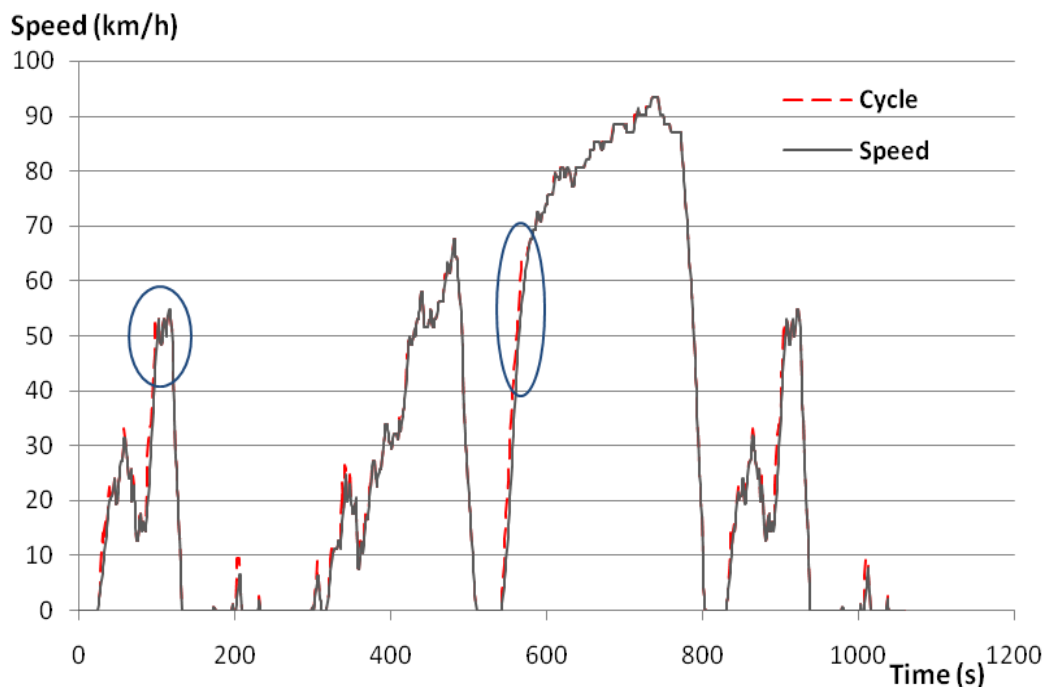


Figure 5-29 Vehicle Speed on the UDDSHEV Cycle

Figure 5-30 shows the simulation result of the vehicle speed on the NYCTRUCK drivecycle. The dashed line is cycle speed requested while the solid line is vehicle speed achieved. The speed differences between the two are circled in the figure. The vehicle showed slightly under power during the rapid acceleration. However, the difference was within the acceptable range.

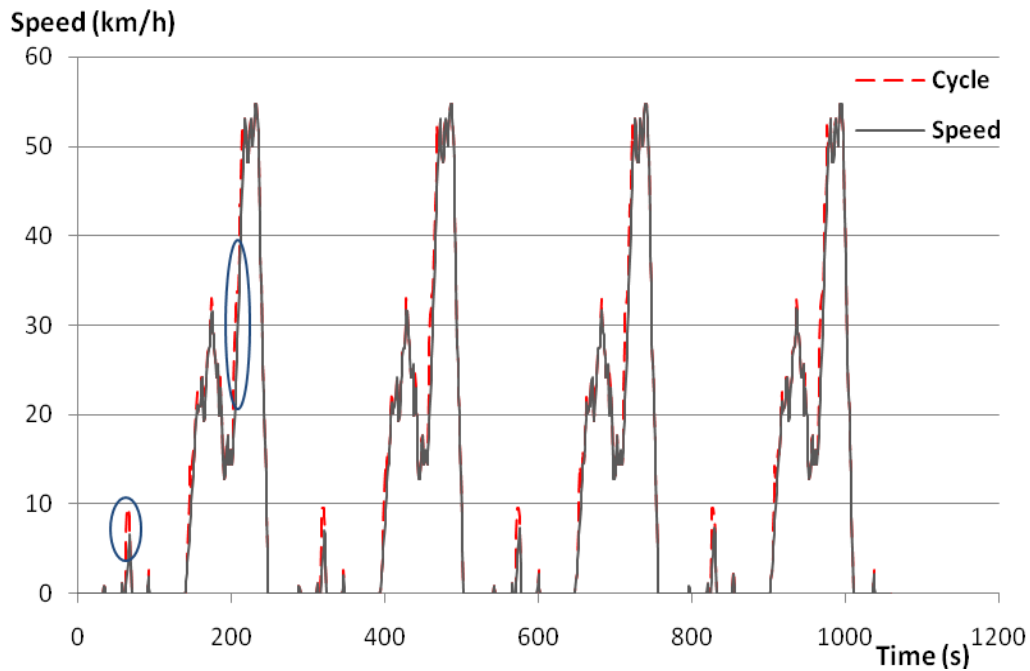


Figure 5-30 Vehicle Speed on NYCTRUCK Cycle

Figure 5-31 shows the simulation result of vehicle speed following the CSHVR drivecycle. The dashed line is cycle speed requested while the solid line is vehicle speed achieved. The average speed difference was 0.67 km/h . The vehicle showed adequate power supply at higher speed. The missing cycle was mostly due to gearbox response at low speed.

The simulation result of vehicle speed on the HWFET cycle is shown in Figure 5-32. The dashed line is cycle speed requested while the solid line is vehicle speed achieved. The average speed difference was 0.7 km/h . The vehicle showed slightly under power during acceleration. The speed curve on the high speed was nicely satisfied. The missing cycles are circled in the figure.

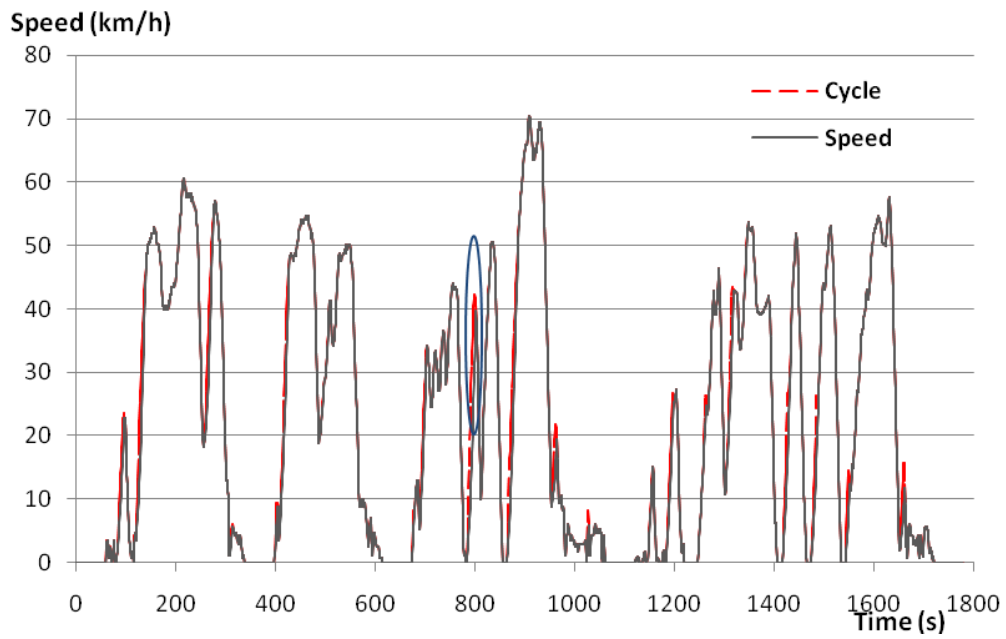


Figure 5-31 Vehicle Speed on CSHVR Cycle

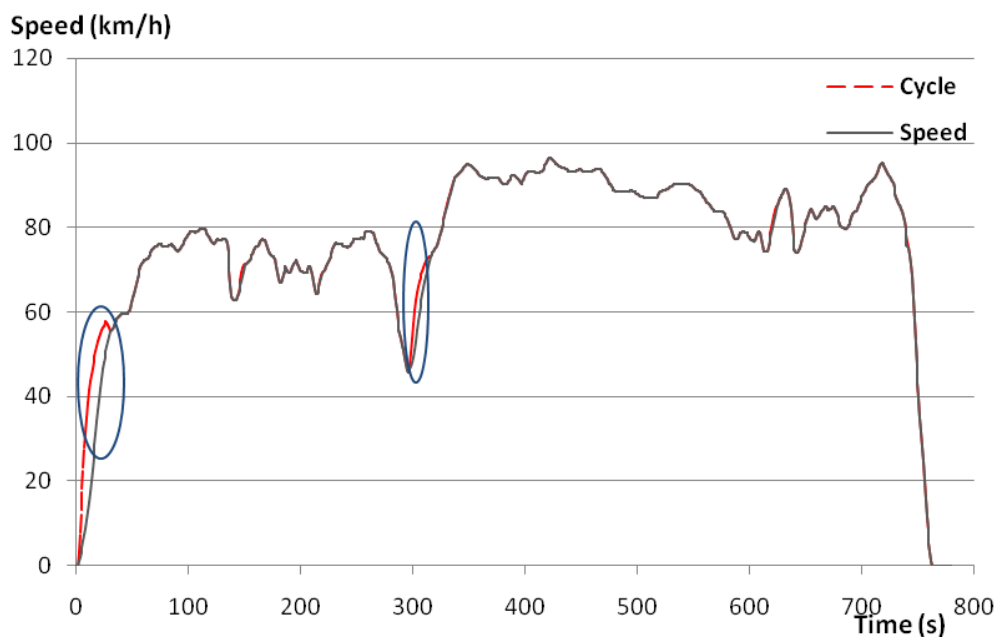


Figure 5-32 Vehicle Speed on HWFET Cycle

5.4.3. System Operation

Using ADVISOR, the performance characteristic of each subsystem can be obtained. In this section, NYCTRUCK cycle was used as the simulation cycle. The operation condition on each of the components were simulated and analyzed. Figure 5-33 shows the engine power and vehicle power demand during NYCTRUCK driving cycle. The engine power demand was calculated based on the average power demand of last 14 seconds. Therefore, the engine power curve was much smoother than the actual real time power demand. A negative value on engine power was a result of engine brake. Figure 5-34 further shows the power demand at both electric motors, where a negative value represent power generation mode. From this result, the output power at M/G2 was in much dramatic changing manner than M/G1.

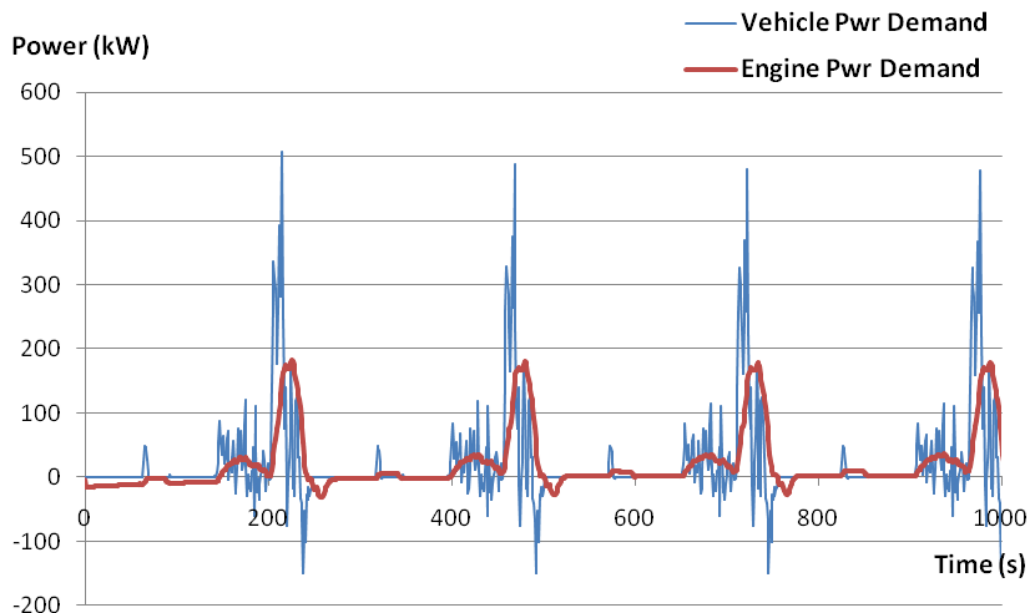


Figure 5-33 Engine Power on NYCCTRUCK Cycle

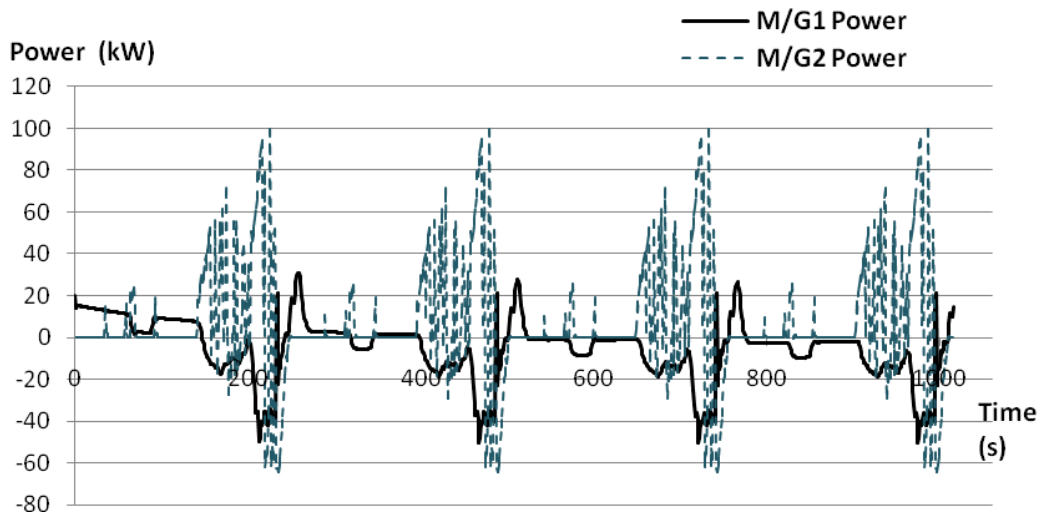


Figure 5-34 Electric Motors Power Demand over NYC TRUCK Cycle

Figure 5-35 shows the speed of the engine, the electric motors and the output shaft. The engine speed was no longer decided by gear ratio but by different control strategies. The engine was designed to operate at an optimal speed regarding to every power demand. The negative value on M/G1 speed reflected the opposite direction of rotation.

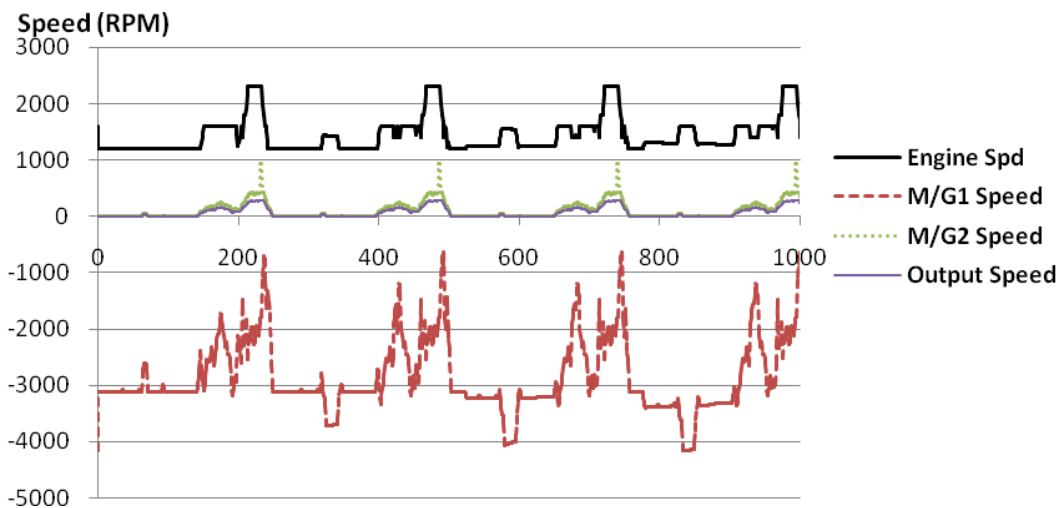


Figure 5-35 Speed of Engine and Electric Motors on NYC TRUCK Cycle

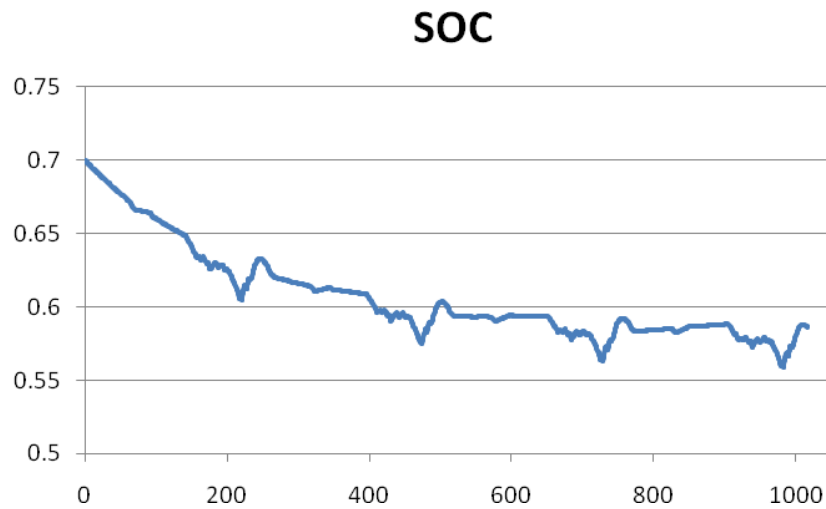


Figure 5-36 Battery SOC History on NYCTRUCK

Figure 5-36 is the history of battery SOC during running the NYCTRUCK cycle. The initial ESS SOC was 0.7. The operation range was between 0.55 and 0.7. The downward trend of the curve reflected the discharging nature during the short simulation period. The fluctuant of SOC was caused by charging power from regenerative braking.

5.4.4. System Efficiency

Hybrid electric vehicles achieve a higher fuel economy by improving efficiency of engine operation. However, electric power loss is introduced due to the additional electric motors and energy storage system. To evaluate the overall system, efficiency of sub components were simulated and analyzed. Engine efficiency was calculated based on mechanical energy produced divided by energy from fuel. Efficiencies of both electric motors considered both power mode and regenerative mode. The axle loss between the two vehicles was the same. The overall efficiency was calculated as Eq. (5.36);

$$\text{System Efficiency} = \frac{\text{aerodynamic drag} + \text{rolling resistance}}{\text{fuel} + \text{ESS SOC}}$$

(5.36)

Figure 5-37 to Figure 5-40 are simulation results of the system efficiency on each subsystem. It shows that the engine efficiency on most driving cycles was improved while an electric loss was also introduced. The added loss was on energy storage systems and both electric motors. The efficiency of electrical components on a conventional vehicle of an ICE engine was assumed to be 100% since it is not equipped with these electrical components. The engine efficiency improvement was considerably greater than the improvement of the overall system. Therefore, efficiency improvement on electrical components (electric motors, energy storage system and power electronics) would further help to improve the overall efficiency.

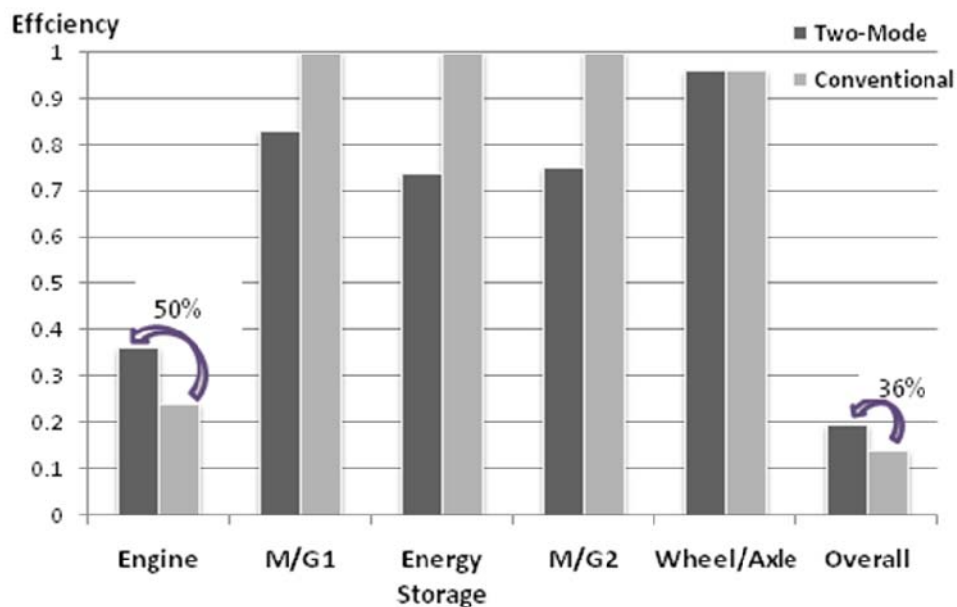


Figure 5-37 Efficiency of Two Mode HEV and Conventional ICE Vehicle on UDDSHEV Cycle

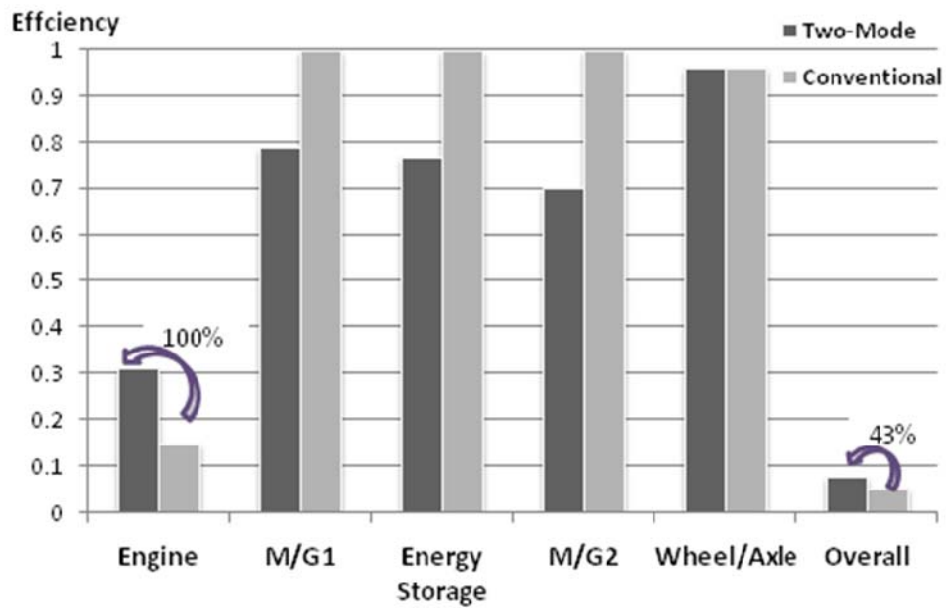


Figure 5-38 Efficiency of Two Mode HEV and Conventional ICE Vehicle on NYCCTRUCK Cycle

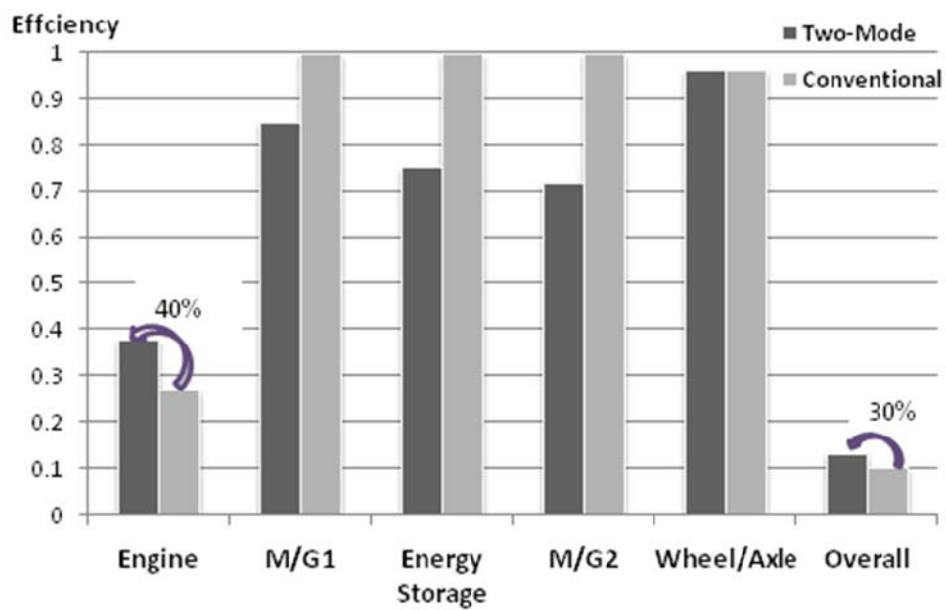


Figure 5-39 Efficiency of Two Mode HEV and Conventional ICE Vehicle on CSHVR Cycle

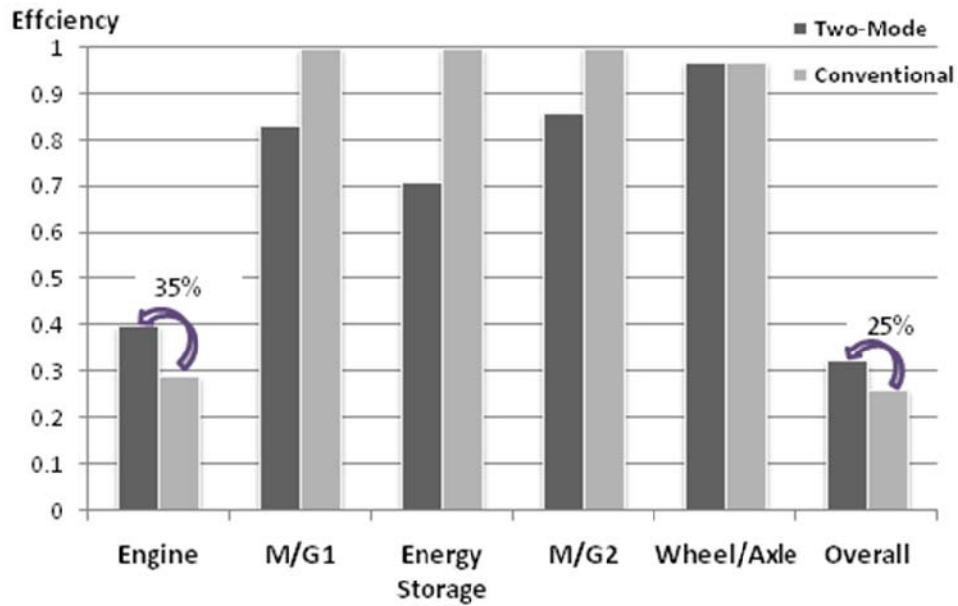


Figure 5-40 Efficiency of Two Mode HEV and Conventional ICE Vehicle on HWFET Cycle

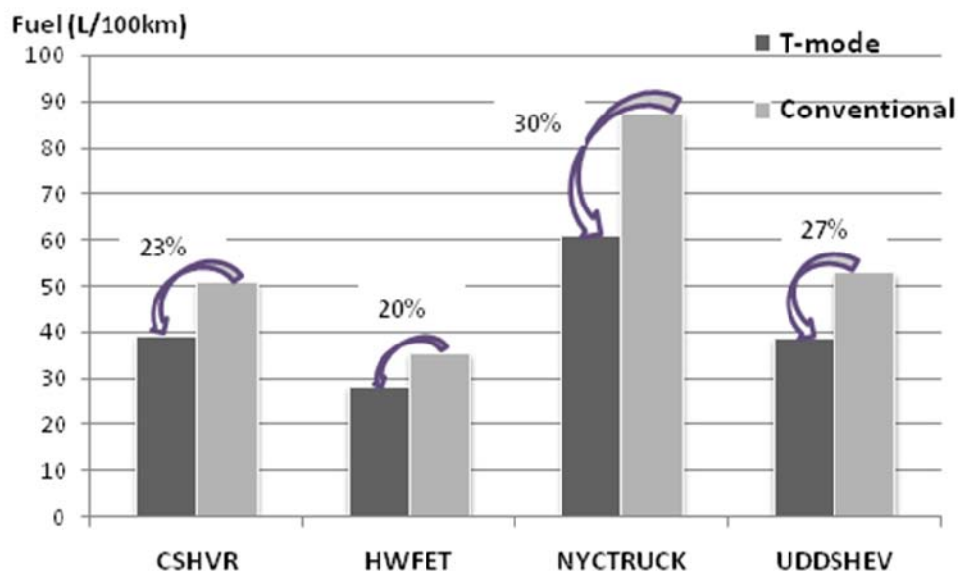


Figure 5-41 Summary of Fuel Consumptions

Figure 5-41 summarized simulation result of vehicle fuel consumptions over the four driving cycles. Two-mode HEV shows 25% improved fuel efficiency on average. The most

significant improvement was on NYCTRUCK cycle which is a busy urban traffic schedule based on New York City. The least improvement is on the HWFET cycle, a highway driving cycle.

5.4.5. All Electric Range

In the end, an all-electric-mode (AEM) was simulated. All electric range was activated when engine was switched off. The intention to keep engine off was largely due to the in-efficient operation of engine at low speed. With limited energy storage system and motor power, all-electric-mode was activated at low speed and low power conditions. Figure 5-42 shows vehicle speed at AEM. The vehicle showed significant under power during acceleration and higher speeds exceed 40 km/h. Therefore, it was only feasible to operate in AEM at low speed.

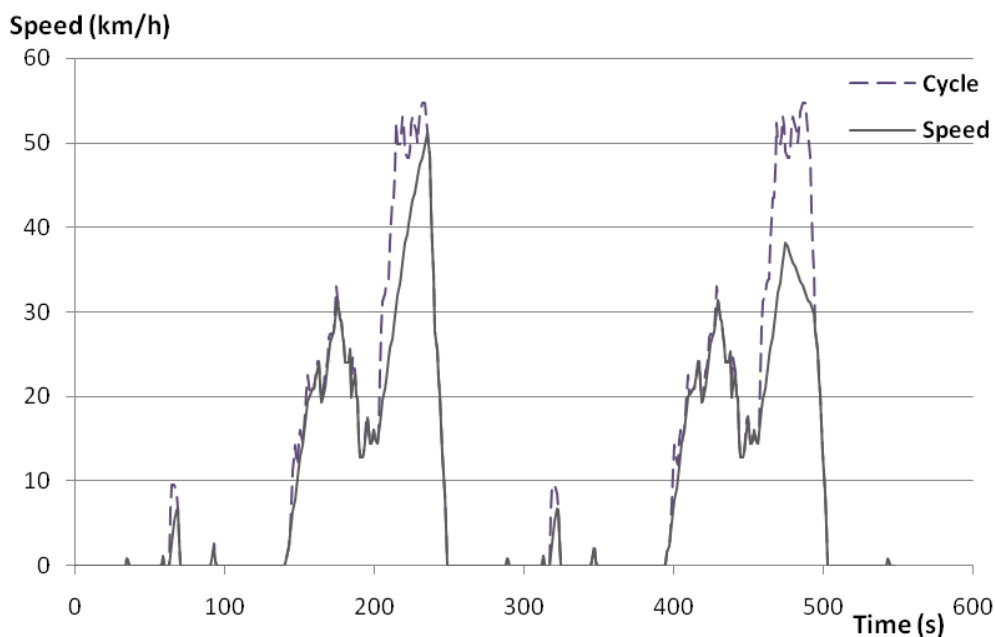


Figure 5-42 All Electric Mode Operation on NYCCTRUCK

Figure 5-43 shows the history of battery SOC when running NYCTRUCK at AEM. The battery SOC dropped from 0.7 to 0.55 at the first load cycle at about 250 seconds. Due to the inefficiency of battery operating at a low SOC, the vehicle had reached a point in which engine had to start. Therefore, the AEM running time in this driving cycle was 250 seconds unless

capacity of energy storage system was increased. The AEM time is always case dependent and there is no definite time or range for it.

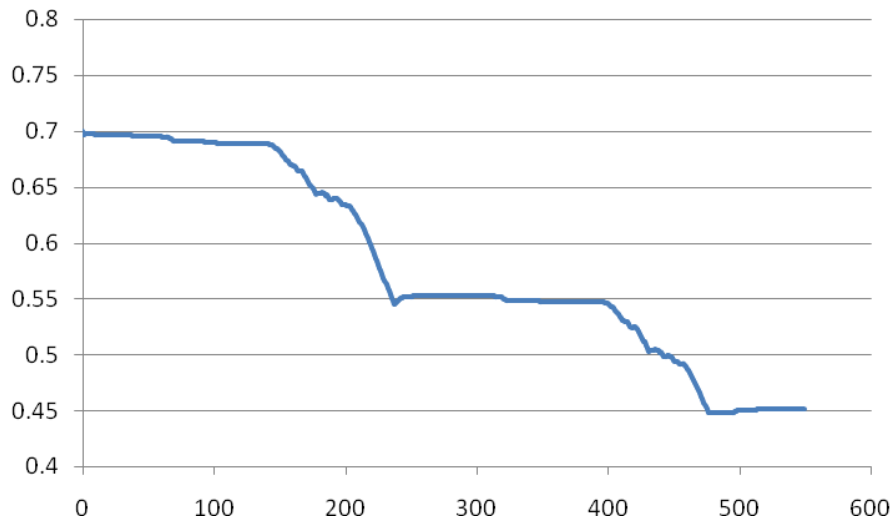


Figure 5-43 Battery SOC on NYCTRUCK at AEM

5.5. Conclusions

In this study, a two-mode HEV model was built. The operation of each powertrain component as well as the overall system was simulated. The results of the study on the two-mode vehicle were both promising and unsatisfactory.

The simulated vehicle succeeded in completing four driving cycles with no significant cycle miss-match. This indicated that the two-mode truck provided adequate power to the road demand. The engine efficiency was improved by at least 35% and an average of 56% over 4 drive cycles. The engine speed was no longer restrained to the vehicle speed and gear ratios. With the added degrees of freedom, the engine speed was decided according to engine power efficiency map. The overall improvement on fuel efficiency was also promising. The vehicle achieved a higher efficiency gain at a busy urban traffic schedule. The improvement on a highway cycle was a bit less but also attractive. Besides, the vehicle power was adequate to

propel the vehicle at a lower speed when engine is switched off. The all electric range was limited but can be improved with increased energy storage capacity.

The future improvements needed on the model is to better reflect the nature of real world vehicles. More refined control strategies have to be developed and electric loss should be reduced. However, there are a series of restrictions to improve the model in ADVISOR. ADVISOR is a well developed tool and fast to simulate. It contains numerous valuable data which were tested by different agencies. The main limitation of it is the nature of empirical model based on fixed testing environments which couldn't be modified to reflect changed operation conditions. One of author's intentions is to develop a "hybrid ESS" which introduces ultracapacitors to work with batteries so that the performance of hybrid energy storage could be explored. Some challenges were found to carry on this work on ADVISOR. Besides, the backward modeling approach of ADVISOR has a distinct difference theory of operation from the real world vehicle driving. To solve these problems and limitations on ADVISOR, a more flexible model tool using a forward modeling approach was studied and introduced in the following chapter.

CHAPTER 6 Modeling of ICE Hybrid Powertrain for a Parallel Hybrid Truck Using Modelica/Dymola and Validation

At the later stage of this study, a collaborative research agreement was made with a leading HEV manufacturer. The objective of this collaboration is to build a computer model that reflects the vehicle in production and also to explore the potential powertrain efficiency gain using other hybrid drivetrain designs.

To further improve the flexibility of vehicle simulations, Dymola was used to perform the work. As previously introduced in CHAPTER 3, Dymola is an efficient tool to develop complex physical models. The programming nature of Dymola is close to Simulink in MatLab. However, with vehicles libraries developed based on Dymola, modeling a hybrid vehicle in Dymola becomes easier. In this study, two libraries were used to facilitate the modeling process, the Powertrain library and the Smart Electric Drive library.

Validation of the Dymola models and simulation using experiment test data of four major powertrain components have shown satisfactory results, although validation at the system level has not yet been completed due to time constraint and the complexity of the task.

6.1. Parallel Hybrid Electric Vehicle

The baseline vehicle in this collaboration work is a parallel hybrid vehicle. The configuration of a parallel hybrid vehicle was introduced in Section 1.3. As the electric motor is located after the transmission, the vehicle is so called a post-transmission parallel hybrid vehicle.

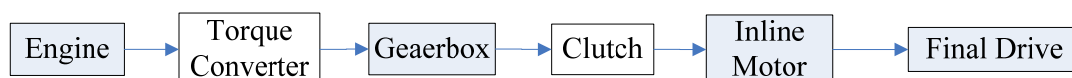


Figure 6-1 a Post-Transmission Parallel HEV Configuration

Figure 6-1 shows the configuration of this parallel HEV. An inline motor was used to couple with the engine torque. A clutch is located prior to inline motor could be used to disengage the gearbox when engine is switched off. The principal torque and speed relations on a parallel HEV are described as Eq. (6.1) and Eq. (6.2), where T_{final} and V_{final} are torque and speed to final drive, T_{engine} and V_{engine} are torque and speed for engine, and T_{motor} and V_{motor} are for electric motor. $R_{gearbox}$ is the gear ratio at gear box.

$$T_{final} = T_{engine} \times R_{gearbox} + T_{motor} \quad (6.1)$$

$$V_{final} = V_{engine} + R_{gearbox} = V_{motor} \quad (6.2)$$

As there is only one electric motor in a Parallel HEV, the motor operates at either powering or generating mode. While engine power supply exceeds power demand at the wheel, the motor regenerates the excess energy and stores it in the ESS. While a power surge is demanded at the wheel which is higher than engine outputting power, the motor withdraws power from ESS and supplies the additional torque. The motor is also used to regenerate energy from braking.

6.2. Vehicle Modeling in Dymola

In contract to a backward modeling approach used in ADVISOR, a forward modeling approach was used in this parallel HEV modeling in Dymola. A forward modeling approach is known to better represent the behavior of a real vehicle and driver. The modeling algorithm of a generic vehicle model is shown in Figure 6-2. A driver model decides pedal and brake signal according to system response. Then the vehicle responses to the operation command and vehicle speed is calculated. The vehicle speed is compared with cycle speed demand. The speed difference (or error) is sent back to driver model to adjust the pedal and brake.

In a conventional vehicle, the pedal signal is directly interpreted as engine fuel injection or torque been generated accordingly. The brake signal on the other hand would be interpreted at braking force applied on the brake disk. In a parallel HEV, the pedal and brake signal is considered differently. As the power sources include both engine and motor, the pedal signal controls the added power from both sources. This is also understood as a control strategy to split the torque load so that the engine operates more efficiently. The brake signal controls both the mechanical brake disk as well as the electric motor because of the regenerative braking. The direct control logic is to maximize the motor regenerative capacity and to use brake disk for further assistance.

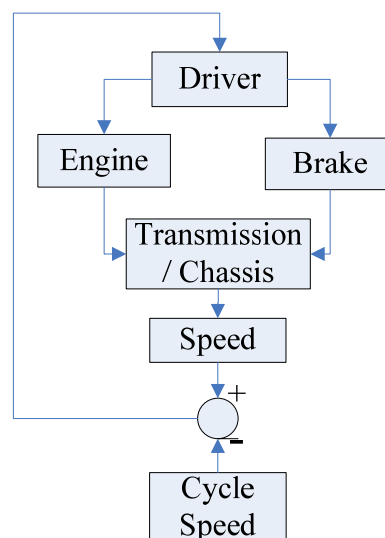


Figure 6-2 Forward Vehicle Modeling Algorithm in Dymola

6.2.1. Engine Modeling

The engine model built in Dymola consists of three parts, a base engine, a starter motor and a speed governor. The base engine receives power request from a driver model and generates the torque accordingly. Engine frictions and other losses are considered. A starter motor is used to generate the starting torque to start the engine. A speed governor is used to confine engine speed. It restricts engine speed between the range of maximum speed and idle speed. The outline of

engine model in Dymola is shown at Figure 6-3.

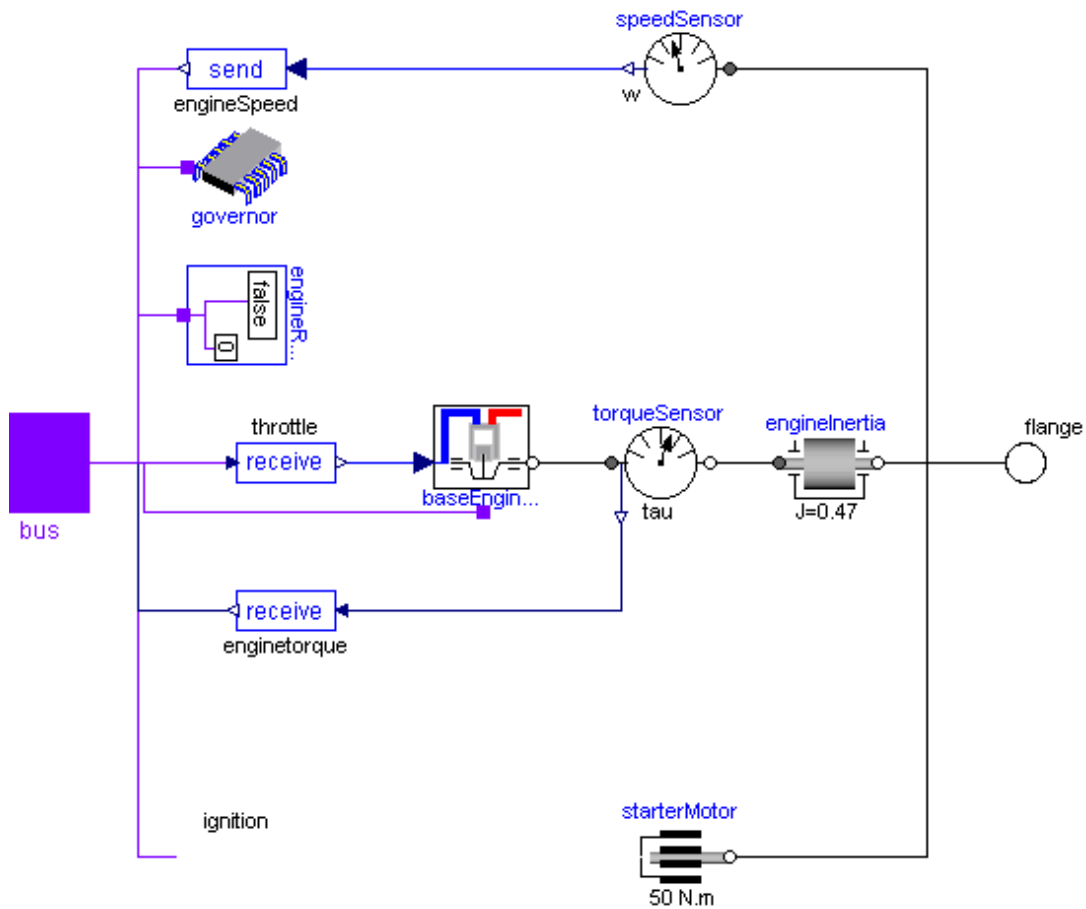


Figure 6-3 Engine Model in Dymola

A simplified base engine model theory is explained in Figure 6-4. The base engine receives pedal signal from driver model and translates it into engine torque request. The engine loss and auxiliary load are calculated according to engine speed. Finally, the engine torque at output shaft is decided. The fuel consumption is calculated based on experimental engine data provided by the industrial partner.

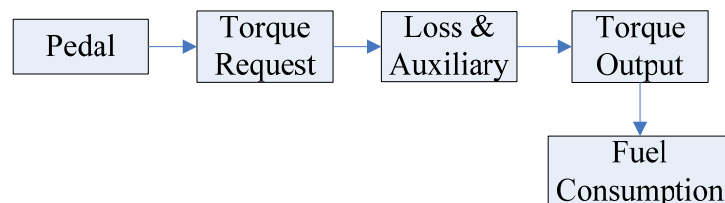


Figure 6-4 Base Engine Modeling

An engine speed governor model is used to confine engine speed within a range. This model receives engine speed V_r and calculates a desirable engine speed V_a . The difference (error) is corrected by controlling the pedal signal through a P controller.

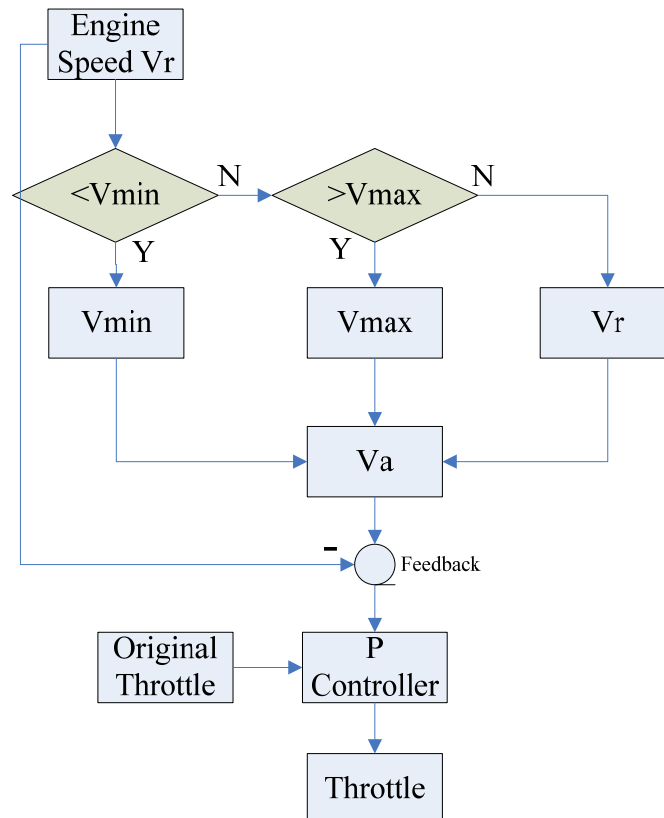


Figure 6-5 Engine Speed Governor Modeling

6.2.2. Transmission Modeling

A 5 speed automatic transmission was used in this vehicle. The transmission model includes a torque converter, two clutches, a gearbox model and two switching controllers. Figure 6-6 shows the transmission model in Dymola. Flange_a receives output torque from engine. Then clutch and Torque converter adjust the input torque for gear shifting. The controlledWheelset decides the dynamic gear ratio change on the gear selected. The last component on drivetrain is

a one way clutch which is used to disengage gearbox in all electric mode (AEM).

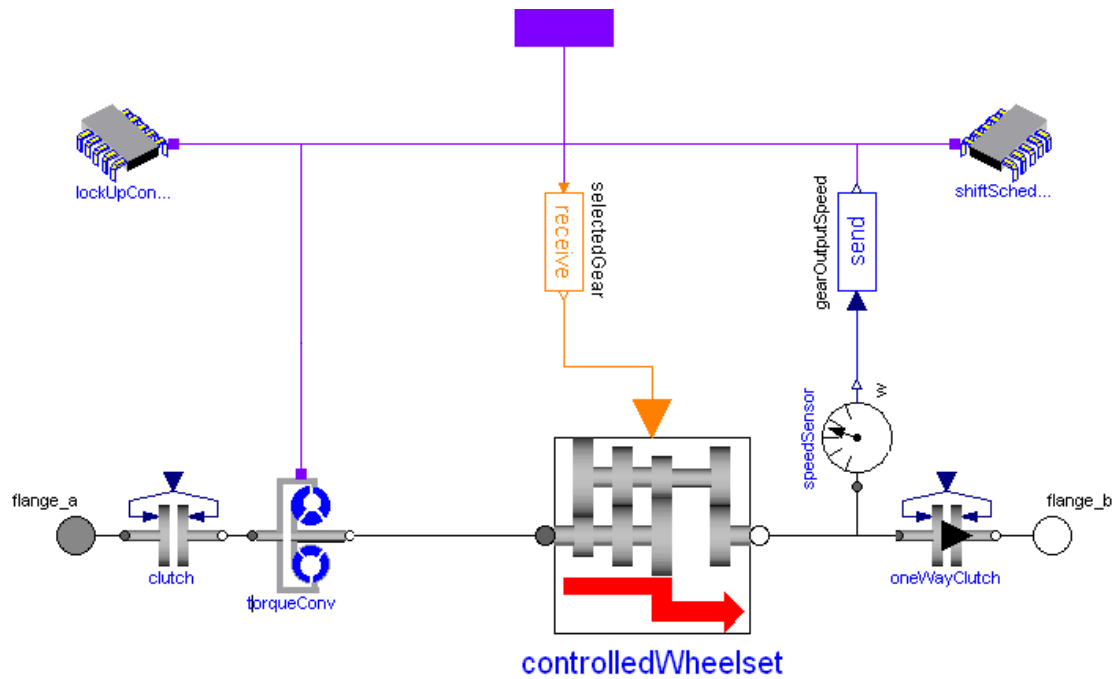


Figure 6-6 Transmission Model in Dymola

The transmission loss consists of two parts, one is spin loss; the other is torque loss. The spin loss is decided by output gear speed and gear selected. The torque loss is decided by turbine torque at torque converter and gear selected.

6.2.3. Chassis and Resistance Modeling

The chassis model in Dymola includes a brake, a differential and two tires as shown in Figure 6-7. The brake signal is inputted from the drive model. The normal force acted on the brake disk is proportional to the brake signal. The differential block was modeled as a fixed ratio gear. A power transmission efficiency of 98% was used.

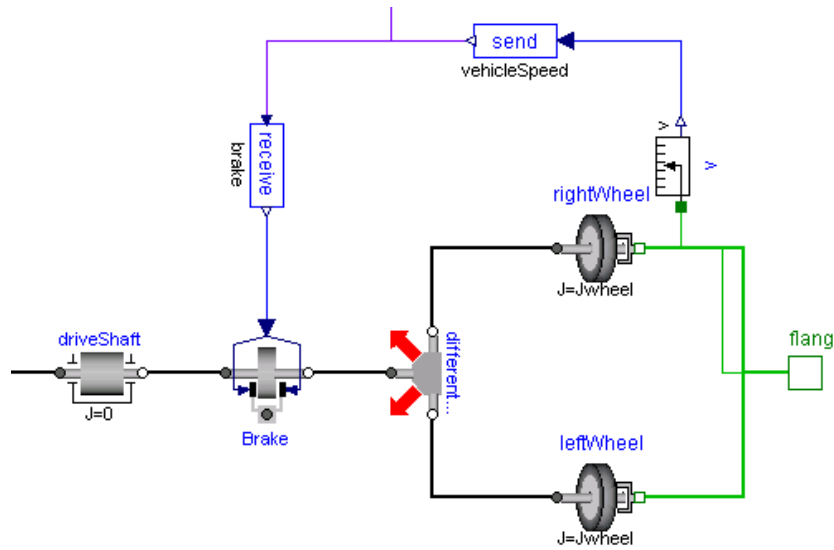


Figure 6-7 Chassis Model in Dymola

The resistance model was modelled similar to drivetrain model described at section 5.2.1. Four forces were considered, acceleration, air-drag, rolling resistance and grade force. The schematic drawing of these forces was shown in Figure 5-19. Figure 6-8 is the modeling diagram of vehicle resistance in Dymola.

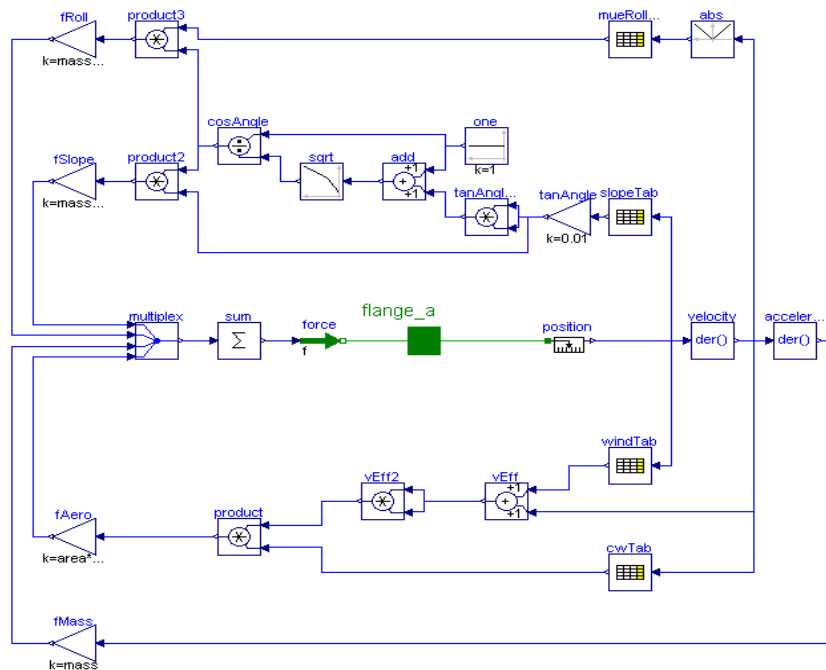


Figure 6-8 Vehicle Resistance Model

6.2.4. Driver Modeling

A driver model in a forward vehicle modeling approach simulates behaviors of a human when operating a motor vehicle. A driver decides whether to accelerate or to brake in order to follow the drivecycle closely. The “brain work” is usually done by using a PI controller or a Lead Compensator. In this model, both controllers were modeled. A PI controller was selected as it provided a better match of the drive cycle from the simulation results.

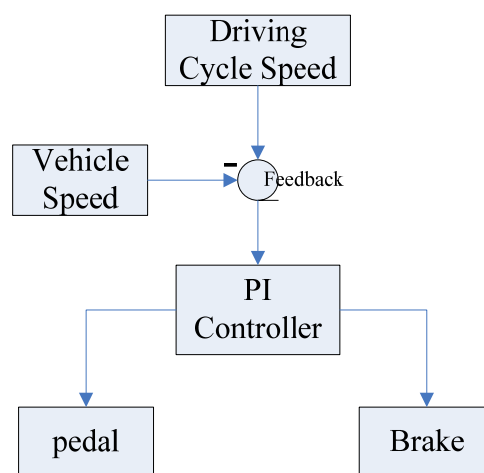


Figure 6-9 Driver Model

6.3. Models Simulation and Validations

Upon completion of the modeling, experimental data provided by the manufacturer were used to validate each component. The experimental data was obtained from the industrial partner. The validated models include the engine, the transmission, the torque converter and the vehicle chassis resistance.

6.3.1. Engine Model Validation

The engine data was based on a ten seconds incremental pedal position from 0 to 1. Figure 6-10 shows the comparison of simulation results and test data. It is shown that the engine model provided a close match to test result. The initial starting period shows a considerable mismatch.

However, the simulation result of engine shows a closer match with the test data after 4 seconds after.

Table 6-1 Engine Model Input

| Input | Description |
|----------------|---------------------------|
| Pedal Position | $Y=0.1t$, for 10 seconds |
| Load | 20 kg.m^2 |

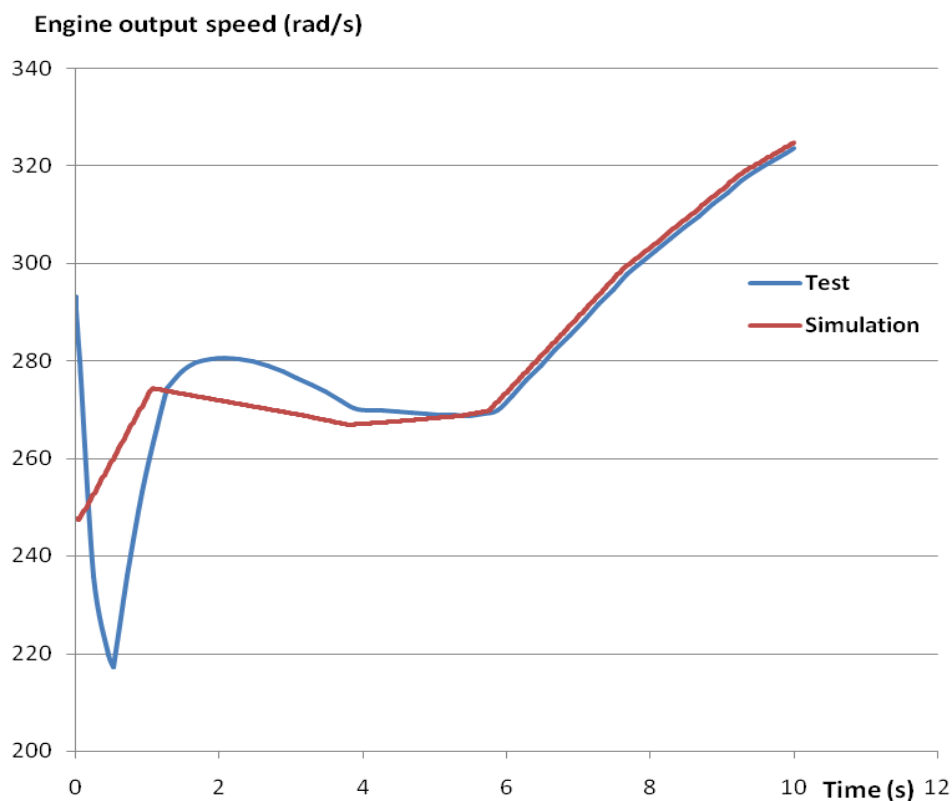


Figure 6-10 Engine Model Validation

6.3.2. Torque Converter Model Validation

A torque converter is used to adjust the torque and speed from the engine to the gearbox for an automatic transmission. The loss at a torque converter sometime is significant which results in a higher fuel consumption of an automatic vehicle compared with its manual transmission counterpart. Therefore, it is important to model a torque converter which accurately reflects the

power transfer and loss on an actual vehicle. In order to evaluate the output from the computer model, a comparison was made using an input as shown in Table 6-2.

Table 6-2 Torque Converter Model Input

| Input | Description |
|--------------|---------------------|
| Torque Input | $T=50\sin(t)+150$ |
| Load | 50 kg.m^2 |

Figure 6-11 and Figure 6-12 show the comparison of simulation result on torque and speed. The comparison shows a close match of the test and the simulation data.

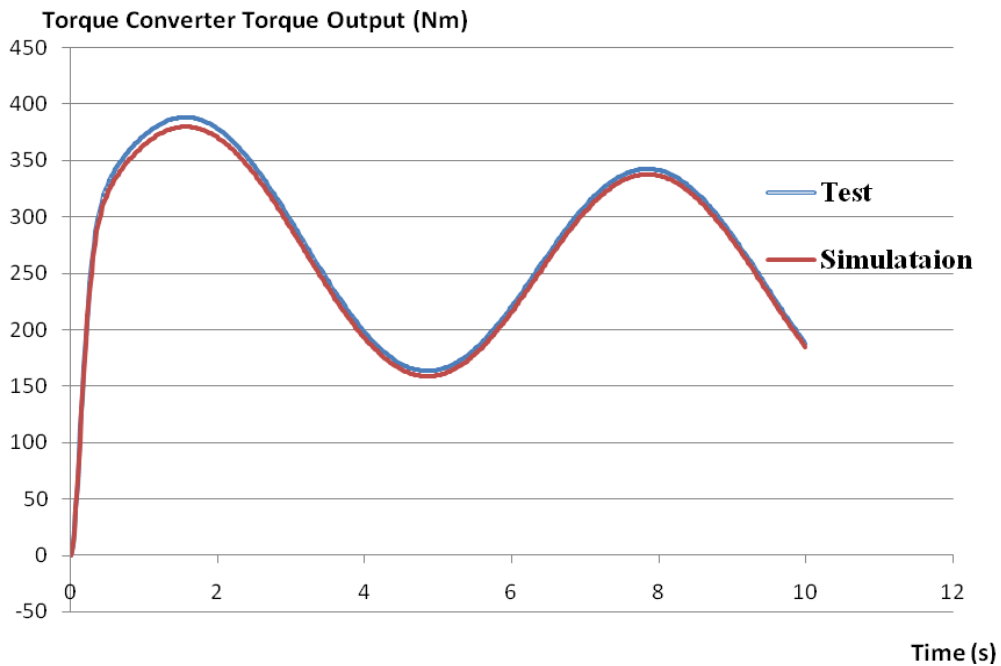


Figure 6-11 Torque Converter Validation - Output Torque

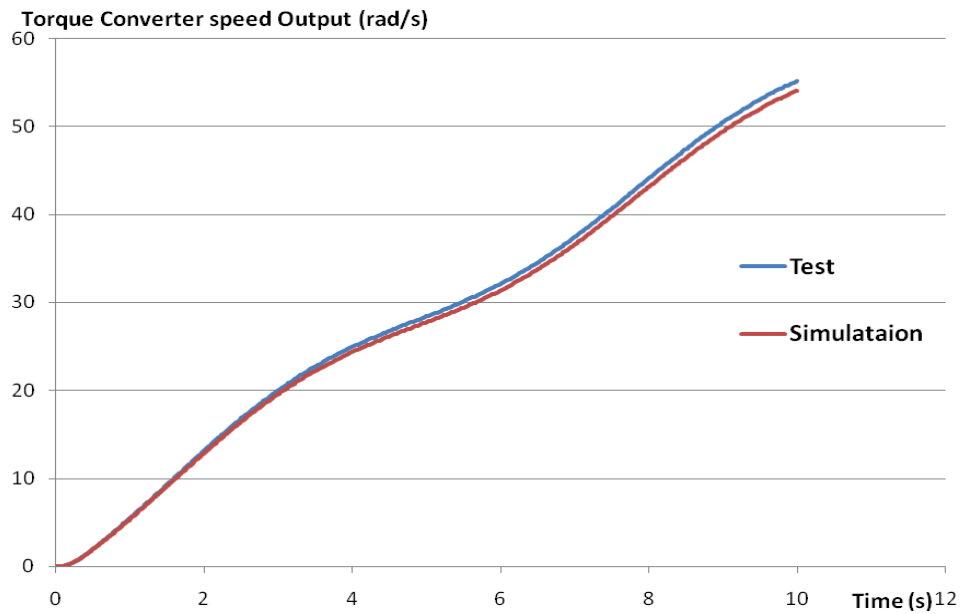


Figure 6-12 Torque Converter Validation - Output Speed

6.3.3. Transmission Model Validation

The transmission model validation was carried out on each of the five gears. A known torque was inputted to the torque converter to simulate an engine torque. A rigid body with inertia of 50 kgm^2 was used to attach to the output shaft to simulate the load. Figure 6-13 shows the comparison of simulation results and data from the manufacturer. The transmission speed at output shaft matched most of the test data. Therefore, the transmission model is considered adequately accurate to represent transmission tested.

Table 6-3 Transmission Input

| Input | Description |
|--------------|---------------------|
| Torque Input | $Y=150+\sin(t)$ |
| Load | 50 kg.m^2 |

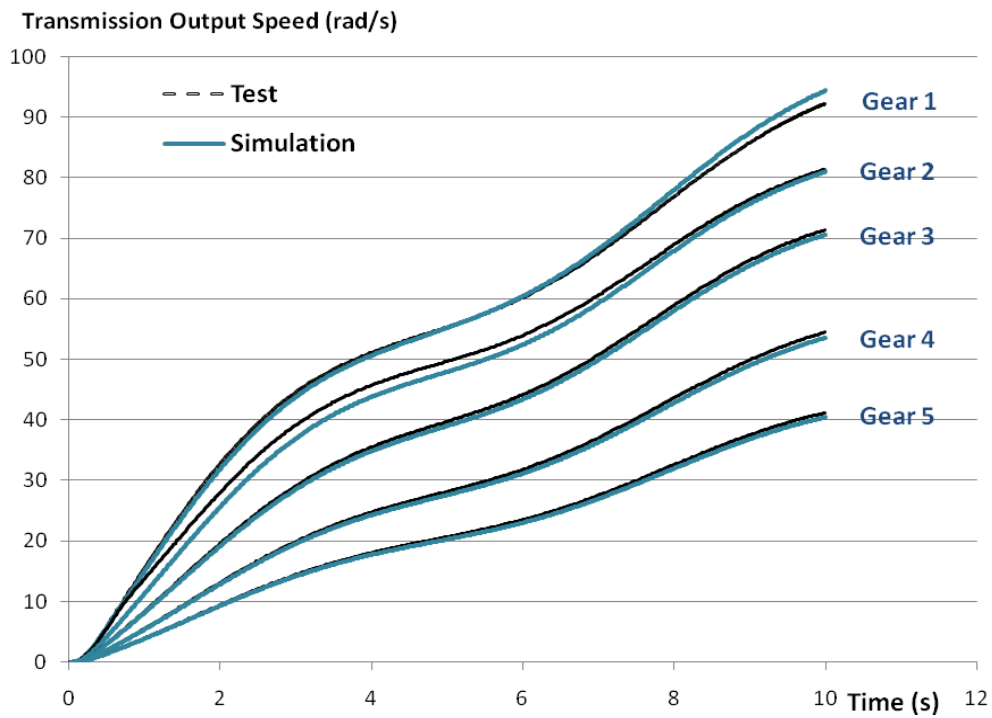


Figure 6-13 Transmission Model Validation - Output Speed

6.3.4. Chassis and Resistance Model Validation

The chassis and resistance model in Dymola was simulated to compare against results provided by manufacturer. A torque was inputted at final axle to simulate a torque output from transmission. The input torque is shown at Table 6-3. The simulated data shows the chassis and resistance model provides a close match with test data.

Table 6-4 Transmission Input

| Input | Description |
|--------------|---------------------|
| Torque Input | $Y=500+3000\sin(t)$ |

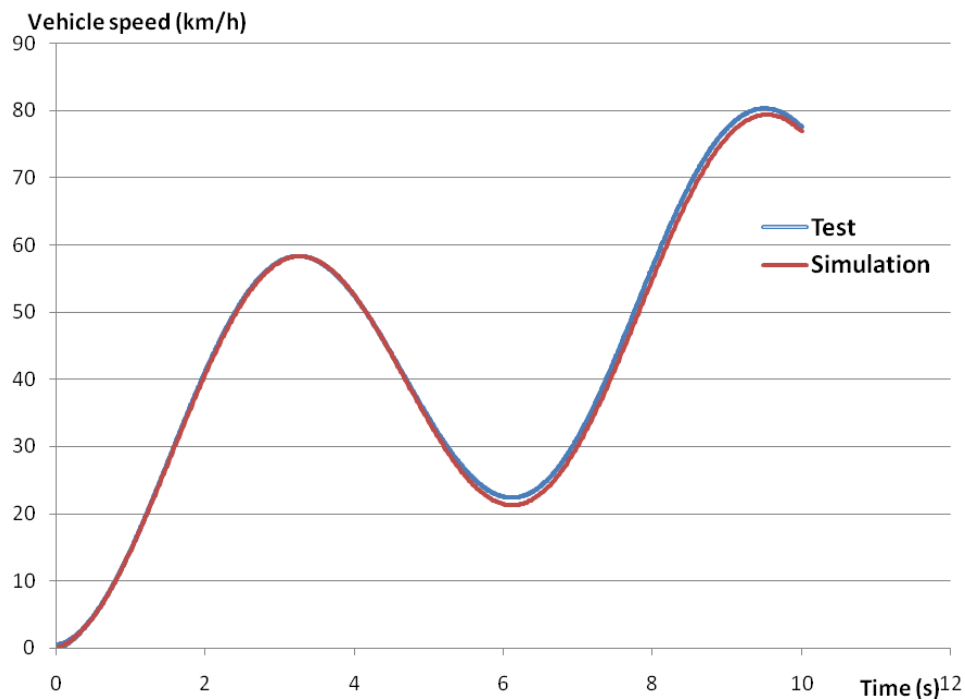


Figure 6-14 Vehicle Chassis Model Validation - Vehicle Speed

6.4. Overview and Conclusions

At the current stage, a simulation using Dymola model at the system level has not yet been carried out. Several key drivetrain components in the system have been modeled. Simulations were run on these models to compare the results with test data provided by the manufacturer. The results on most simulations showed a very good match to experimental data. It is therefore demonstrated that Dymola is capable of modeling a complex vehicle system.

To complete the modeling of a parallel HEV, additional work in several areas has to be carried out. The motor, energy storage device and power electronics units have to be modeled and validated. Afterwards an optimal control strategy should be introduced and applied on the vehicle model. Improvements on efficiency and performance using the optimized control strategy need be verified.

CHAPTER 7 Summary

7.1. Research Problem

The improvement of HEV design over conventional vehicle is largely on better powertrain efficiency. To verify the optimal design of vehicle powertrain, validation using costly prototype is expensive and sometime impractical. Vehicle simulation is a method for fast and systematic investigation of different design options and configurations, including the choice of various types of battery, transmission, fuel cells, fuel reformer, etc as well as their parameters. Therefore, simulation based analysis on vehicle performance is both useful and crucial to the development of new hybrid vehicles. At present, the available vehicle simulation tools cannot support the modeling and analysis of all vehicle design options, rather than focusing on very specific applications. Considerable work is needed to introduce more capable and reliable powertrain modeling and simulation tools to guide new hybrid vehicle design.

7.2. Technology Review

In this study, two general issues of hybrid electric vehicles were reviewed, including the state-of-the-art powertrain configurations and advanced energy storage systems. Comparisons were made to find optimal design for certain application. A review of vehicle simulation tool was carried out. Two modeling platforms introduced in detail were Matlab/Simulink and Modelica/Dymola. These simulation packages were used extensively through this study.

7.3. Vehicle Modeling

To better assist the design and development of future generation HEV, three distinct vehicular systems were studied and modeled using two vehicle modeling packages, ADVISOR and Dymola.

The first model is a fuel cell based hybrid power backup system used for an elevator in a high-rise building. It is modified from an electric vehicle model built in ADVISOR. The simulation results demonstrated the technical and cost feasibility of using fuel cell power system to provide uninterrupted power to the elevator system. A second model built is a Class 7 commercial truck using a two-mode truck model built on ADVISOR. The simulation results showed that the two-mode hybrid powertrain has adequate power as well as a dramatic improvement on fuel efficiency. The last vehicle model of a parallel hybrid electric vehicle was done on the Dymola platform. Computer models of key vehicle powertrain components, engine, transmission, and chassis were built. The simulation results are validated using test data provided by the vehicle manufacturer. The integrated system model is not yet completed and vehicle simulation was not performed.

7.4. Future Work

The research forms the foundation for further studies on the modeling and analysis of advanced hybrid vehicle powertrain configurations using advanced modeling and simulation tools.

The preliminary studies on fuel cell hybrid power system for elevator power backup system; the two mode hybrid vehicle powertrain configuration; and the use of Dymola to model complex hybrid vehicle powertrain and ESS provide promising research directions that deserve further study.

REFERENCES

1. Cacciola, R.R. and M. Sarva, *Adverse respiratory effects and allergic susceptibility in relation to particulate air pollution: flirting with disaster*. . Allergy, 2002(2002): p. 58:281-6.
2. Maples, J., Moore Jr., Schaper, *Transportation and fuel technologies: performance analysis methodology*. 1998, Washington, DC: US Department of Energy.
3. Administration, E.I. [cited 2007 Sep 17]; Available from: <http://www.eia.doe.gov/neic/quickfacts/quickoil.html>.
4. Lew, F., *Reducing Oil Consumption in Transport: Combining Three Approaches*. 2004, Office of Energy Efficiency, Technology and R&D International Energy Agency.
5. Chiang, P.K., *Two-Mode Urban Transit Hybrid Bus In-Use Fuel Economy Results From 20 Million Fleet Miles*. 2007, SAE.
6. Carlson, E., P. Kopf, and J. Sinha, *Fuel Cell seminar*. 2005, TIAX LLC: Cambridge MA.
7. Westbrook, M., *The Electric Car: Development and future of battery, hybrid and fuel-cell cars*. IEE Power and Energy Series 38, ed. A. Johns and D. Warne. 2001, London, United Kingdom: Institution of Electrical Engineers.
8. Miller, J., *Propulsion Systems for Hybrid Vehicles*,
. Institution of Electrical Engineers: London, United Kingdom., 2004.
9. Jong-Seob, W., R. Langari, and M. Ehsani, *An energy management and charge sustaining strategy for a parallel hybrid vehicle with CVT*. IEEE Transactions on Control Systems Technology, 2005. **13**(2): p. 313-20.
10. Meisel, J. *An analytic foundation for the Toyota Prius THS-II powertrain with a comparison to a strong parallel hybrid-electric powertrain*. in *SAE 2006 World Congress*. 2006. Detroit, MI.
11. Wishart, J.D., Y. Zhou, and Z. Dong. *Review, Modelling and Simulation of Two-Mode Hybrid Vehicle Architecture*. in *9th International Conference on Advanced Vehicle and Tire Technologies (AVTT)*. 2007. Las Vegas, NV, US.
12. Balch, R.C., A. Burke, and A.A. Frank. *The affect of battery pack technology and size choices on hybrid electric vehicle performance and fuel economy*. in *16th Annual Battery*

-
- Conference on Applications and Advances, Jan 9-12 2001*. 2001. Long Beach, CL: Institute of Electrical and Electronics Engineers Inc.
13. Stienecker, A.W., T. Stuart, and C. Ashtiani, *An ultracapacitor circuit for reducing sulfation in lead acid batteries for Mild Hybrid Electric Vehicles*. Journal of Power Sources, 2006. **156**(2): p. 755-762.
 14. Karden, E., et al., *Energy storage devices for future hybrid electric vehicles*. Journal of Power Sources, 2007. **168**(1): p. 2-11.
 15. Douglas, H. and P. Pillay. *Sizing ultracapacitors for hybrid electric vehicles*. 2005. Raleigh, NC, United States: Institute of Electrical and Electronics Engineers Computer Society, Piscataway, NJ 08855-1331, United States.
 16. Staunton, R.H., et al., *Evaluation of 2004 Toyota Prius Hybrid Electric Drive System*. 2006: United States. p. Size: 4 Mb.
 17. Markel, T. and A. Simpson. *Energy storage systems considerations for grid-charged hybrid electric vehicles*. 2005. Chicago, IL, United States: Institute of Electrical and Electronics Engineers Computer Society, Piscataway, NJ 08855-1331, United States.
 18. Ito, K. and M. Ohnishi, *Development of prismatic type nickel/metal-hydride battery for HEV*, in *Proceedings of the 20th Electric Vehicle Symposium*. 2003: Long Beach.
 19. Horiba, T., et al., *Applications of high power density lithium ion batteries*. Journal of Power Sources, 2005. **146**(1-2): p. 107-10.
 20. Taniguchi, A., et al., *Development of nickel/metal-hydride batteries for EVs and HEVs*. Journal of Power Sources, 2001. **100**(1-2): p. 117-124.
 21. Congress, G.C. 2007 [cited 2007 7.1]; Available from: http://www.greencarcongress.com/2007/06/report_toyota_w.html.
 22. Kotz, R. and M. Carlen, *Principles and applications of electrochemical capacitors*. Electrochimica Acta, 2000. **45**(15-16): p. 2483-2498.
 23. Rufer, A. and P. Barrade. *A supercapacitor-based energy storage system for elevators with soft commutated interface*. in *36th IAS Annual Meeting -Conference Record of the 2001 Industry Applications, Sep 30-Oct 4 2001*. 2001. Chicago, IL: Institute of Electrical and Electronics Engineers Inc.
 24. Arulepp, M., et al., *The advanced carbide-derived carbon based supercapacitor*. Journal of Power Sources, 2006. **162**(2 SPEC ISS): p. 1460-1466.
 25. Anstrom, J.R., et al. *Simulation and field-testing of hybrid ultra-capacitor/battery energy storage systems for electric and hybrid-electric transit vehicles*. 2005. Austin, TX, United States: Institute of Electrical and Electronics Engineers Inc., Piscataway, NJ 08855-1331, United States.

-
26. Schupbach, R.M., et al. *Design methodology of a combined battery-ultracapacitor energy storage unit for vehicle power management*. 2003. Acapulco, Mexico: IEEE.
 27. Santi, E., et al. *A fuel cell based domestic uninterruptible power supply*. in *17th Annual IEEE Applied Power Electronics Conference and Exposition, Mar 10-14 2002*. 2002. Dalas, TX: Institute of Electrical and Electronics Engineers Inc.
 28. Markel, T., et al., *ADVISOR: A systems analysis tool for advanced vehicle modeling*. *Journal of Power Sources*, 2002. **110**(2): p. 255-266.
 29. Wipke, K.B., M.R. Cuddy, and S.D. Burch, *ADVISOR 2.1: A user-friendly advanced powertrain simulation using a combined backward/forward approach*. *IEEE Transactions on Vehicular Technology*, 1999. **48**(6): p. 1751-1761.
 30. Guenther, M. and Z. Dong, *Modelling, Testing and Design Optimization of PEM Fuel Cell System for Low-speed Electric Vehicles*. 2005, Department of Mechanical Engineering and Institute for Integrated Energy Systems.
 31. Markel, T. and K. Wipke. *Modeling grid-connected hybrid electric vehicles using ADVISOR*. in *16th Annual Battery Conference on Applications and Advances, Jan 9-12 2001*. Long Beach, CL: Institute of Electrical and Electronics Engineers Inc.
 32. German aerospace center, I.o.R.a.M. [cited; Available from: <http://www.dlr.de/rm/en/>, contact Martin.Otter@dlr.de.
 33. Research, A. [cited; Available from: http://www.arsenal.ac.at/home_en.html modelica@arsenal.ac.at.
 34. BAUR, M. and J. UNGETH UM, *Alternative Vehicles- Modelica Bibliothek zur Simulation von alternativen Fahrzeugkonzepten*, in *in Steuerung und Regelung von Fahrzeugen und Motoren – AUTOREG 2006*,. 2006: Wiesloch, Germany,.
 35. [cited 2007 July 1st]; Available from: <http://www.ricardo.com/default.aspx> dynamic.simulation@ricardo.com.
 36. Gray, L., *A brief history of residential elevators: Part one. The flying chair*. *Elevator World*, 2005. **53**(1): p. 110-111.
 37. Kulkarni, A.B., H. Nguyen, and E.W. Gaudet. *Comparative evaluation of line regenerative and non-regenerative vector controlled drives for AC gearless elevators*. 2000. Rome, Italy: Institute of Electrical and Electronics Engineers Inc., Piscataway, NJ, USA.
 38. Tominaga, S., et al. *Development of energy-saving elevator using regenerated power storage system*. in *Proceedings of Power Conversion Conference - Osaka PCC 2002, 2-5 April 2002*. 2002. Osaka, Japan: IEEE.
 39. Wiegers, R.G., D.M. Blacketter, and H.L. Hess, *Modelling performance of ultracapacitor arrays in hybrid electric vehicles*. *International Journal of Alternative Propulsion*, 2006.

-
- 1(1): p. 32-46.
40. Burke, A.F. *Prospects for ultracapacitors in electric and hybrid vehicles*. 1996. Long Beach, CA, USA: IEEE, Piscataway, NJ, USA.
 41. Burke, A.F. *Review of Ultracapacitor Technologies for Vehicle Applications*. in *Proceedings of the First Annual Advanced Automotive Battery Conference*,. 2001. Las Vegas.
 42. Gagliardi, F. and M. Pagano. *Experimental results of on-board battery-ultracapacitor system for electric vehicle applications*. 2002. L'Aquila, Italy: IEEE.
 43. Zhang, X.-g., et al., *Study on hybrid system of MH/Ni battery and carbon-based supercapacitor*. *Battery Bimonthly*, 2003. **33**(4): p. 226-7.
 44. Gao, L., R.A. Dougal, and S. Liu. *Active power sharing in hybrid battery/capacitor power sources*. 2003. Miami Beach, FL, USA: IEEE.
 45. Baisden, A.C. and A. Emadi, *ADVISOR-based model of a battery and an ultra-capacitor energy source for hybrid electric vehicles*. *IEEE Transactions on Vehicular Technology*, 2004. **53**(1): p. 199-205.
 46. Anderman, M. *Analysis of an ultracapacitor/VRLA hybrid power source for hybrid vehicles*. 2004: Proceedings of the Ninth European Lead Battery.
 47. Solero, L., A. Lidozzi, and J.A. Pomilio, *Design of multiple-input power converter for hybrid vehicles*. *IEEE Transactions on Power Electronics*, 2005. **20**(5): p. 1007-1016.
 48. Di Napoli, A., et al. *Multiple input DC-DC power converter for fuel-cell powered hybrid vehicles*. in *2002 IEEE 33rd Annual Power Electronics Specialists Conference (PESC), Jun 23-27 2002*. 2002. Cairns, Australia: Institute of Electrical and Electronics Engineers Inc.
 49. Todorovic, M.H., L. Palma, and P. Enjeti. *Design of a wide input range DC-DC converter with a robust power control scheme suitable for fuel cell power conversion*. in *19th Annual IEEE Applied Power Electronics Conference and Exposition - APEC 2004, Feb 22-26 2004*. 2004. Anaheim, CA., United States: Institute of Electrical and Electronics Engineers Inc.
 50. Strakosch, G.R., *Vertical Transportation: Elevator and Escalators*. 1983, New York: John Wiley & Sons.
 51. Zhu, W.D. and L.J. Teppo, *Design and analysis of a scaled model of a high-rise, high-speed elevator*. *Journal of Sound and Vibration*, 2003. **264**(3): p. 707-731.
 52. Haraldsson, K. and K. Wipke, *Evaluating PEM fuel cell system models*. *Journal of Power Sources*, 2004. **126**(1-2): p. 88-97.

-
53. Amphlett, J.C., et al., *Performance modeling of the Ballard Mark IV solid polymer electrolyte fuel cell II. Empirical model development*. Journal of the Electrochemical Society, 1995. **142**(1): p. 9-15.
 54. Fowler, M.W., et al. *Incorporation of voltage degradation into a generalised steady state electrochemical model for a PEM fuel cell*. in *7th Grove Fuel Cell Symposium, Grove VII, Sep 11-13 2001*. London: Elsevier Science B.V.
 55. Xue, D. and Z. Dong, *Optimal fuel cell system design considering functional performance and production costs*. Journal of Power Sources, 1998. **76**(1): p. 69-80.
 56. Cownden, R., M. Nahon, and M.A. Rosen, *Modeling and Analysis of a Solid Polymer Fuel Cell System for Transportation Applications*. International Journal of Hydrogen Energy, 2001. **26**(6): p. 615-623.
 57. Wishart, J.D. and Z. Dong, *Optimization of Fuel Cell System Based on Empirical Data of PEM Fuel Cell Stack and Generalized Electrochemical Semi-Empirical Model*. Journal of Power Sources, 2006. **161**: p. 1041-1055.
 58. Cameron, D.S., *Building and commercialisation of a fuel cell industry*. 2006: The Interact Consultancy.
 59. Maxwell, *Maxwell*.
 60. Cegnar, E.J., H.L. Hess, and B.K. Johnson. *A purely ultracapacitor energy storage system for hybrid electric vehicles utilizing a microcontroller-based dc-dc boost converter*. 2004. Anaheim, CA., United States: Institute of Electrical and Electronics Engineers Inc.
 61. Gao, L., R.A. Dougal, and S. Liu, *Power enhancement of an actively controlled battery/ultracapacitor hybrid*. IEEE Transactions on Power Electronics, 2005. **20**(1): p. 236-243.
 62. Hu, M., *Power flow and efficiency of planetary gear transmission*. Chinese Journal of Mechanical Transmission, 1998(2): p. 13-16.
 63. Lin, C.C., et al. *Energy management strategy for a parallel hybrid electric truck*. in *2001 American Control Conference, Jun 25-27 2001*. 2001. Arlington, VA: Institute of Electrical and Electronics Engineers Inc.
 64. Chan-Chiao, L., et al., *Power management strategy for a parallel hybrid electric truck*. IEEE Transactions on Control Systems Technology, 2003. **11**(6): p. 839-49.
 65. Boyali, A., et al. *Modeling and control of a four wheel drive parallel hybrid electric vehicle*. 2006. Munich, Germany: IEEE.
 66. Jeon, S., J.-M. Lee, and Y.-I. Park. *Adaptive multi-mode control strategy for a parallel hybrid electric vehicle based on driving pattern recognition*. 2003. Washington, DC., United States: American Society of Mechanical Engineers, New York, NY 10016-5990,

United States.

67. Jong-Seon, W. and R. Langari. *Intelligent energy management agent for a parallel hybrid vehicle*. 2003. Denver, CO, USA: IEEE.
68. Hannoun, H., D. Diallo, and C. Marchand. *Energy management strategy for a parallel hybrid electric vehicle using fuzzy logic*. 2006. Taormina, Italy: Institute of Electrical and Electronics Engineers Computer Society, Piscataway, NJ 08855-1331, United States.
69. Yan, W., V. Utkin, and G. Rizzoni. *Power flow control for a series hybrid electric vehicle*. in *IEEE International Symposium on Industrial Electronics 2005, ISIE 2005, Jun 20-23 2005*. 2005. Dubrovnik, Croatia: Institute of Electrical and Electronics Engineers Inc., Piscataway, NJ 08855-1331, United States.
70. Gielniak, M.J. and Z.J. Shen. *Power management strategy based on game theory for fuel cell hybrid electric vehicles*. in *2004 IEEE 60th Vehicular Technology Conference, VTC2004-Fall: Wireless Technologies for Global Security, Sep 26-29 2004*. 2004. Los Angeles, CA, United States: Institute of Electrical and Electronics Engineers Inc., Piscataway, NJ 08855-1331, United States.
71. Min Joong, K., et al. *Testing, modeling, and control of a fuel cell hybrid vehicle*. in *Proceedings of the 2005 American Control Conference, 8-10 June 2005*. 2005. Portland, OR, USA: IEEE.